MICROCOPY RESOLUTION TEST CHART

NATIONAL BUREAU OF STANDARDS-1963-A

AD-A148 731

NAVAL POSTGRADUATE SCHOOL
Monterey, California

THESIS

A CRITICAL ANALYSIS OF OCEAN THERMAL ANALYSIS
MODELS IN OPERATION AT FNOC

by

Brian James Brady

September 1984

Thesis Advisor: C. N. K. Mooers

Approved for public release, distribution unlimited

84   12   17   027

DTIC
SELECTED
DEC 28 1984

E

NAVAL POSTGRADUATE SCHOOL
Monterey, California

Commodore R.H. Shumaker
Superintendent

David A. Schrady
Provost

Released as a
Technical Report by:

John N. Dyer
Dean of Science and Engineering

REPORT DOCUMENTATION PAGE	READ INSTRUCTIONS BEFORE COMPLETING FORM	
1. REPORT NUMBER NPS-68-84-015	2. GOVT ACCESSION NO. AD-A148731	3. RECIPIENT'S CATALOG NUMBER
4. TITLE (and Subtitle) A CRITICAL ANALYSIS OF OCEAN THERMAL ANALYSIS MODELS IN OPERATION AT FNOC		5. TYPE OF REPORT & PERIOD COVERED Master's Thesis; September 1984
		6. PERFORMING ORG. REPORT NUMBER
7. AUTHOR(s) Brian James Brady		8. CONTRACT OR GRANT NUMBER(s) N0001483AF00001
9. PERFORMING ORGANIZATION NAME AND ADDRESS Naval Postgraduate School Monterey, California 93943		10. PROGRAM ELEMENT, PROJECT, TASK AREA & WORK UNIT NUMBERS Program Element: 61153N Project: RR031-03-01 RR033-02-01
11. CONTROLLING OFFICE NAME AND ADDRESS Office of Naval Research, Arlington, VA 22217 Code 422PO Naval Postgraduate School, Monterey, CA 93943		12. REPORT DATE September 1984
		13. NUMBER OF PAGES 160
14. MONITORING AGENCY NAME & ADDRESS(if different from Controlling Office)		15. SECURITY CLASS. (of this report) Unclassified
		15a. DECLASSIFICATION/DOWNGRADING SCHEDULE

16. DISTRIBUTION STATEMENT (of this Report)

Approved for public release, distribution unlimited

17. DISTRIBUTION STATEMENT (of the abstract entered in Block 20, if different from Report)

18. SUPPLEMENTARY NOTES

19. KEY WORDS (Continue on reverse side if necessary and identify by block number)

Thermal Structure, OPTOMA, California Current System, TEOTS, EOTS, Mixed Layer Depth, Acoustic Propagation, FACT9H and PE Transmission Loss Models, Interannual Variability, El Nino

20. ABSTRACT (Continue on reverse side if necessary and identify by block number)

Horizontal and vertical thermal structures were examined in a region of the Northeastern Pacific Ocean off Northern California. The observations were acquired on three cruises as part of the ONR-sponsored Ocean Prediction Through Observation, Modeling and Analysis (OPTOMA) research program, centered in a region of the California Current System, ca. 37 to 39°N, 124 to 126°W, during June and July, 1983.

1

#20 - ABSTRACT - (CONTINUED)

The horizontal temperature correlation scale was between 30 and 50km, which was a significant factor when comparisons were made between measured horizontal thermal structures and those retrieved from Fleet Numerical Oceanography Center's (FNOC) analyses, which had grid spacing of 320km (TEOTS) and 40km (EOTS).

Operational (modeled) analysis fields were not in agreement with the observed fields. The major discrepancies occurred in the magnitude of the mixed layer depth and the shape of the horizontal temperature fields (maps).

The operational significance of differences between modeled and observed thermal structures was assessed in terms of their effect on low-frequency; i.e., less than 1Khz, acoustic propagation utilizing the FACT9H and PE Transmission Loss models.

Mixed layer depth differences produced significant disagreements between direct ranges computed from modeled and observed temperature profiles. The effect was most pronounced at higher frequencies and when both source and receiver were shallow; i.e., both at 20m.

A comparison was made between average depth/temperature profiles from July, 1982, July, 1983, and FNOC climatology to obtain a measure of the effect of interannual variability in the domain. This comparison showed that a significant temperature anomaly existed in the upper 400m in 1983 compared to 1982 due to El Nino and that this anomaly was not represented by the FNOC climatology.

The difference between modeled and measured thermal structures are believed to be related to thermal structure model resolution, model sensitivity to input data, short scales of spatial variability and non-representative climatology for the domain.

A Critical Analysis of Ocean Thermal Analysis Models
in
Cperation at FNOC

by

Brian J. Brady
Lieutenant Commander, Royal Navy
B.S., Salford University, 1971

Submitted in partial fulfillment of the
requirements for the degree of

MASTER OF SCIENCE IN OCEANOGRAPHY
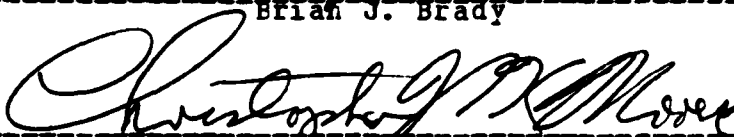
from the

NAVAL POSTGRADUATE SCHOOL
September 1984

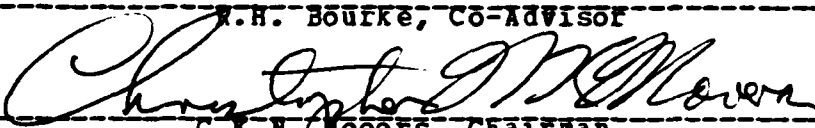Author: _____
Brian J. Brady

Approved by: _____
C.R.N. Mooers, Thesis Advisor

_____
R.H. Bourke, Co-Advisor

_____
C.R.N. Mooers, Chairman,
Department of Oceanography

_____
J.N. Dyer,
Dean of Science and Engineering

3

ABSTRACT

Horizontal and vertical thermal structures were examined in a region of the Northeastern Pacific Ocean off Northern California. The observations were acquired on three cruises as part of the ONR-sponsored Ocean Prediction Through Observation, Modeling and Analysis (OPTOMA) research program, centered in a region of the California Current System, ca. 37 to 39°N, 124 to 126°W, during June and July, 1983.

The horizontal temperature correlation scale was between 30 and 50km, which was a significant factor when comparisons were made between measured horizontal thermal structures and those retrieved from Fleet Numerical Oceanography Center's (FNOC) analyses, which had grid spacing of 320km (TEOTS) and 40km (EOTS).

Operational (modeled) analysis fields were not in agreement with the observed fields. The major discrepancies occurred in the magnitude of the mixed layer depth and the shape of the horizontal temperature fields (maps).

The operational significance of differences between modeled and observed thermal structures was assessed in terms of their effect on low-frequency; i.e.,less than 1Khz, acoustic propagation utilizing the FACT9H and PE Transmission Loss models.

Mixed layer depth differences produced significant disagreements between direct ranges computed from model and observed temperature profiles. The effect was most pronounced at higher frequencies and when both source and receiver were shallow; i.e., both at 20m.

A comparison was made between average depth/temperature profiles from July, 1982, July, 1983, and FNOC climatology

to obtain a measure of the effect of interannual variability
in the domain.   This comparison showed that a significant
temperature anomaly existed in the upper 400m in 1983
compared to 1982 due to El Nino and that this anomaly was
not represented by the PNOC climatology.

The differences between modeled and measured thermal
structures are believed to be related to thermal structure
model resolution,   model sensitivity to input data, short
scales of spatial variability and non-representative clima-
tology for the domain.

TABLE OF CONTENTS

LIST OF TABLES

LIST OF FIGURES

ACKNOWLEDGEMENT

I. INTRODUCTION

A. BACKGROUND AND OBJECTIVES

The dependence of acoustic propagation on the ocean thermal structure and the increased demand from the Navy for accurate acoustic forecasts to facilitate planning and economical use of resources has led to an increasing requirement for a reliable and accurate model to represent ocean thermal structure. Such a requirement is not easily met, however, because of the limited number of observations in the typical ocean thermal structure data base, approximately 150 XBT measurements per day in the northern hemisphere [Clancy et al., 1983]. In view of the upper ocean's spatial and temporal scales of variability such a small data base represents a significant handicap to the performance of any ocean analysis model.

The availability of an ocean thermal structure data base from a relatively densely sampled area of the Northeastern Pacific Ocean (approximately 200km west of point Arena, Northern California) made it possible to evaluate the accuracy of the output of two operational ocean thermal structure analysis systems.

The objectives of this research are firstly to obtain a description of the characteristics of the ocean thermal structure from a portion of the ocean (ca. 37°N to 39°N; 124°W to 126°W) sampled during the three cruises comprising OPTOMA5 which took place in June and July 1983. (OPTOMA - Ocean Prediction Through Observations, Modeling, and Analysis, is a joint Harvard/NPS project 'intended to acquire field data to characterise synoptic scale eddies over a domain in the California Current off Northern

15

California, and to 'set-up' an eddy-resolving, statistical/ dynamical, limited domain, open boundary numerical ocean prediction model.'The '5' indicates the fifth series of cruises of the project). Secondly, the analysed ocean thermal structure is to be used as a 'sea truth' by which to evaluate the accuracy of two real-time ocean thermal analysis systems presently in use at the Fleet Numerical Cceanography Center (FNOC), namely, the Expanded Ocean Thermal Structure (ECTS) analysis and the Thermodynamic Ocean Prediction System (TOPS)-Coupled EOTS (TEOTS) analysis. The final objective is to determine the operational significance of deviations in the modeled thermal structure from the 'sea truth' by utilizing the output from operational acoustic models to provide a quantitative measure of the effect of these thermal structure differences on acoustic propagation in the ocean. Two low-frequency, passive-acoustic models were used to provide a measure of the variability of acoustic energy propagation which could be expected from the acoustic models alone. These then, would provide a benchmark by which the variability due to differences between modeled and analysed thermal structures could be judged significant or not. The two acoustic models used were the FACT9H (Fast Asymptotic Ccherrent Transmission) transmission loss model and the AESD (Acoustic Enviromental Support Detachment) PE (Parabolic Equation) model [Brock,1978].

B. STUDY AREA AND ITS OCEANOGRAPHY

The area investigated is located in the California Current System (CCS), south of the Mendocino Escarpment. The region is approximately bounded by 37° to 39° N and 124° to 126°W. The bathymetry, Fig. 1.1 , shows the area to be offshore of the continental slope, with an average water depth of 4000m.
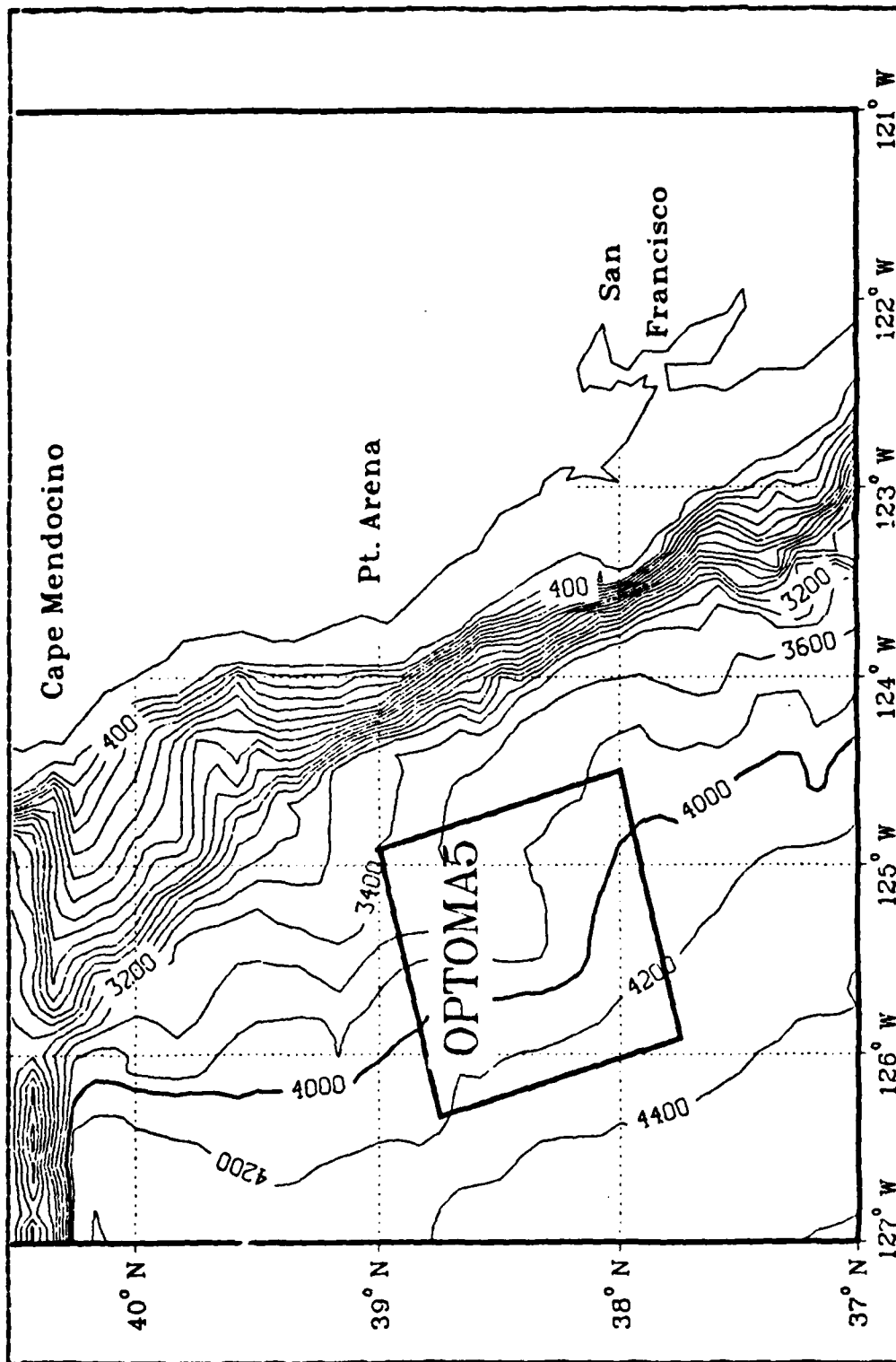
Figure 1.1   Bathymetry of Study Domain and Adjacent Area.

17

The CCS is composed of four currents: the California
Current, the Davidson Current, the California Undercurrent,
and the Southern California Current. Of these four currents
the southward flowing California Current is the major influ-
ence in the study domain. This current forms the eastern
boundary current of the large anticyclonic gyre centred near
the Hawiian Islands. As an extension of the Westwind Drift,
the California Current occurs between the North Pacific
atmospheric high pressure system and the semi-permanent
thermal low positioned over Central California. Contrary to
the classical picture of a broad, slow, shallow climatolo-
gical mean eastern boundary current, the CCS is known to
comprise mesoscale eddies, meandering jets and turbulent
filaments [Mooers and Robinson, 1984] together with their
associated complex horizontal and vertical thermal struc-
tures. The mean current is broad (approx. 1000km wide),
shallow (less than 500m deep) and sluggish moving (approx
0.9km/hr). The southward to southeastward winds, which
prevail during the spring to the fall months south of 40° N,
produce upwelling along the coast, extending 50 to 100km
offshore. Upwelling begins in February or March and
continues through August in the study domain. The cold,
usually high salinity water, brought into the surface layers
by this process, is then moved offshore by the smaller scale
perterbations in the CCS, further complicating the ocean
thermal structure. The most intense upwelling sites occur to
the south of capes and headlands [Reid et al.,1958] with the
most conspicuous centres of upwelling adjacent to the study
domain at 35° N and 41° N [Sverdrup et al., 1942 and Reid et
al., 1958].

Mean monthly upwelling velocities for the west coast of
North America(Fig 1.2; from Heath (1983)), based on Nelson's
(1977) wind stress curl data, clearly show upwelling to be
at its most intense in July off Northern California. Hence,

18

the maximum horizontal and, because of the differing water masses involved, vertical variations in thermal structure should be expected to occur in the study domain during the period under investigation.

In addition to the seasonal variations in thermal structure, inter-annual variability is also evident. Significant increases in temperature off Central and Northern California occurred during the winters of 1972, 1976, 1979 and 1983, corresponding to El Nino episodes [Breaker, 1983]. Of particular interest are the effects of the major El Nino warming of 1982-83. A brief analysis of the possible operational consequences of such an anomolous event is presented in Chapter V.
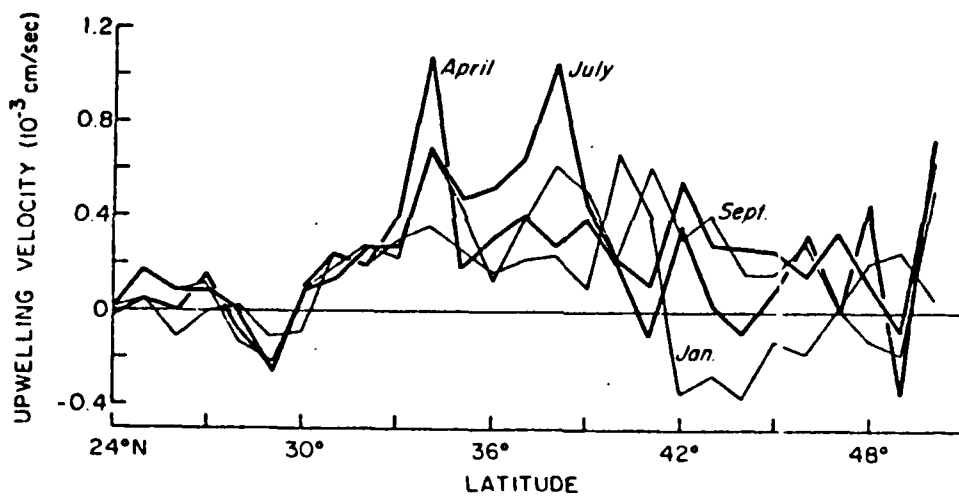
Figure 1.2   Mean Monthly Upwelling Indices.

II. DESCRIPTION OF COMPUTER MODELS

A. OCEAN ANALYSIS MODELS

1. Expanded Ocean Thermal Structure (EOTS) Analysis Model

The Expanded Ocean Thermal Structure (EOTS) analysis [Mendenhall et al., 1978] has been the US Navy's operational thermal analysis system for the past several years and provides ocean thermal structure input to most of the acoustic predictions generated at FNOC.

EOTS is run on a 63x63 grid for both hemispheric and regional coverage. The grid spacing for the hemispheric product is 200 to 400km, while that of the regional version is typically 40 to 80km. For the SOCAL region, in which the study domain resides, the spacings are 320km and 40km respectively.

The EOTS analysis system is based on a Fields-by-Information-Blending (FIB) methodology [Holl and Mendenhall, 1971; Holl, Cuming and Mendenhall, 1979] and is a numerical blending technique whereby the difference between a first guess field (in this case the previous analysis weighted towards climatology at a specied rate) and the assembly field, are eliminated in a weighted, least mean squares sense. The first guess field provides shape information for the horizontal blending procedure. The assembly field, into which all new observations are assembled, is obtained in a two-step process. First, the assembly field from the previous analysis is trended towards climatology in the same manner as the first guess field, and a weight field associated with it is decayed an arbitrary amount. Then, a weighted average of the assembly and first guess fields is

21

FIXED LEVELS

FLOATING LEVELS

The vertical grid on which the twenty-six EOTS parameters are defined. Columns labeled T, T', T" are temperature, first vertical temperature derivative, and second vertical temperature derivative, respectively. Parameters 9-26 are associated with fixed levels. Parameters 2-8 are associated with floating levels defined relative to parameter 1, Primary Layer Depth (PLD).

Figure 2.1   Analysis Levels for FNOC Analyses.

formed (using a low, specified weight for the first guess field) to provide a new assembly field. New observations are interpolated to the nearest analysis grid point using shape information from the first guess field. At each grid point, a weighted average of the interpolated observations and the assembly field is formed and a final assembly field determined. It is upon this final assembly field and the first guess field that the FIB analysis is performed. The procedure is designed to spread information from data-rich points to data-sparse points and produces a smoothed, horizontally and vertically blended field. During the blending, both first guess and assembly fields are weighted towards climatology, and, in the absence of inputs, they will revert to climatology over a period of approximately fifteen days [Pollack, personal communication].

The analysis is performed on twenty-six parameters at fixed and floating levels from the surface to 400m, Fig 2.1 . Parameter 1 is the Primary Layer Depth (PLD) which in general equates to the depth of the surface mixed layer. The remaining parameters are temperature at selected depths and vertical temperature gradients. Parameters 2 to 8 are analysed at floating levels defined relative to the PLD. Parameters 9 to 26 are associated with fixed levels. Below 400m the thermal field is constructed from climatological archives modified to blend smoothly with the analysed temperature profiles above.

Selection of the PLD (point 1) is accomplished by applying an algorithm to all BT observations made during a specified number of days (typically five) prior to the analysis time to identify PLD candidates (i.e., the depth(s) at which the criteria prescribed by the PLD algorithm are satisfied) from each profile. The algorithm assigns the PLD to the depth(s) (below the surface) of maximum rate of curvature in the vertical profile. Then a preliminary

23

three-cycle FIB is performed using the selected PLD
candidates as input, and the PLD and assembly fields from
the previous analysis, trended towards climatology, as the
first guess and initial assembly fields. Any recent BT's are
then examined and the PLD candidate from each that is
closest to the PLD produced by the preliminary FIB analysis
is selected and entered into a second three-cycle FIB
analysis. This produces the final analysed PLD.

2. TOPS-Coupled EOTS (TEOTS) Analysis

The TEOTS system is an attempt to incorporate
oceanic physics and air-sea interactive processes into the
analysis by coupling the ocean thermal analysis to the
atmospheric forcing via the physics of the TOPS mixed layer
model.

The TOPS mixed layer model is the Navy's vertical
ocean thermal structure forecast system. Given that the
ocean is primarily atmospherically forced, and that mixed
layer depths have proved 'highly predictable with a variety
of models', such as the Denman (1973) or Mellor and Durbin
(1975) models, TOPS was developed by NORDA (Naval Ocean
Research and Development Activity); it is based largely on
the use of rather well-defined atmospheric variables to
drive a model to describe the relatively data sparse oceans.
Surface wind, solar heat fluxes, and precipitation fields
are among those necessary to drive the TOPS/TEOTS models.
The surface fluxes are supplied by NOGAPS (Naval Operational
Global Atmospheric Prediction System) and the physics of the
model are based on the Mellor and Yamada (1974) level-2
turbulence model with the added effects of advection by
instantaneous wind drift and climatologically averaged geos-
trophic currents. The TOPS model produces a twenty-four
hour forecast for temperature fields at seventeen depths
from the surface to 500m on a horizontal grid spacing

24

identical to that used in the teots analysis to which j
coupled. The main purpose behind the TOPS/TEOTS approac
to de-couple the objective analysis component (EOTS) SS1
MLD fields from climatology, and to provide realistic]
boundary conditions for the atmospheric models.

TEOTS is coupled to TOPS in cyclical fas1
providing initial conditions for a 24hr TOPS forecast
is subsequently fed back into EOTS as a first guess 1
for the following day's analysis. With the exception o1
lock-step procedure described above and a diff(
prescription for certain parameters, the TEOTS ana1
system is the same as EOTS, relying on the FIB technigt
combine the various types of data. Clancy and Pollack ('
give a more rigorous description of both EOTS and TEOTS.

For the study domain EOTS was used for the reg:
(NOCAL) analysis and TEOTS for the hemispherical analys:

B. ACOUSTIC MODELS

1. The FACT9H Model

The FACT9H Transmission Loss Model is the
Interim Standard Transmission Model for ocean regions
may be treated with a single sound-speed profile and a
ocean bottom [Jacobs, 1982]. It is a ray-acoustics
designed for the computation of transmission loss as a
tion of range and frequency for a source and receiv
fixed depths. The classical ray treatment has been augm
with the addition of higher order asymptotic correctio
the vicinity of caustics, and the phase addition of ce
ray paths.

Wave theory for acoustic propagation states
there is a frequency below which no 'trapped' normal
may exist for a given channel or duct (waveguide) [Cc
et al., 1980]. The FACT9H model attempts to translate

25

condition to ray-acoustics by applying an algorithm [Clay, 1968] to characterize the gross features of ducted propagation. The intensity in the surface duct is found from the principle of conservation of energy modified by additional losses (proportional to range) caused by duct leakage and rough-surface scattering of energy from the duct [Marsh and Schulkin, 1967]. For both source and receiver within the surface duct the transmission loss (TL) as a function of range (R) is given by Eqn. 2.1

$$TL(R) = 22 + 10\log(R \cdot \theta) + b \cdot R \qquad (eqn\ 2.1)$$

where θ is the angle for the ray at the surface which just grazes the bottom of the duct and b contains the duct-leakage and rough-surface losses, Eqn. 2.2

$$b = 14.88 \times 10^5\ f^{-5/3}\ g^{-4/3}\ z^{-3} + W\ f^{1/2}\ z^{-1/2} \qquad (eqn\ 2.2)$$

In the above expression f is the frequency, g the magnitude of the below layer gradient, z the duct depth, and W is a factor determined by surface wave height.

The 9H is a model designator and reflects the stage of development of the model physics (FACT 10 is presently in operation at FNOC).

2. The PE Model

The PE Model replaces the reduced elliptic wave equation with a parabolic partial differential equation that can be integrated numerically using the Tappert-Hardin split-step Fourier Algorithm [Brock, 1978]. The parabolic wave equation includes diffraction and all other full-wave effects as well as range depedent environments. The entire range and depth dependent acoustic field is computed as the solution is marched forward in range. The model assumes a

26

flat pressure release ocean surface and a vanishing field at the depth of the finite Fourier transform (i.e., for bottom grazing angles greater than the maximum permissible 33°, the acoustic energy is smoothly attenuated to zero and back reflection of acoustic energy into the water column is avoided). For grazing angles less than the maximum, a pseudo radiation condition is introduced at the water-bottom interface by smoothly attenuating the field. Since the error in the parabolic approximation increases as angles increase from the horizontal, steep bottom slopes can cause inaccuracies. The model is primarily considered useful for predicting low-frequency acoustic propagation of energy along waterborne or shallow-angle, bottom-bounce paths in deep water.

III. DATA BASE

A. DATA ACQUISITION

The XBT and CTD data from the surface to 500m acquired from the OPTOMA5 cruises formed the primary source of field data. OPTOMA5 consisted of three separate cruises undertaken between 15 June and 19 July, 1983 by R/V ACANIA. The three cruises, designated AI, AII and AIII each sampled approximately the same area of the CCS, Fig. 3.1

A secondary source of field data was provided by deep CTD casts from the cruise undertaken by the R/V DE STEIGUER between 10 and 21 June, 1983. A section of this cruise sampled the OPTOMA5 area and provided CTD data to 3000m. Satellite imagery was also used, when available, to provide a qualitative measure of the sea surface temperature distribution.

Temperature profiles, to be compared later with the field data, were retrieved from the archives of FNOC for the same area and period. Both EOTS and TEOTS depth/temperature profiles for the beginning and end of each OPTOMA5 cruise were obtained for selected positions, Fig. 3.2 .

Details of the data base are given in Table I .

B. DESCRIPTION OF DATA AND DATA PROCESSING

1. ACANIA Data

The positions of the XBT/CTD casts for the Acania cruises are documented, Figs. 3.3 to 3.5. All XBT/CTD data were edited thus eliminating any obviously erroneous profiles. A secondary visual inspection of each profile was undertaken with the result that a final data base for each cruise was obtained, Table I

28
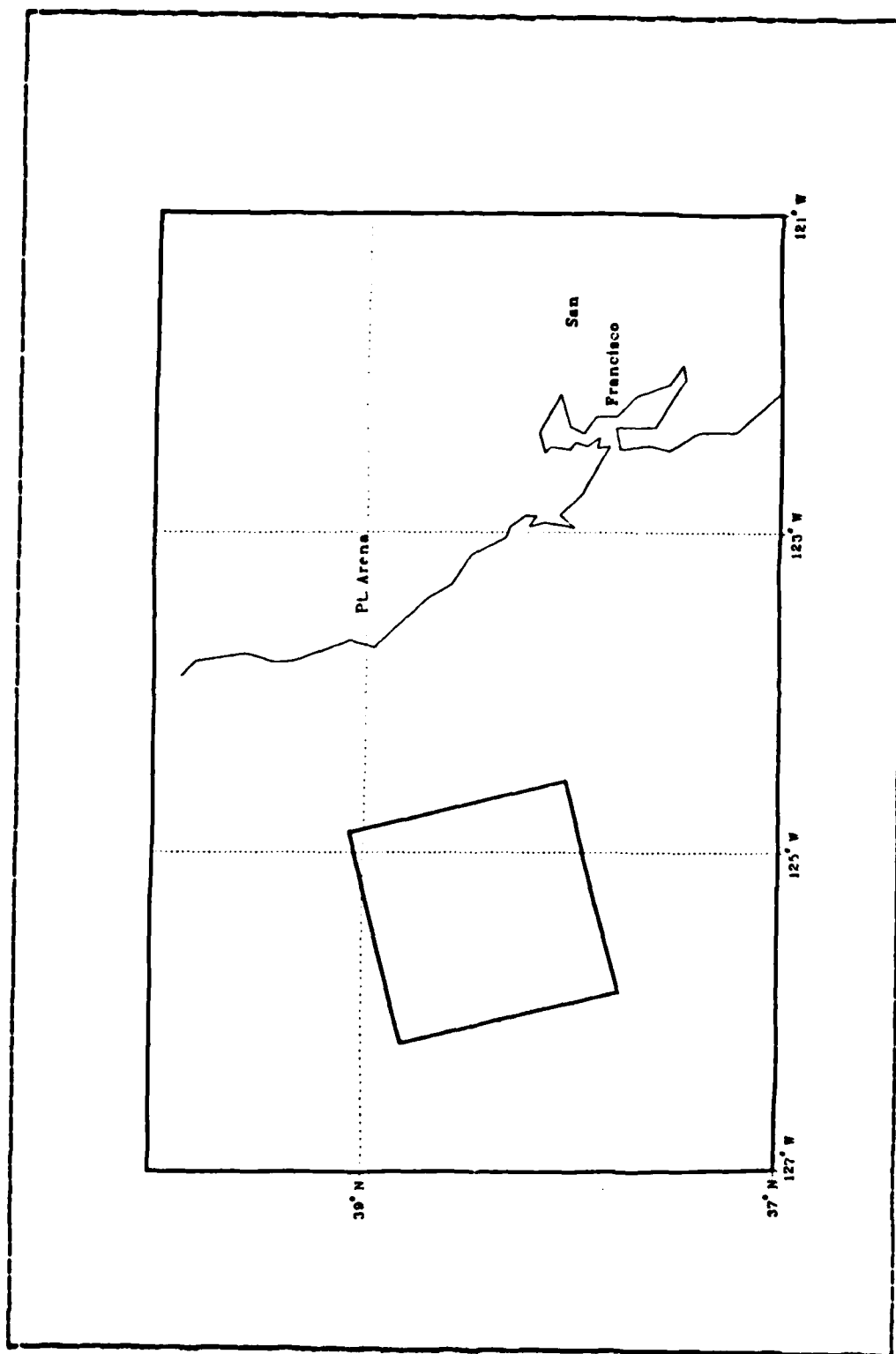
Figure 3.1   OPTOMA5 Study Domain.

29
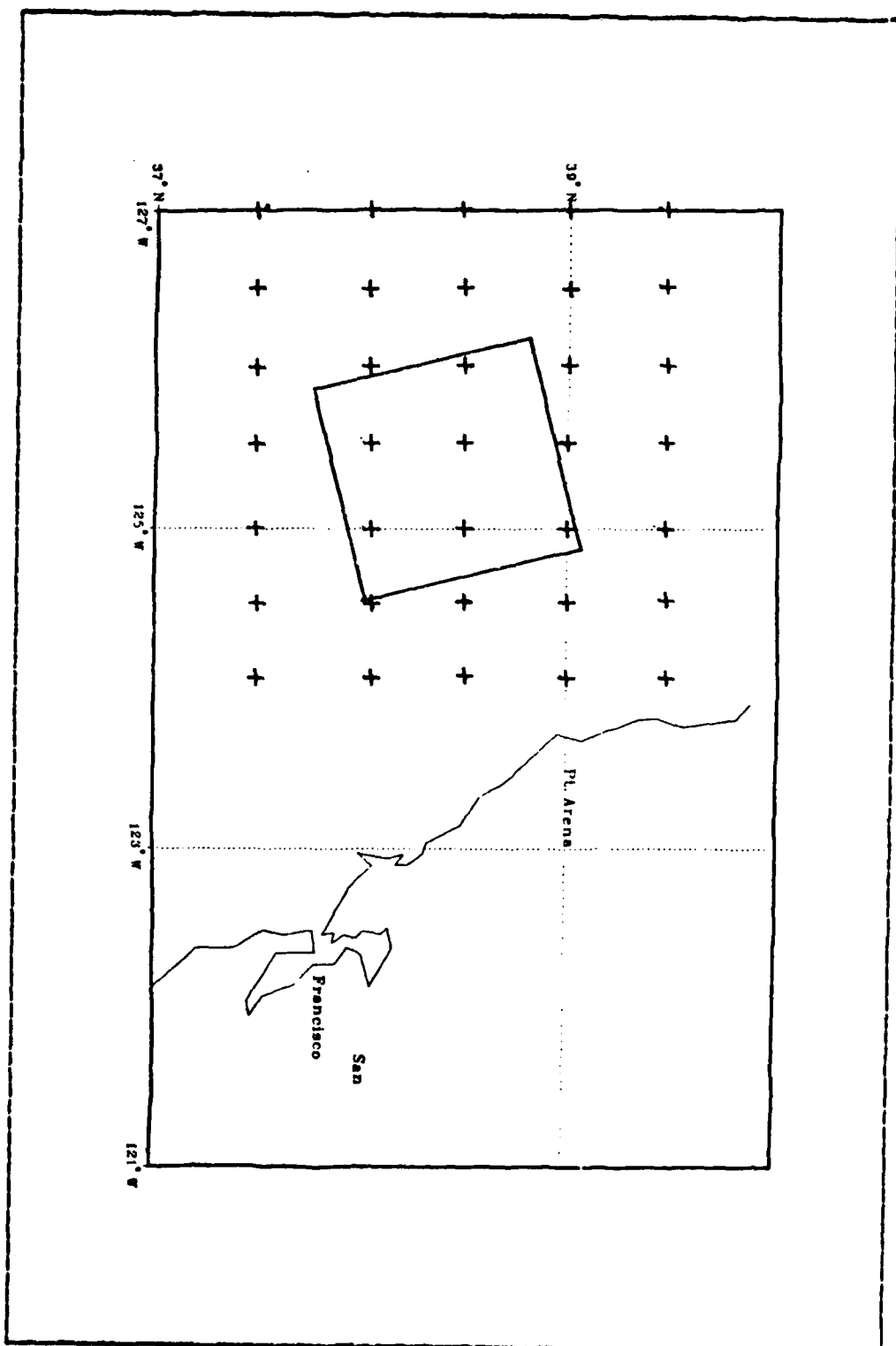
Figure 3.2   Locations of FNOC Depth/Temperature Profiles.
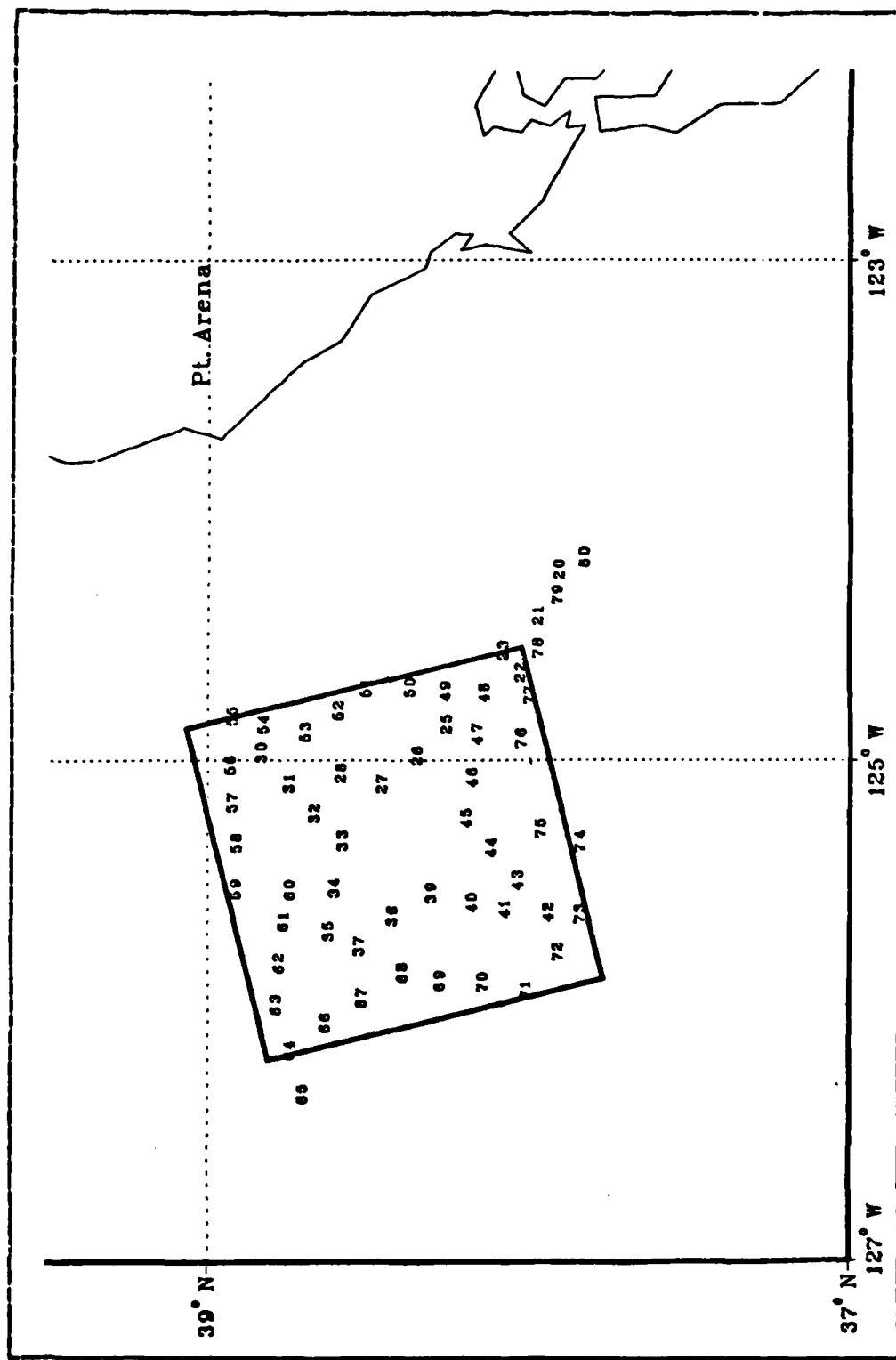
Figure 3.3   XBT Station Locations—Cruise AI.

31
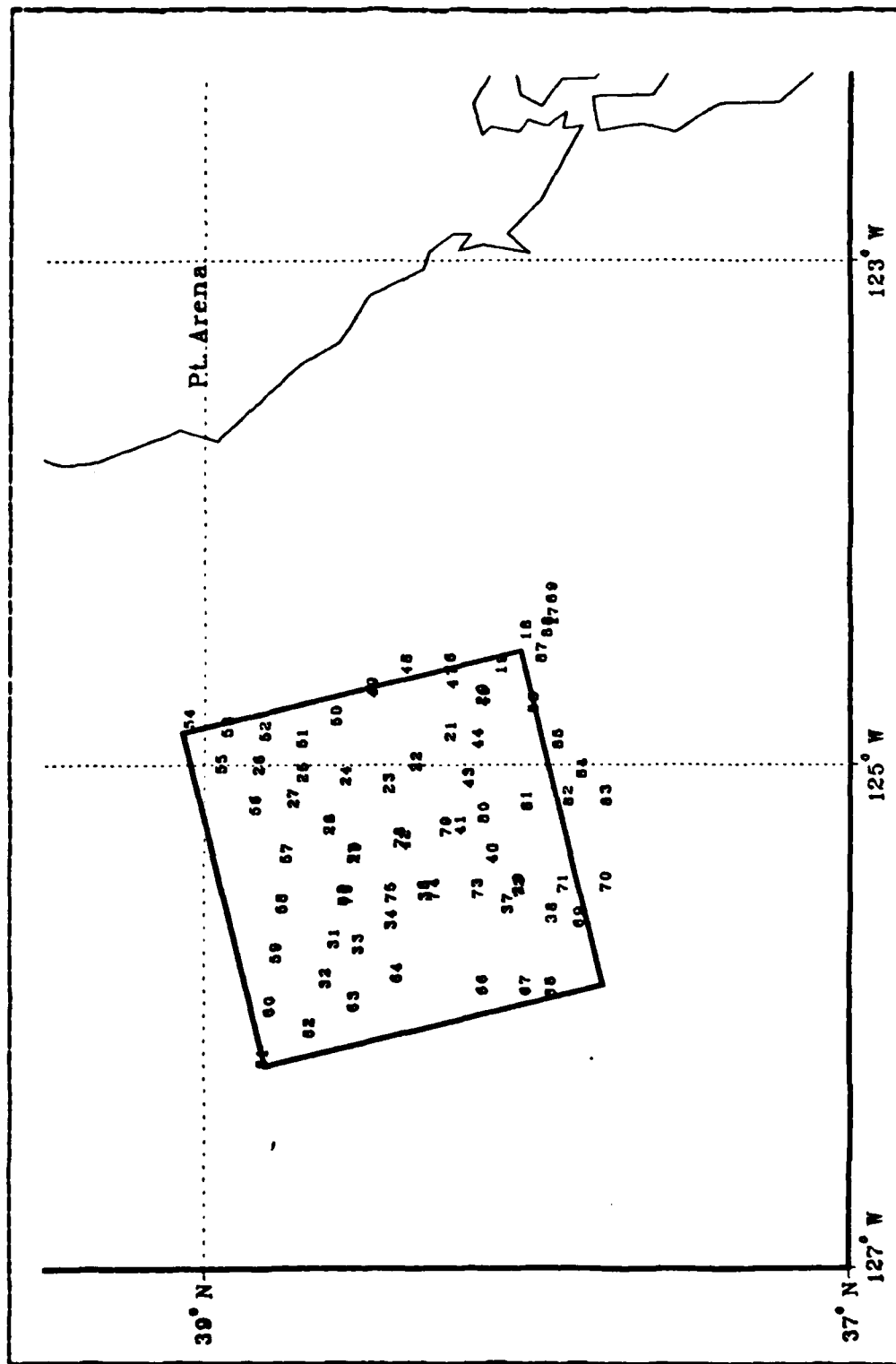
Figure 3.4   XBT Station Locations-Cruise AII.

32
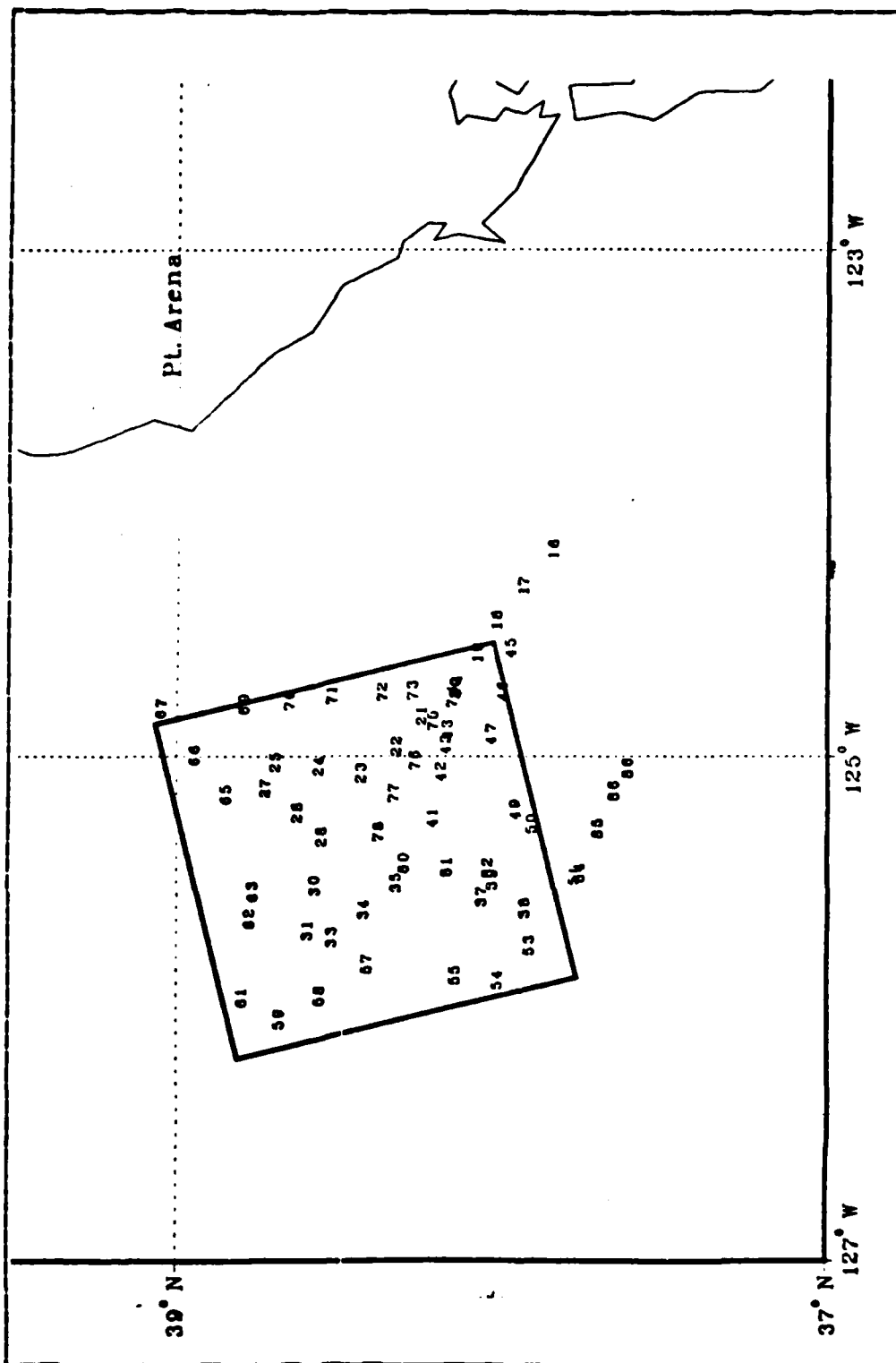
Figure 3.5   XBT Station Locations—Cruise AIII.

33

TABLE I
Details of Data Base

SOURCE	PERIOD	NO. OF ACCEPTABLE PROFILES	RANGE OF PROFILES
OPTOMA AI	6/15-6/22	74	0-500m
OPTOMA AII	6/29-7/4	89	0-500m
OPTOMA AIII	7/13-7/19	86	0-500m
DE STEIGUER	6/10-6/21	8	0-3000m
EOTS/IEOTS	6/16,6/23, 6/30,7/7, 7/10,7/21	42	0-400m

The XBT's were then interpolated in the vertical to standard 5m depths from the surface to 500m. The loss of temperature microstructure resulting from this interpolation was assumed unimportant in view of the goals of this study. These edited, 'smoothed' depth/temperature profiles formed the field data upon which the later analysis was to be based.

Information from each cruise was assumed 'quasi-synoptic' (i.e. the region was believed to have varied somewhat over the period of sampling). This assumption is weakest in the near surface layers where the time scale of variability can be of the order of a day or less. The validity of this assumption in the context of the present study is addressed in Chapter V.

2. DE STEIGUER Data

The DE STEIGUER sampling provided CTD casts from the surface to a maximum depth of 3000m. These profiles were

also interpolated vertically to 5m depth intervals and, based on the assumption that the water column was near stationary below the thermocline (approximately 500m), they were used to extend the ACANIA and FNOC profiles to a depth of 3000m. These profiles were then extrapolated linearly to the ocean bottom (assumed flat at 4000m).

An average salinity/depth profile was calculated from the 'in-area' DE STEIGUER CTD casts and this average profile was assumed as the standard salinity profile for all sound speed calculations.

3. Satellite Imagery

Advanced Very High-Resolution Radiometer (AVHRR) infrared images from the NOAA-7 satellite were used to qual- itatively show the more obvious features of the SST field. These images were obtained on an 'as available' basis during each of the ACANIA cruises. Details of the major features shown in these images were sketched, Figs. 3.6 to 3.8 The satellite images were also used to qualitively assess the assumption of quasi-synopticity.

4. FNOC Archived Data

Temperature profiles for the standard positions, Fig. 3.2 , were extracted from the archives of FNOC. These profiles were used for both EOTS and TEOTS analyses on the dates closest to the commencement and termination of each ACANIA cruise.
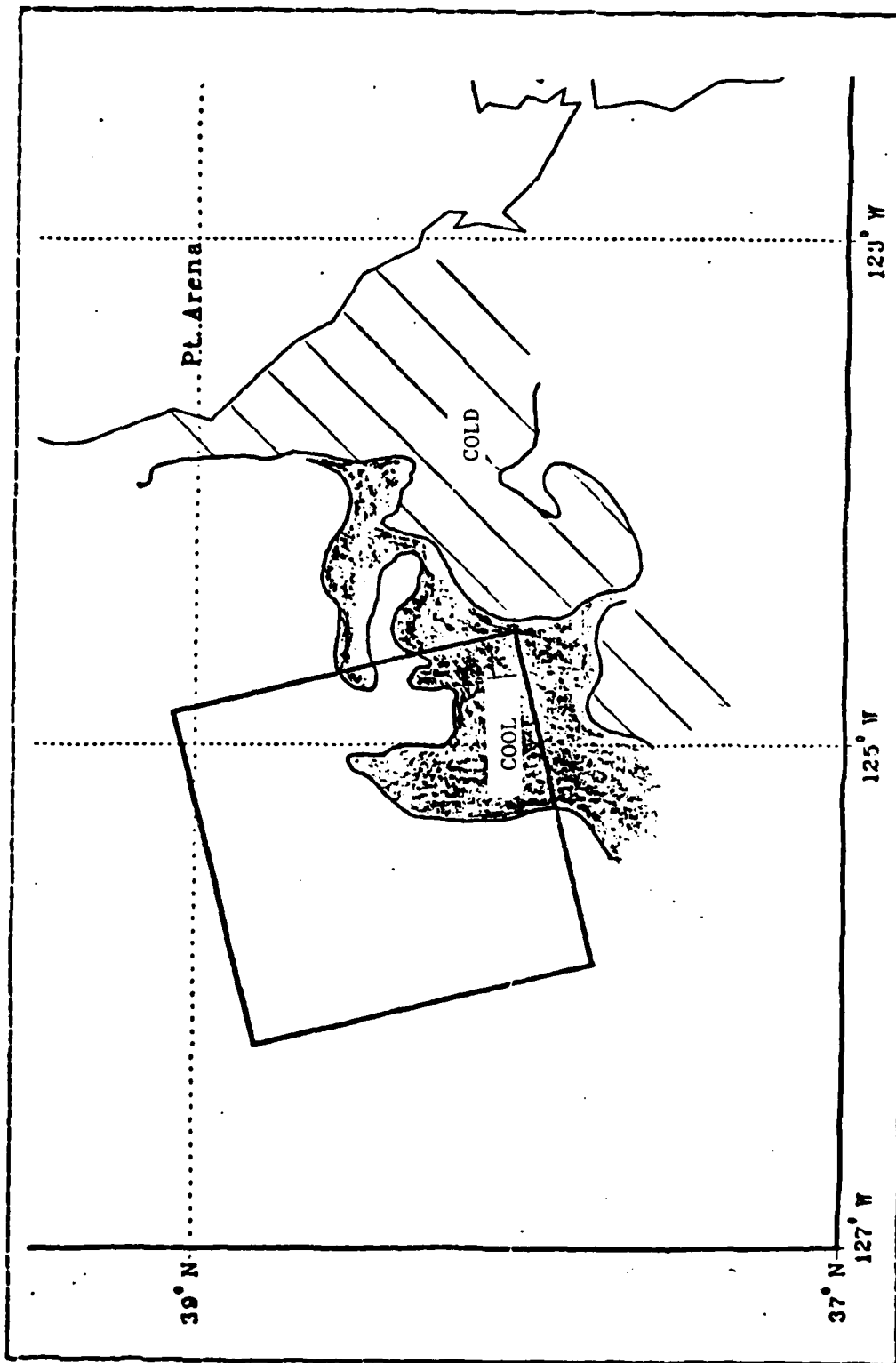
Figure 3.6   Satellite Observed SST Features-Cruise AI.
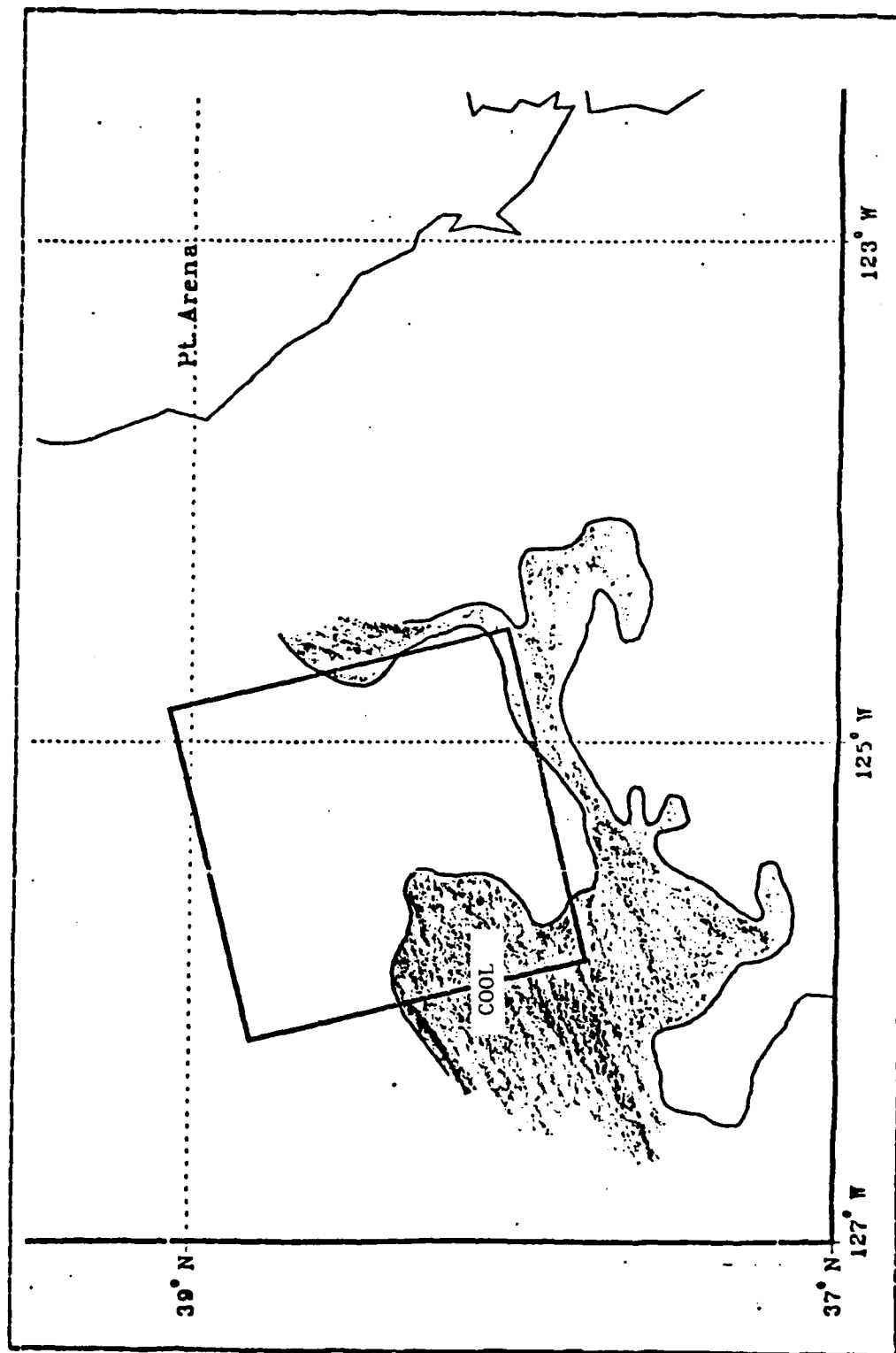
Figure 3.7   Satellite Observed SST Features-Cruise AII.

39° N

37° N

127° W

125° W

123° W

Pt.Arena

COOL
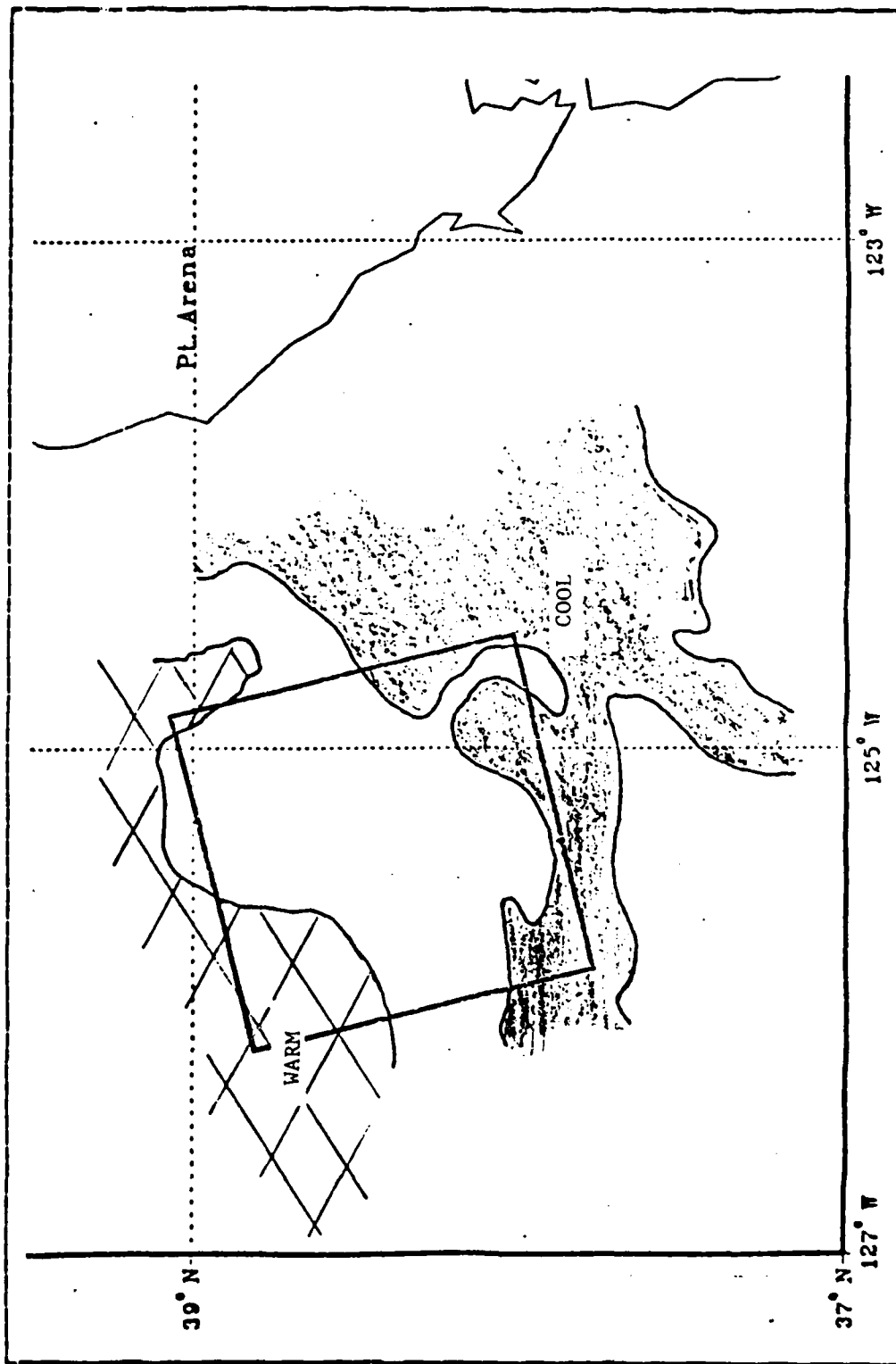
Figure 3.8   Satellite Observed SST Features-Cruise AIII.

38

IV. DATA ANALYSIS

A. DATA PROCESSING

To facilitate comparison with FNOC's data fields,
study domain was divided into a 7x7, square grid w:
grid-spacing of 20km and the irregularly spaced XB'
profiles interpolated onto this grid.

The horizontal correlation of the temperature fie:
various depth intervals in the top 150m of the water co
were evaluated. The correlation at various levels disp:
similar chracteristics showing zero crossings occurri:
approximately 80km with a 0.5 correlation at approxim:
30km (approximately the e-folding distance between
origin and the zero crossing distance). It was, there:
reasonable to assume that the temperature variation:
points within 30 km of a given position within the d
were related (i.e. all points within 30km could be exp:
to influence a given point). As an example, the SST l
zontal correlations for each cruise are presented, Figs.
to 4.3 . The correlation information thus derived was
when interpolating the field data onto the grid.
observations within 30km of each grid point were use:
each observation value was weighted according to the in'
of its distance from the grid point. The interpolated
thus formed were then automatically contoured at FNOC {
erature levels, Fig. 2.1 The mixed layer depth (MLD) ca
lated from the field data was equated to the PLD in the
analyses (point 1 Fig. 2.1) and was defined as the :
lowest depth below which a negative temperature gradien{
found with a magnitude greater than $3^{\circ}C$ /100m over
consecutive 5m depth intervals. The algorithm use:

calculate the MLD was designed to yeild the true MLD even in the presence of strong, near-surface negative temperature gradients caused by diurnal heating the "afternoon effect" which seldom exceeded 7m in depth. MLD's calculated by this method agreed well with manually determined MLD's for the sampled profiles. FNOC EOTS and TEOTS profiles were also interpolated and contoured in a similar manner and on the same grid. The MLC computed for the model profiles using the algorithm described above was in agreement with the PLD.

By contouring the fields in the manner described, it was possible to extract a depth/temperature profile from the surface to 4000m for any position within the study domain.

Throughout the study domain, temperature variations at 400m were small enough (<0.5°C) for all profiles (including those provided by FNOC) to be smoothly blended between shallow and deep profiles above the depth of the deep sound channel axis (ca. 500m).

The feasibility of using discrete depth/temperature levels, with depth separations dictated by the EOTS analysis levels, to represent the vertical temperature structure of the area was tested by examining the vertical pattern correlation between temperatures in the near surface layers (the zone of maximum variation of temperature with depth), Figs. 4.4 to 4.6 . These pattern correlations are similar for each cruise and have zero crossings at depths of the order of 300m when the SST is correlated with deeper levels. Such a pattern correlation gives an good indication of the probability that variations in temperature at one depth are related to variations in temperature at another depth. At the e-folding depth (approximately 100m), the correlation is approximately 0.7. It was therefore considered reasonable to represent the vertical temperature structure at the discrete levels dictated by the EOTS analysis. The EOTS depth interval between temperature levels in the near surface

40
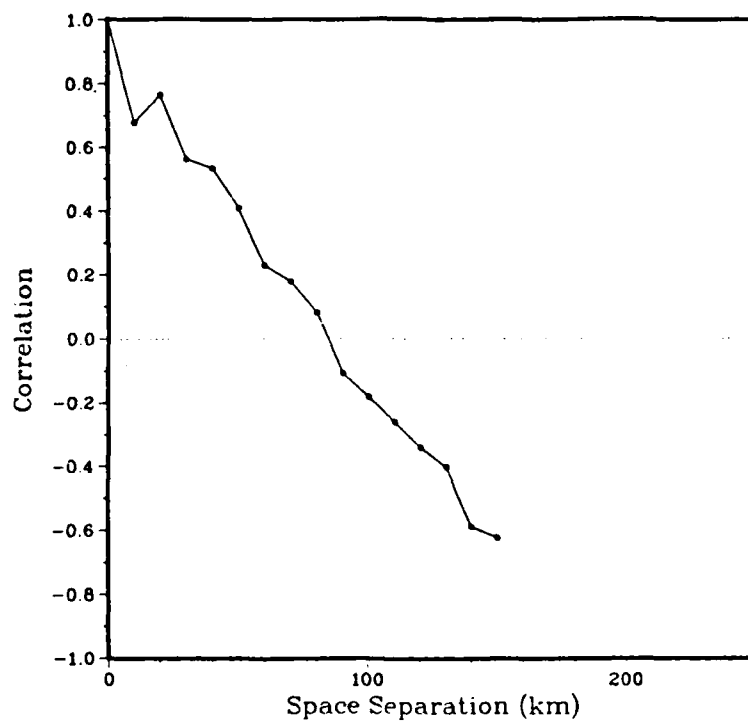
Figure 4.1   SST Horizontal Correlation-Cruise AI.

41
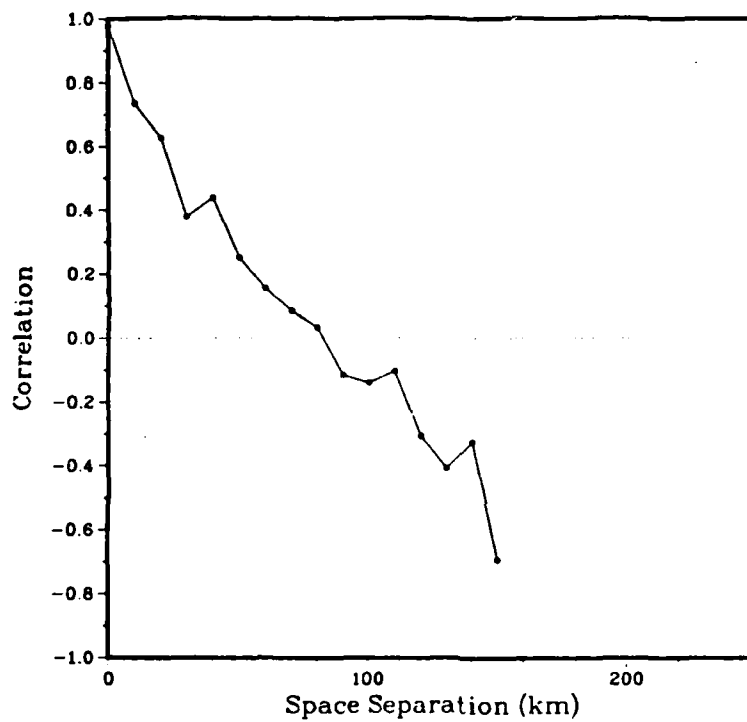
Figure 4.2   SST Horizontal Correlation-Cruise AII.
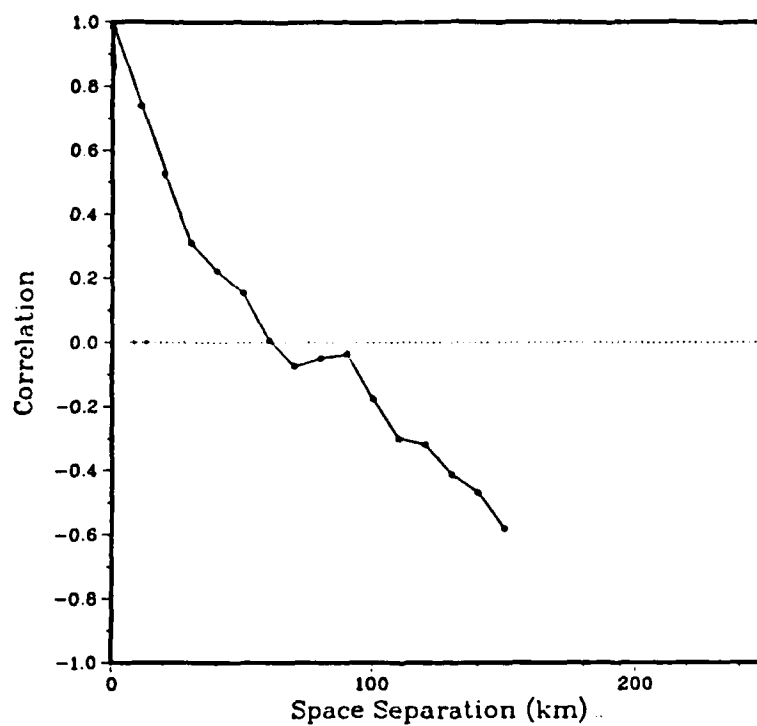
Figure 4.3   SST Horizontal Correlation-Cruise AIII.

43

layer is of the order of 50m which yields a pattern correlation coefficient ranging from 0.6 for cruise AII to 0.8 for cruises AI and AIII. Below the mixed layer (approximately 50m) the correlation improves to 0.8 or better between adjacent contoured levels.

The smoothing effect of deriving profiles as described above (i.e. the higher frequency fluctuations of temperature with depth are removed) was not considered important, because the profiles thus derived were later to be used as inputs to low frequency (<1000Hz) acoustic models and the essential shape of the profile was maintained. Additionally, ray theory is only valid if sound velocity does not change much in a wavelength, therefore, the inclusion of the higher wavenumber fluctuations of temperature (and, therefore, sound speed) with depth could invalidate the use of this theory [Urick, 1983].

Four features of the vertical temperature profile were selected as being of primary importance in describing the thermal structure for low frequency passive acoustic applications. These were: sea surface temperature (SST), mixed layer depth (MLD) (previously defined), the below layer gradient (BLG) (defined as the temperature gradient in the 25m immediately below the MLD) and the thermocline gradient (THG) (Defined as the temperature gradient between the MLD and the deep sound channel axis depth). The contour fields derived for each of these parameters, Figs. 4.7 to 4.10 , are described in detail in Section B of this chapter.

B. DESCRIPTION OF AREA THERMAL STRUCTURE

The following is a brief description of the thermal structures measured in the study domain during the three OPTOMA5 cruises. The desciption in limited to the four parameters defined in section A above.
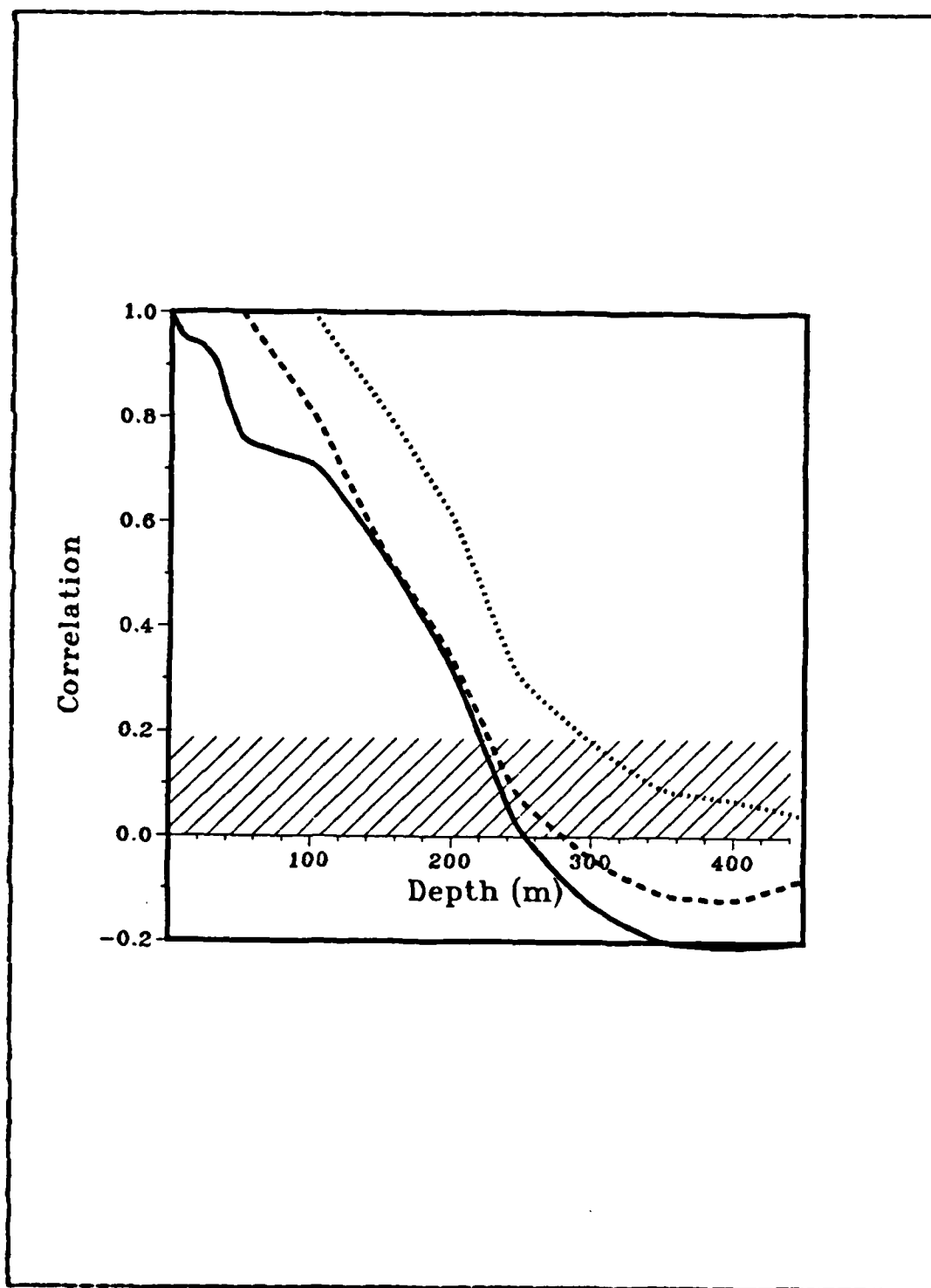
Figure 4.4   Pattern Correlation-Cruise AI.

45
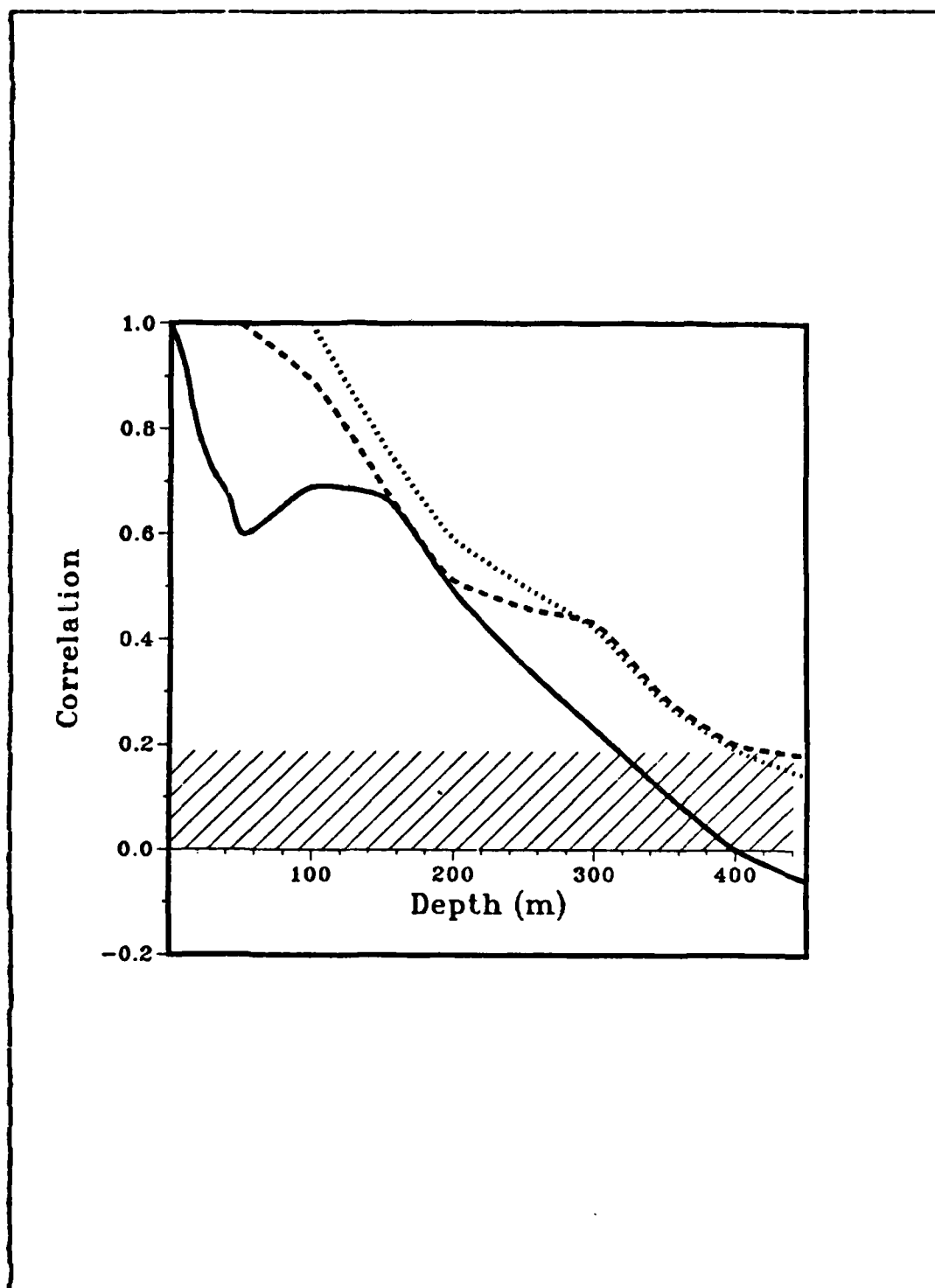
Figure 4.5   Pattern Correlation-Cruise AII.

46
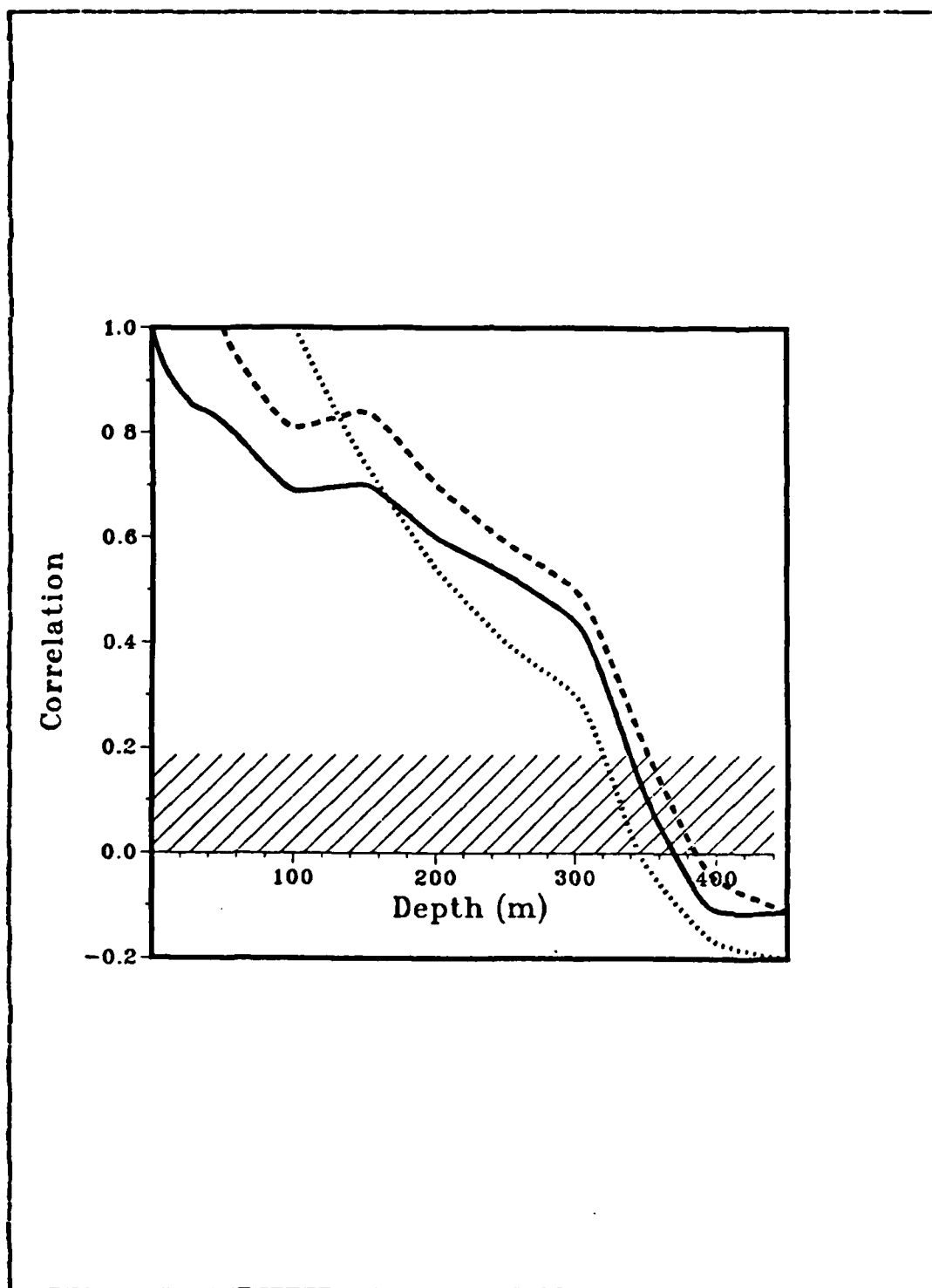
Figure 4.6   Pattern Correlation-Cruise AIII.

47
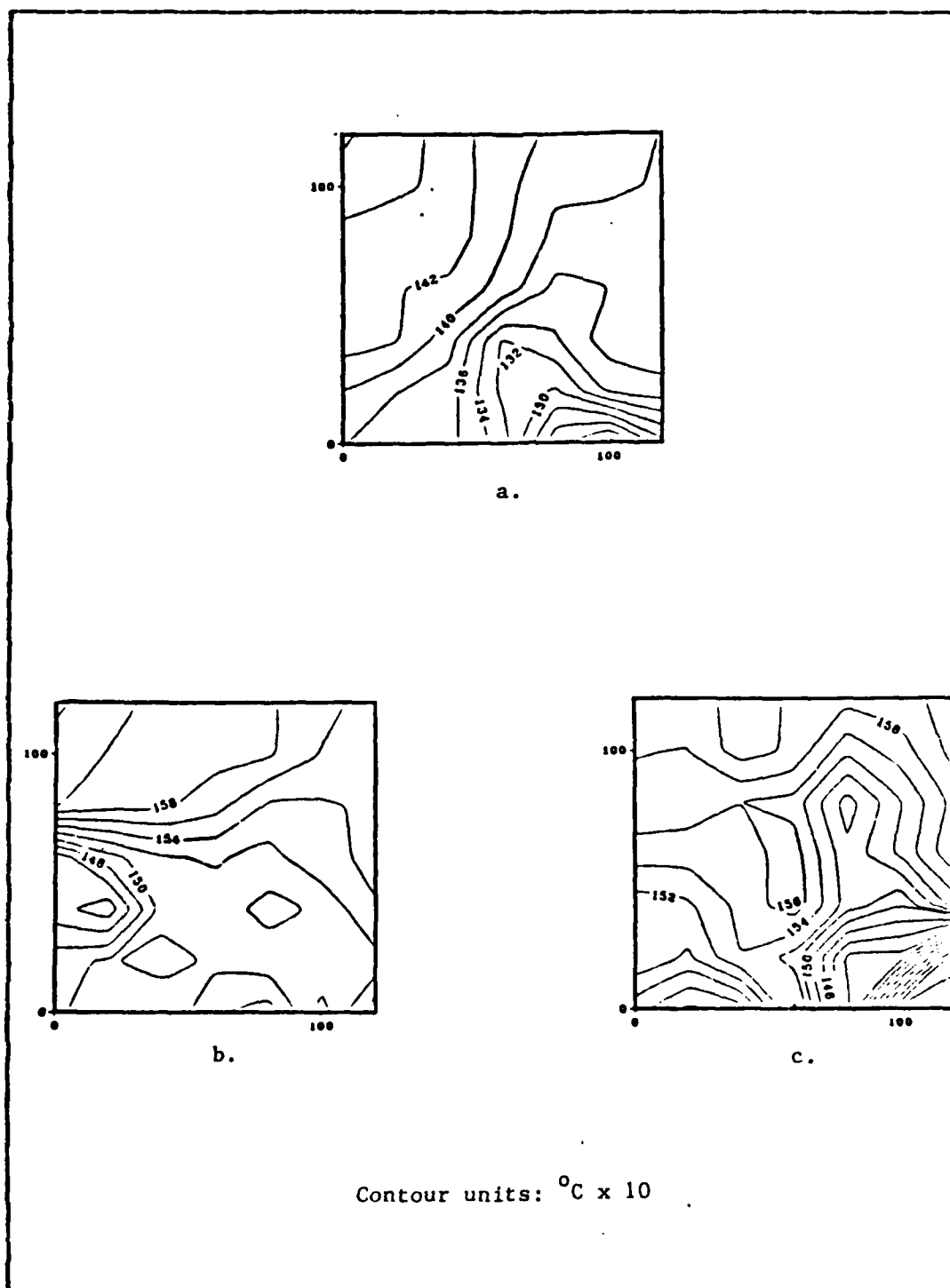
Contour units: $^{o}C \times 10$

Figure 4.7   SST Contours
a. Cruise AI   b. Cruise AII   c. Cruise AIII.

48

a.

b.   c.
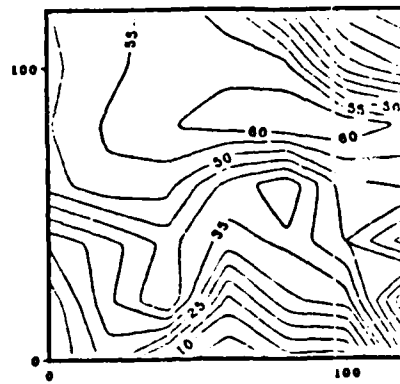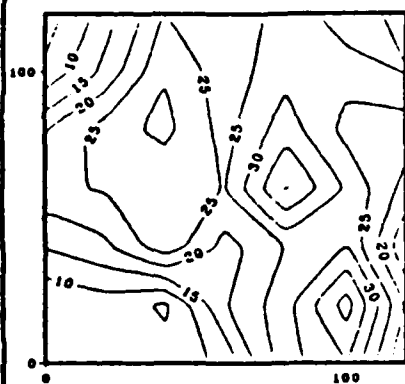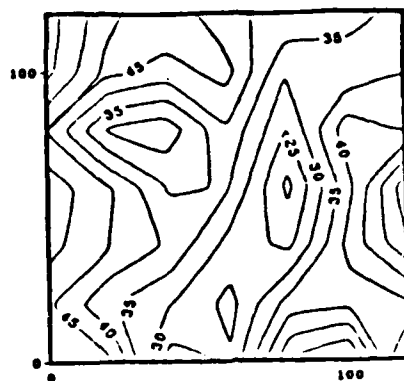
Contour units: metres

Figure 4.8   MLD Contours
a. Cruise AI   b. Cruise AII   c. Cruise AIII.

49

Contour units: ^{o}C/1000m
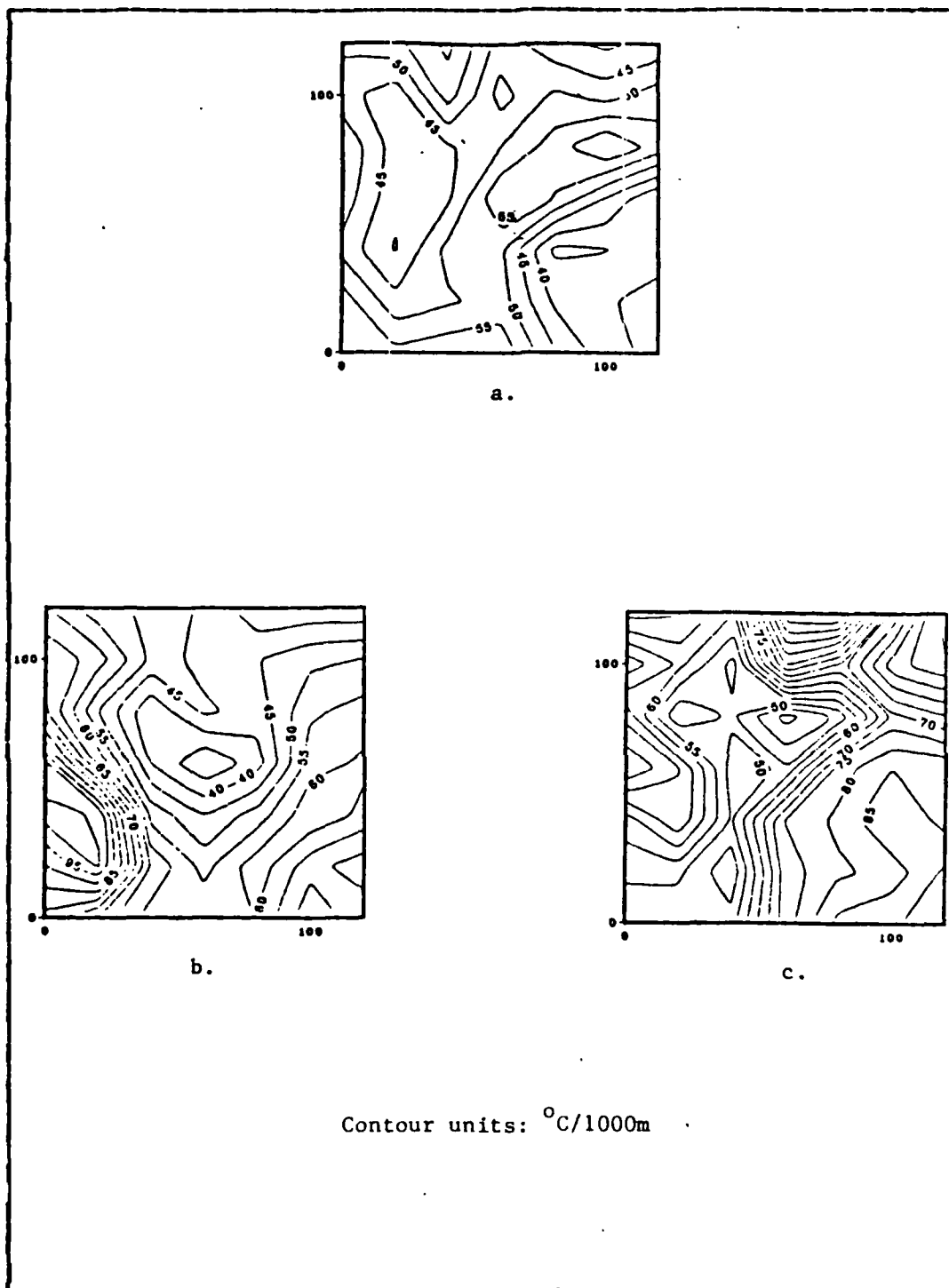
Figure 4.9   BLG Contours
a. Cruise AI   b. Cruise AII   c. Cruise AIII.

50

Contour units: °C/1000m
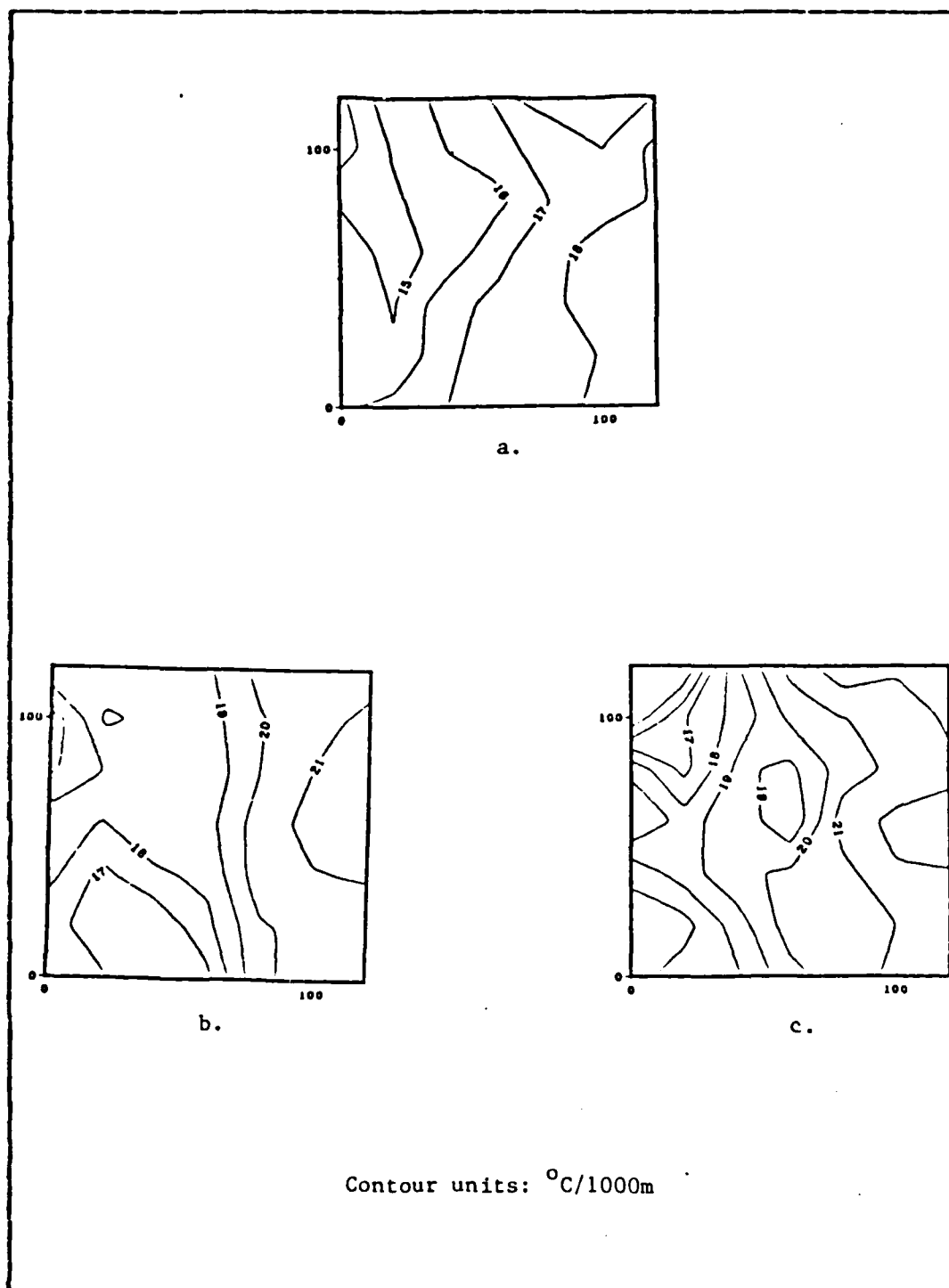
Figure 4.10   THG Contours
a. Cruise AI   b. Cruise AII   c. Cruise AIII.

51

The significant weather for each cruise (i.e. wind speed and cloud cover) were obtained from R/V ACANIA's hourly log. The wind was from a generally southeastward throughout all three cruises, and, for the most part, wind speeds were between 15 and 20 knots. The major excursions from this norm were (a) at the beginning of cruise AI when wind speeds were greater than 30 knots on the first and second days (16 and 17 Jun), (b) during the latter part of cruise AI and early in cruise AII when winds of 10 to 15 knots were recorded and (c) during the first two days of cruise AIII when wind speeds again increased to 30 knots or more. Throughout the three cruises, partly cloudy to clear skies prevailed, with predominantly less than 4 oktas of cloud cover. Pressure remained nearly steady at approximately 1030 mb.

1. **Cruise AI (15 Jun-22 Jun, 1983)**

SST's ranged from 14.6°C in the northwest of the domain to 12.2°C associated with a cool feature protruding into the southeast, Fig. 4.7 (a). The effect of the cool intrusion was to intensify the horizontal temperature gradient in its vicinity and to, locally, distort the otherwise nearly meridional SST structure. The maximum temperature gradient intensification occurred on the northern flank of the cool feature, where a gradient of 7.0°C/100m was observed. The position of the cooler water agreed well with the position obtained from satellite imagery, Fig 3.6.

The depth of the mixed layer, Fig. 4.8 (a) , varied from 20 to 55m in a complex manner throughout the area with the shallowest depths in a 50km-wide swath southeast to northwest across the centre of the area. No discernable correlation was observed between the SST and MLD patterns.

Below layer gradients ranged from 3.5°C/100m in the sector affected by the cold feature in the southeast to 5.0°C/100m in an area apparently associated with the

52

shallower MLD's, Fig 4.9 (a). Thermocline gradients var
in a near meridional manner with the weaker gradients in
west. The magnitude of the gradient varied from 1.5°C/1
to 1.8°C/100m, Fig 4.10 (a).

2. **Cruise AII (29 Jun-4 Jul, 1983)**

A general warming trend was apparent between the
of cruise AI and the beginning of cruise AII with SS
generally 2.0°C warmer throughout the domain. There was a
a distinct change in the SST pattern, Fig 4.7 (b). The c
feature initially observed in the southeast sector
relaxed southwards and a second cool feature was observed
extend northward into the southwest of the domain.
warmest water remained in the far northwest sector, wit
near meridional structure throughout the remainder of
area. Temperatures ranged from 14.4°C to 16.2°C. The warm
trend was to be expected for the period involv
Climatology [Podeszoa, 1976] shows the SST increasing f
14.1°C in June to 16.5°C in July. The mainly light to fr
winds and clear skies prevailing through the latter part
AI and early days of AII could be expected to produce
warming trend noted. Satellite imagery once more agr
well, qualititavely, with the position of the major surf
features shown by the analysis, Fig 3.7.

Associated with the warming trend and genera
lighter winds, the MLD shoaled over the period between
and AII. Layer depths, some 20m shallower than than th
observed during AI, were measured with depths varying f
near surface in the northwest to 40m in the southeast
with a complex structure throughout the area.

The strengthening of the BLG, Fig 4.9 (b) compa
to those observed during cruise AI indicated that
warming trend had been limited to the upper layers of
ocean and was, therefore, probably atmospherically driv

Magnitudes ranged from 10.0°C/100m in the west in association with the lower SST's to 3.5°C/100m in the centre of the domain, loosely associated with the deeper MLD's. An increase in THG's to between 1.7°C/100m and 2.1°C/100m with a generally similar pattern to that of cruise AI, emphasized the supposition that the warming had been limited to the upper layers of the ocean.

3. Cruise AIII (13 Jul-19 Jul, 1983)

The SST analysis, Fig. 4.7 (c) showed the presence of cool water along the southern edge of the domain with the cool feature in the southwest during cruise AII, having relaxed southward and a further intrusion of cool water extending northward into the area from the southeast. Satellite imagery agreed well with the position of these features, Fig. 3.8 . However, coverage was too intermittent to allow the feature in the southeast to be positively related to the cool feature measured in a similar position during cruise AI. Temperatures ranged from 12.4 to 16.0°C with the warmest water remaining as an almost stationary feature in the far northwest of the domain. A relatively intense horizontal temperature gradient of 10.0°C/100m was measured in a 30km-wide band around the cool feature in the southeast.

MLD's, Fig. 4.8 (c) were, on average, deeper than those measured during cruise AII, indicative of the higher winds prevailing during the early part of the cruise producing significant mixing in the surface layers. However, shoaling of the MLD, in both the north and south of the area, to 10m or less would tend to indicate that the wind mixing was restricted to the area being sampled by ACANIA during that period. The general horizontal structure of the MLD remained complex.

54

The magnitude of neither the BLG nor the THG changed much from those measured during cruise AII. However, the distribution of the maximum and minimum BLG was significantly different from that of AII, although there was a weak increase in BLG in association with the cool feature in the southeast of the domain.

V. COMPARISON OF OBSERVED AND MODELED TEMPERATURE STRUCTURE

For each of the parameters discussed in the Chapter IV, namely, SST, MLD, BLG and THG, a difference field was produced by subtracting the magnitude of the parameter derived from the model analysis from that derived from the OPTOMA5 data. The procedure was carried out for each model analysis at each of the 49 grid points in the domain. The difference fields thus calculated were contoured, Figs. 5.1 to 5.24.

Statistics were calculated from the contoured difference fields by examining the percentage of the total domain enclosed by discrete contour intervals in each difference field, and for each parameter. The 'bin-size' for each field was established by examining the individual plots and subjectively selecting an appropriate difference interval such that each bin would represent between 10 and 20% of the dynamic range of the variable, whilst keeping the area covered by each bin large enough to make measurement practical. The bin-sizes selected were:

$$SST - 0.4^\circ C$$
$$MLD - 10.0 m$$
$$BLG - 1.0^\circ C/100m$$
$$THG - 0.1^\circ C/100m$$

The areas within each bin were measured using a Planimeter. Figs. 5.25 to 5.48 show the histograms of the distributions obtained by the above method and Tables II to IV list the relevant statistics for each histogram.

A negative value in the difference calculations implies that the model analysis was overestimating that particular parameter (i.e., Difference = Sea truth - Model value).

56

Because of a corruption in the data supplied by FNOC it was not possible to derive contour fields of the model analyses for the termination of cruise AIII.

The larger grid spacing used in the TEOTS, hemispherical analyses (ca. 320km) meant that TEOTS comparisons were, necessarily, general in nature and should be viewed in terms of average values , since it is unlikely that such a large grid spacing will allow the analysis to retrieve the mesoscale variability present in the area (horizontal variability on a scale of the order of tens of kilometers).

The following sections discuss the statistics obtained and qualitatively estimate the effectiveness of the model analysis in representing the sea-truth. A summary of the model performances is given in Section A.6 of this chapter. Throughout the Chapter, sea truth refers to OPTOMA5 derived data.

A. CCMPARISONS

1. Cruise AI

The analysis dates for cruise AI were 16 June, 1983 (initial) and 23 June, 1983 (final). FNOC data files showed inputs into the the analyses for the study domain of three BT's for the initial, and twenty-three BT's (from R/V ACANIA) for the final analyses. The statistics for the difference fields derived for this cruise are given in Table II and the histograms from which these statistics were derived are shown in Figs. 5.25 to 5.32

a. EOTS Analysis

The initial SST analysis, Fig. 5.1 (b) showed a nearly meridional structure with the warmest water in the west of the domain and a weakly strengthening horizontal temperature gradient in the east. The difference field, Fig.

57

5.1 (c) showed the analysis to be overestimating the meas-
ured SST for the majority of the area. The mean difference
was -0.8°C and the maximum difference was -2.0°C associated
with the intrusion of cool water into the southeastern
sector, Fig. 5.1 (a). The final analysis, Fig. 5.1 (d)
showed a general movement of the analysis field towards the
sea truth in both shape and magnitude. The shape field was
only marginaly improved and continued to neglect the pres-
ence of the cool feature in the southeast. The mean differ-
ence reduced to 0.1°C and the spread of the difference field
about this mean was also reduced compared to that of the
initial analysis. The maximum difference remained in the
vicinity of the cool feature but with a reduced magnitude of
-0.8°C.

The MLD was overestimated in both initial and
final analyses, Fig 5.2 (b) and (d). The slight shoaling of
the layer between the two analyses (2m) had no significant
effect on the difference fields, Fig. 5.2 (c) and (e). The
modeled MLD was, on average, 18 to 19.5m greater than the
sea truth and the maximum difference was between 30 and 40m.
The near uniform structure of the modeled MLD in both anal-
yses was a gross misrepresentation of the complex structure
evident in the sea truth contour field, Fig. 5.2 (a).

The average magnitude of both the BLG, Fig. 5.3
and THG, Fig 5.4 model analysis fields also moved closer to
the sea truth between the initial and final model analyses.
The BLG analyses, however, showed a marked difference
between modeled and sea truth shape fields for both
analyses.

    b. TEOTS Analysis

The initial TEOTS SST analysis, Fig. 5.5 (b)
overestimated the sea truth in a similar manner to that
observed in the equivalent EOTS analysis and by

58

approximately the same average amount i.e., a mean difference of -0.9°C. The mean difference was almost halved in the final analysis, Fig. 5.5 (c). However, the error in the modeled shape field remained constant as, therefore, did the difference distribution about the mean. The difference fields are shown in Fig. 5.5 (d) and (e).

The modeled MLD was unresponsive to input data and showed a lack of features. The TEOTS analyses overestimated the MLD by an average of 12m. TEOTS MLD's were closer to the mean sea truth MLD than were the EOTS analyses but, because of the lack of shape agreement between model and sea truth the distribution of the difference field about the mean was similar to that observed in the EOTS analyses.

The BLG, Fig. 5.7 and THG, Fig. 5.8 appear to respond to the input data by moving closer to the sea truth in the mean. However, the lack of shape agreement between model and sea truth contour fields remained unchanged. The TEOTS analysis was initially further from the sea truth and responded more slowly to input data than the EOTS analysis.

2. Cruise AII

The analysis dates for cruise AII were 30 June, 1983 (initial) and 7 July, 1983 (final). The inputs to the analyses were 3 BT's and nil for the initial and final analyses, respectively. Statistics for the model/sea truth comparisons are given in Table III and the histograms from which the statistics were derived are shown in Figs. 5.33 to 5.40

a. EOTS Analysis

The initial SST analysis, Fig. 5.9 (b) showed similar shape characteristics to those observed in the 23 June EOTS analysis (cruise AI) and a general warming trend of 0.5°C was indicated. Over the same period the sea truth analysis, Fig. 5.9 (a) indicated an increase in SST of 2.0°C

59

and a marked change in the shape of the contour field.   The initial difference field, Fig. 5.9 (c) showed the analysis to be an underestimate of the sea truth by an average of 1.0°C with a maximum difference of 1.6°C and a general lack of agreement between model and sea truth shape fields was apparent.

The final model analysis, Fig. 5.9 (d), showed a trend towards a meridional SST structure (away from the zonal structure apparent in the sea truth field)   with no change in the average SST. The mean difference remained similar to that calculated for the initial analysis. However, because of the increased disagreement between the model and sea truth shape fields, the spread of the differ- ence distribution about the mean increased.

The   FNOC   climatological   depth/temperature profile for the June/July period in the region of the study domain predicts a SST of 14.2°C which was in close agreement with the mean SST of 14.4°C observed in the model analysis.

The initial MLD analysis, Fig. 5.10 (b) showed no significant change, in shape or magnitude from that observed in the 23 June analysis, Fig.   5.2 (d).   However, changes in the sea truth field,   Fig. 5.10 (a) , between cruises AI and AII meant that the difference field, Fig. 5.10 (c) , was markedly different from that of the 23 June analysis. Although the final MLD analysis, Fig 5.10 (d) did indicate a slight shoaling (5m to 10m), the MLD was overes- timated by the model analyses throughout.

The shoaling of the MLD between the initial and final analyses noted above is compatible with the model analysis moving towards the FNOC July climatology for the region which shows a change in MLD from 55m in June to 37m in July.

The model BLG's were overestimated and the shape of the contour field in poor agreement with that of the sea

60

truth. A smoothing of the modeled BLG field to a near constant value in the final analysis did, however, reduce the mean difference from the 1.2°C/100m observed in the initial analysis to 0.3°C/100m. The results of the comparisons are shown in Fig. 5.11.

Model and sea truth THG's were in good agreement for both analyses, Fig. 5.12.

b. TEOTS Analysis

The warming trend noted in the EOTS analyses was also observed in the TEOTS analyses, Fig. 5.13 The mean difference decreased from 0.4°C in the initial TEOTS analysis to near zero in the final analysis. The horizontal structure of the TEOTS analyses remained meridional with a weakly strengthening horizontal temperature gradient in the east of the domain compared to the complex near zonal structure observed in the sea truth SST.

Modeled MLD's, Fig. 5.14 remained unchanged by any significant amount in both magnitude and structure from those of the TEOTS analyses of cruise AI. The modeled MLD's were overestimated by between 5m and 35m, when compared to the sea truth.

The BLG, Fig. 5.15 was overestimated by the model in both the initial and final analyses with the magnitude of the mean difference increasing by the final analysis.

The THG, Fig. 5.16 was in reasonably good agreement with the sea truth throughout.

3. Cruise AIII

As previously stated, model analyses were not available for the termination of this cruise. There were no BT inputs to either model for the 10 July, 1983 analysis.

The only significant change in either model was a general increase in the SST (0.5°C) indicated in the EOTS analysis.

The significant changes in the difference fields, Figs. 5.17 to 5.24 were due to changes in the sea truth fields between cruises AII and AIII.

The statistics of the difference fields and the relevant histograms are shown in Table IV and Figs. 5.41 to 5.48 As with cruise AII, the TEOTS SST and MLD analyses were, on average, in closer agreement with the sea truth than the EOTS analyses.

4. Effectiveness of the EOTS Analysis in Representing Input Data

To estimate the accuracy of the EOTS analysis in responding to input data the author's analysis program was revised to operate on a 4x4 grid with a 40km grid spacing, similar to that used in the EOTS analysis program. The twenty-three BT's input to the EOTS 23 June analysis were used as input. The resulting SST contour field and that produced by the equivalent EOTS analysis are shown in Fig. 5.49.

From Fig. 5.49 it can be seen that the EOTS analysis did not respond accurately to the input data. The accuracy of the author's analysis program had previously been veri-fied by comparisons with manually contoured SST fields with favourable results. The reason for the lack of resolution in the EOTS analysis is not fully understood but is probably due to excess weighting on the first guess field used in the EOTS FIB analysis. This first guess field provides the shape information to which any input data is fitted in a least squares sense.

62

5. Validity of Quasi-Synoptic Assumption

Lack of synopticity in the OPTOMA5 data proved to be unimportant since the only inputs, of any significance, to the FNOC models were the twenty-seven BT submissions prior to the 23 June analyses. The fact that the BT's were input to the models as one data set made them synoptic to the computer model and, therefore, a synoptic assumption is valid for the sea truth analysis with which the model analyses were compared.

6. Summary

a. SST

The EOTS SST analysis responded to the magnitude changes dictated by input data (when sufficient data was available) but horizontal structure was not resolved on a scale commensurate with the resolution capability of the 40km grid spacing used. In the absence of input data the EOTS SST moved towards climatology and became even less structured.

There was a measureable response to input data in the TEOTS SST analysis. The magnitude of the response was less than that observed in the EOTS analysis and the lack of agreement in the shape field between model and sea truth was even more pronounced, as might have been expected from the larger grid spacing used in the TEOTS analysis. TEOTS perfomed better, in a general sense, than EOTS when data were not available and the move towards climatology noted in the ECTS analysis was not observed.

b. MLD

Neither model produced a realistic analysis of the sea truth MLD whether input data were available or not. Both analyses tended to overestimate the magnitude of the

63

MLD, with the TEOTS analysis giving a consistently better estimate of the sea truth MLD than the EOTS analysis.

c. BLG and THG

The lack of agreement between modeled and sea truth MLD made comparisons of BLG and THG difficult (Both parameters were defined in terms of the layer depth). Any agreement noted between these two parameters was therefore regarded as purely coincidental.

B. INTER-ANNUAL VARIABILITY

The mesoscale variability of the study domain has been dealt with in some detail in the previous sections. Underlying this mesoscale variability is a variability with a time scale of the order of years (the effect of El Nino). The region was known to be influenced by such an event during the period of the present study. To illustrate the effect of such an anomaly, mean depth/temperature profiles were compared for July, 1983 and July/August, 1982 in the study domain. The mean profiles were also compared to FNOC July climatology for the region. The mean profile for 1982 was derived from XBT data collected during the OPTOMA2 cruise of July/August, 1982 (The area of the CCS sampled by this cruise was very close to that sampled in the OPTOMA5 series of cruises) and that for 1983 was derived from XBT data collected during cruise AIII of the OPTOMA5 series (July, 1983). Figs. 5.50 to 5.52 show the results of the comparisons.

FNOC climatology was in reasonable agreement with the 1982 mean profile (assumed non-El Nino year), Fig 5.50 . The major discrepancy between climatological and measured profiles occurred in the upper part of the water column (surface to 50m) which could be expected since this is the

64

region subject to maximum atmospheric forcing and, therefore, the short time scale variability impossible to predict with climatology.

The presence of a thermal anomaly in the depth/temperature profile was clearly evident when the 1982 profile was compared to that from 1983, Fig. 5.51. The assumed El Nino event was present as a layer of warmer waters between the near surface and approximately 200m with a maximum anomaly of 2.5°C at a depth of 60m. The inability of a static climatology to represent such an event was demonstrated by comparing the 1983 mean depth/temperature profile with that obtained from FNOC climatology, Fig. 5.52.

To obtain a measure of the operational significance of an anomalous event such as the one described above transmission loss curves were computed from the FACT9H transmission loss model for the July 1983 climatological and mean depth/temperature profiles . The only measurable effect, Figs. 5.53 to 5.55 was a reduction in convergence zone range in the curves derived from the climatological profiles (approximately 3%) and a decrease in convergence zone gain (approximately 5db).

C. RESULTS OF RECENT FNOC STUDIES

Recent modifications have been made to both EOTS and TEOTS analysis models (Frost, pers. comm.) and, in particular, the model sensitivity to input changes in PLD (MLD) has been modified. The incorporation of the TEOTS analysis into the finer grid regional model has also been achieved for certain areas. The effect of these modifications is the subject of an ongoing investigation by FNOC, based on inputs from the Bay of Biscay and the Western Mediterranean Sea regional analyses.

The initial results from the study are promising with TEOTS apparently showing considerable skill in predicting changes in layer depth even in the absence of input data (Frost, pers. comm.). No information is available from this study related to the skill of the analysis in resolving the horizontal structure in the region.
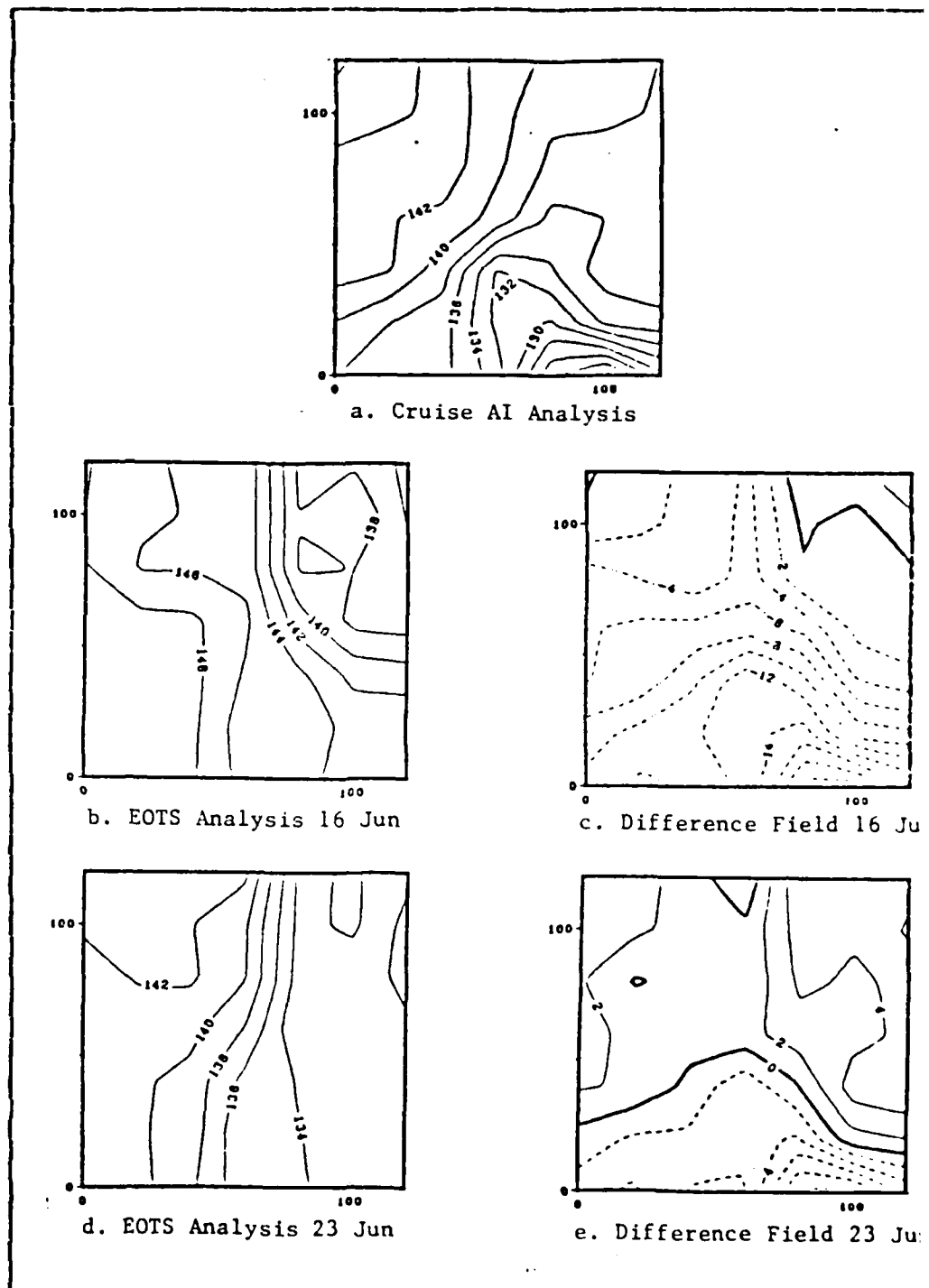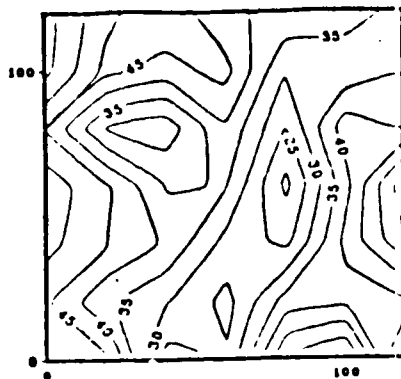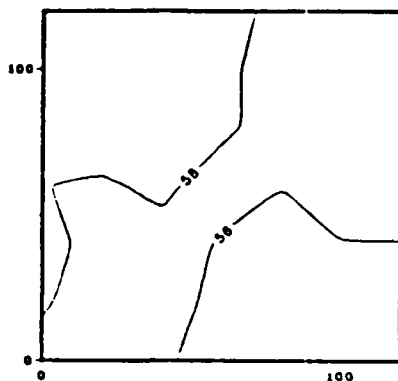
a. Cruise AI Analysis

b. EOTS Analysis 16 Jun

c. Difference Field 16 Ju

d. EOTS Analysis 23 Jun

e. Difference Field 23 Ju

Figure 5.1   Contoured SST Fields for EOTS/Cruise AI
(contour units °Cx10).

67

a. Cruise AI Analysis

b. EOTS Analysis 16 Jun

c. Difference Field 16 Jun

d. EOTS Analysis 23 Jun

e. Difference Field 23 Jun

Figure 5.2   Contoured MLD Fields for EOTS/Cruise AI
(contour units m).

68

a. Cruise AI Analysis

b. EOTS Analysis 16 Jun   c. Difference Field 16 Jun

d. EOTS Analysis 23 Jun   e. Difference Field 23 Jun
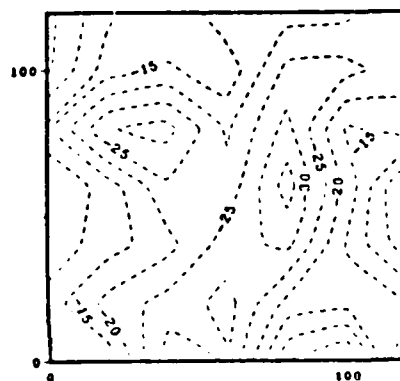
Figure 5.3   Contoured BLG Fields for EOTS/Cruise AI (contour units °C/1000m).
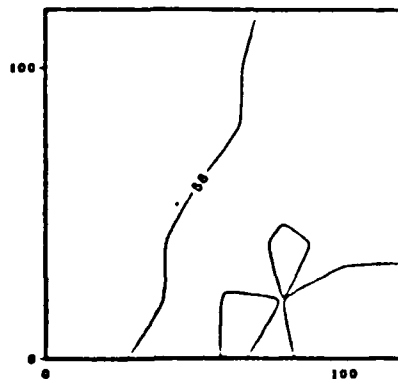
69

a. Cruise AI Analysis

b. EOTS Analysis 16 Jun

c. Difference Field 16 Jun

d. EOTS Analysis 23 Jun

e. Difference Field 23 Jun
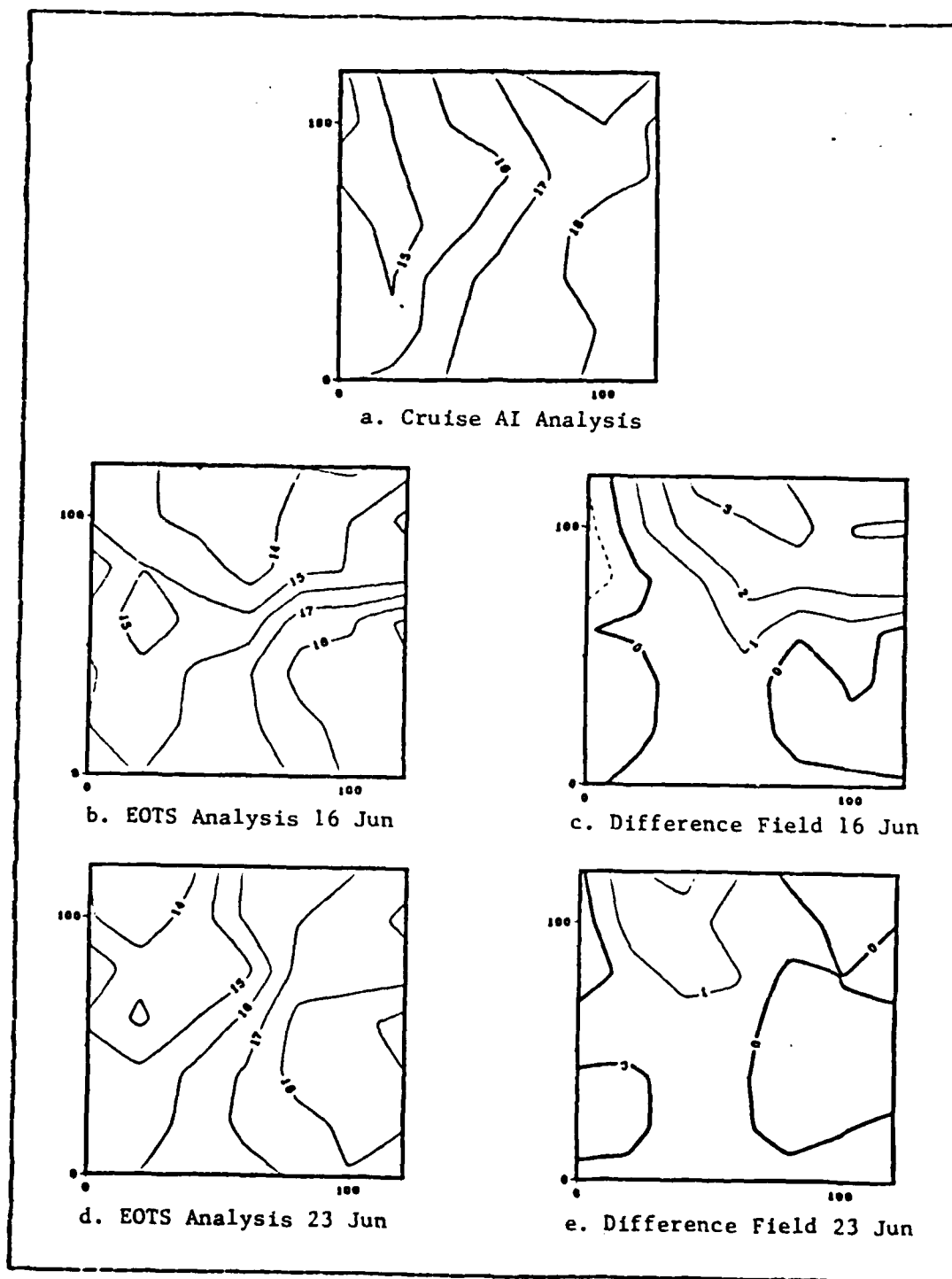
Figure 5.4   Contoured THG Fields for EOTS/Cruise AI
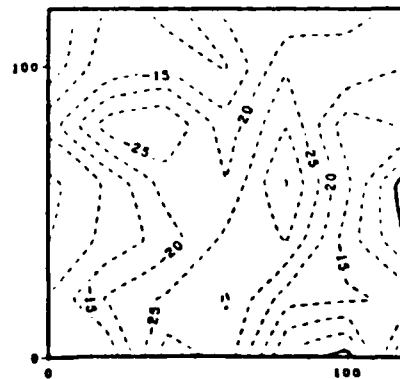(contour units °C/1000m).
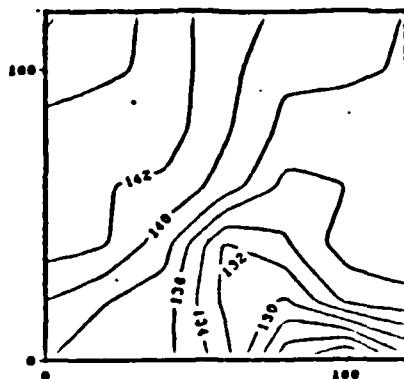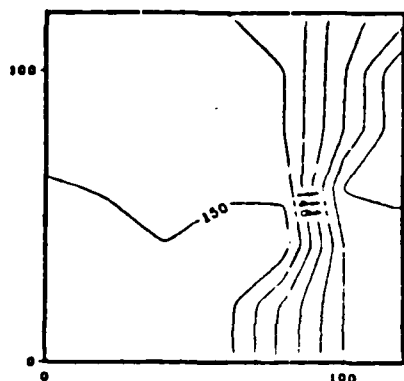
70

a. Cruise AI Analysis

b. TEOTS Analysis 16 Jun

c. Difference Field 16 Jun

d. TEOTS Analysis 23 Jun

e. Difference Field 23 Jun

Figure 5.5   Contoured SST Fields for TEOTS/Cruise AI
(contour units °Cx10).

71

a. Cruise AI Analysis

b. TEOTS Analysis 16 Jun

c. Difference Field 16 Jun

d. TEOTS Analysis 23 Jun

e. Difference Field 23 Jun

Figure 5.6   Contoured MLD Fields for TEOTS/Cruise AI (contour units m).
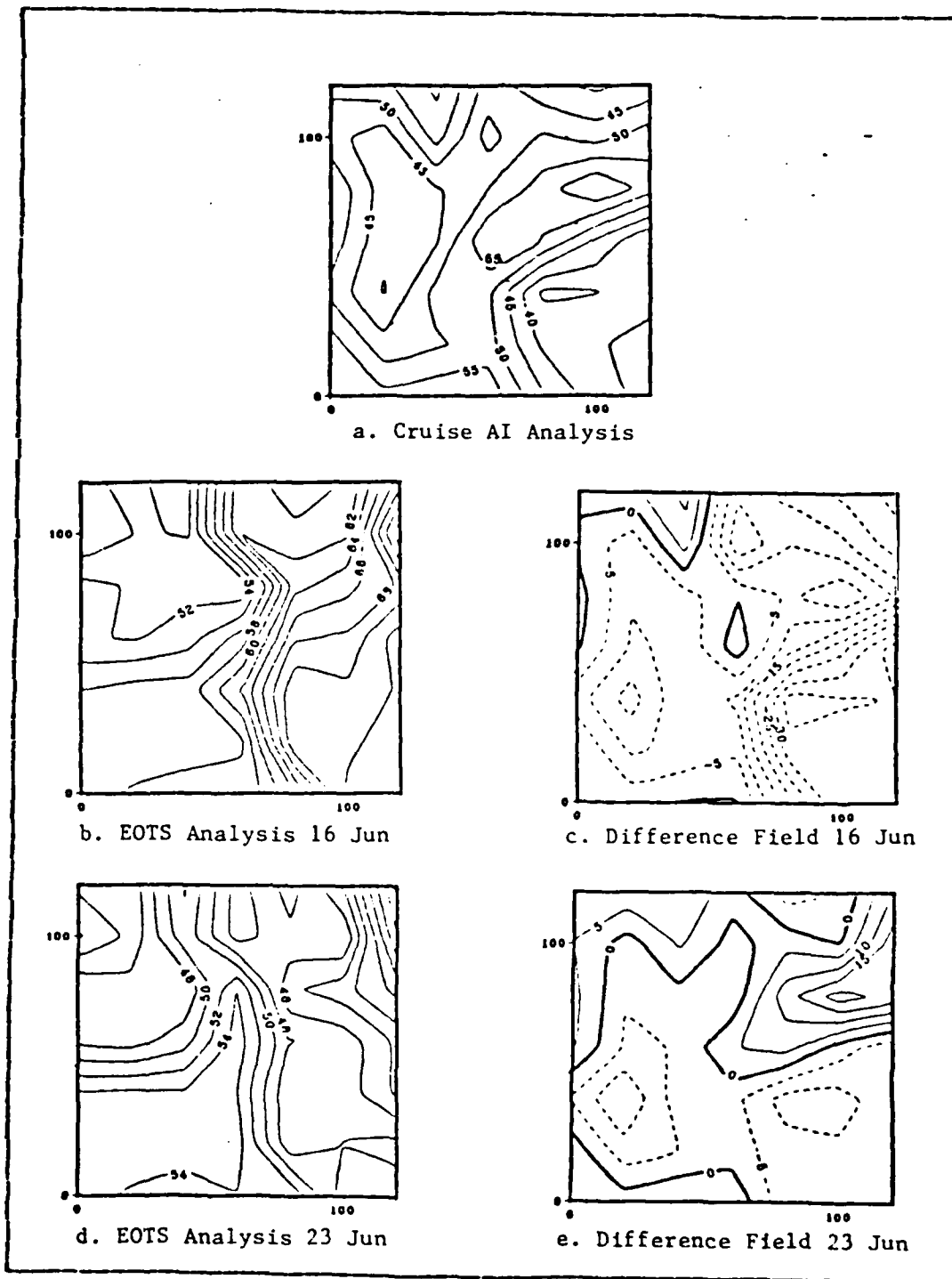
72

a. Cruise AI Analysis

b. TEOTS Analysis 16 Jun

c. Difference Field 16 Jun

d. TEOTS Analysis 23 Jun
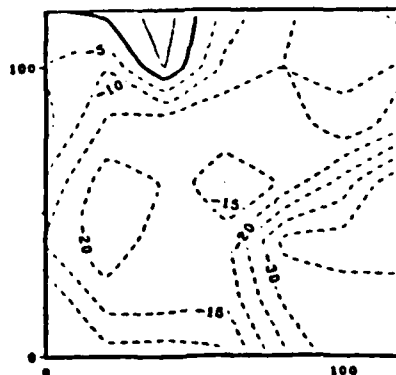
e. Difference Field 23 Jun

Figure 5.7   Contoured BLG Fields for TEOTS/Cruise AI
(contour units °C/1000m).

73

a. Cruise AI Analysis

b. TEOTS Analysis 16 Jun

c. Difference Field 16 Jun

d. TEOTS Analysis 23 Jun

e. Difference Field 23 Jun
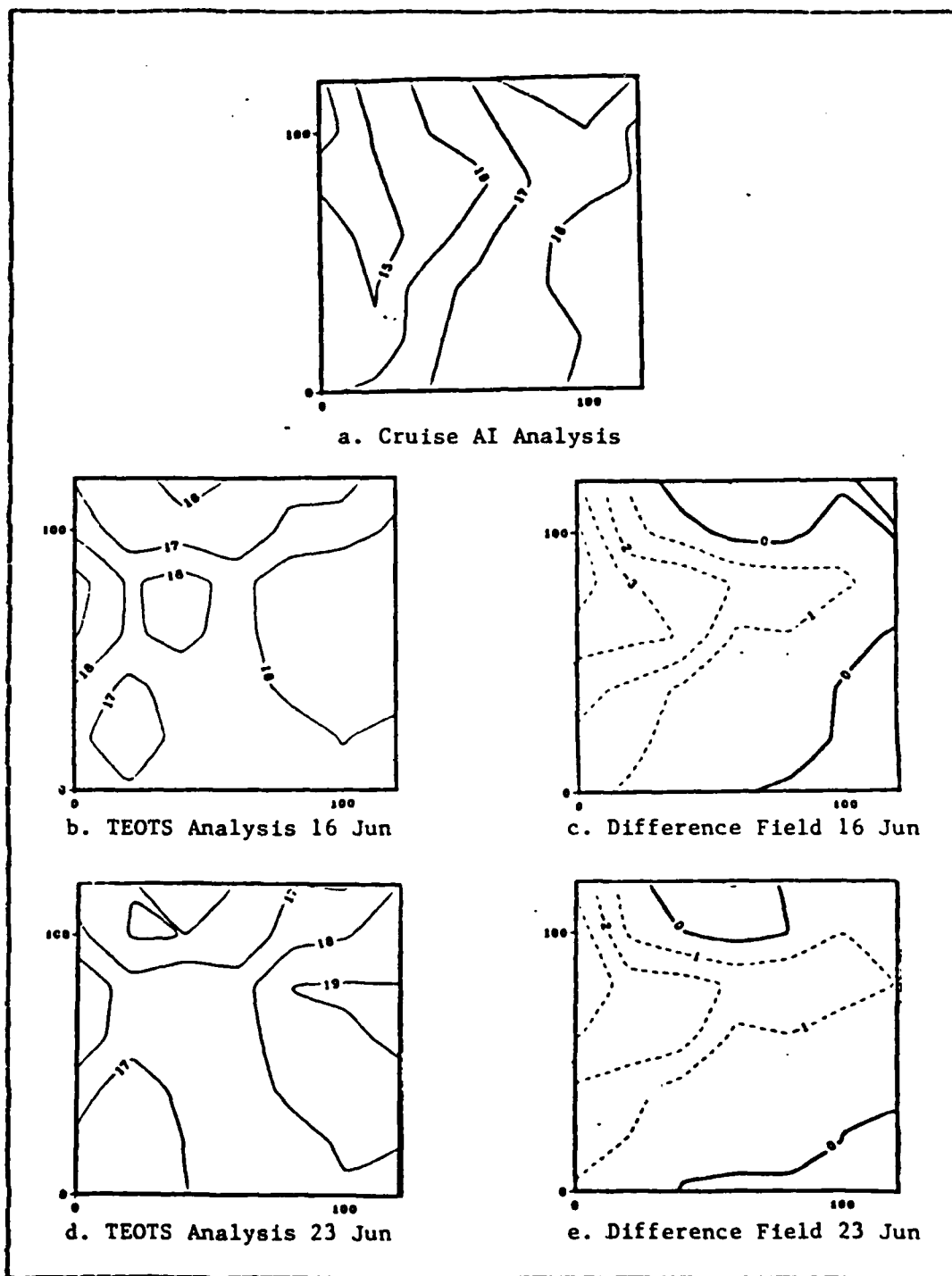
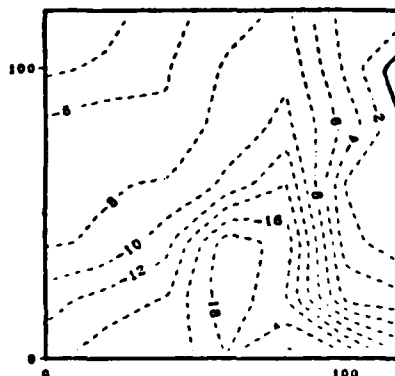**Figure 5.8   Contoured THG Fields for TEOTS/Cruise AI (contour units °C/1000m).**

74

a. Cruise AII Analysis

b. EOTS Analysis 30 Jun

c. Difference Field 30 Jun

d. EOTS Analysis 7 Jul

e. Difference Field 7 Jul
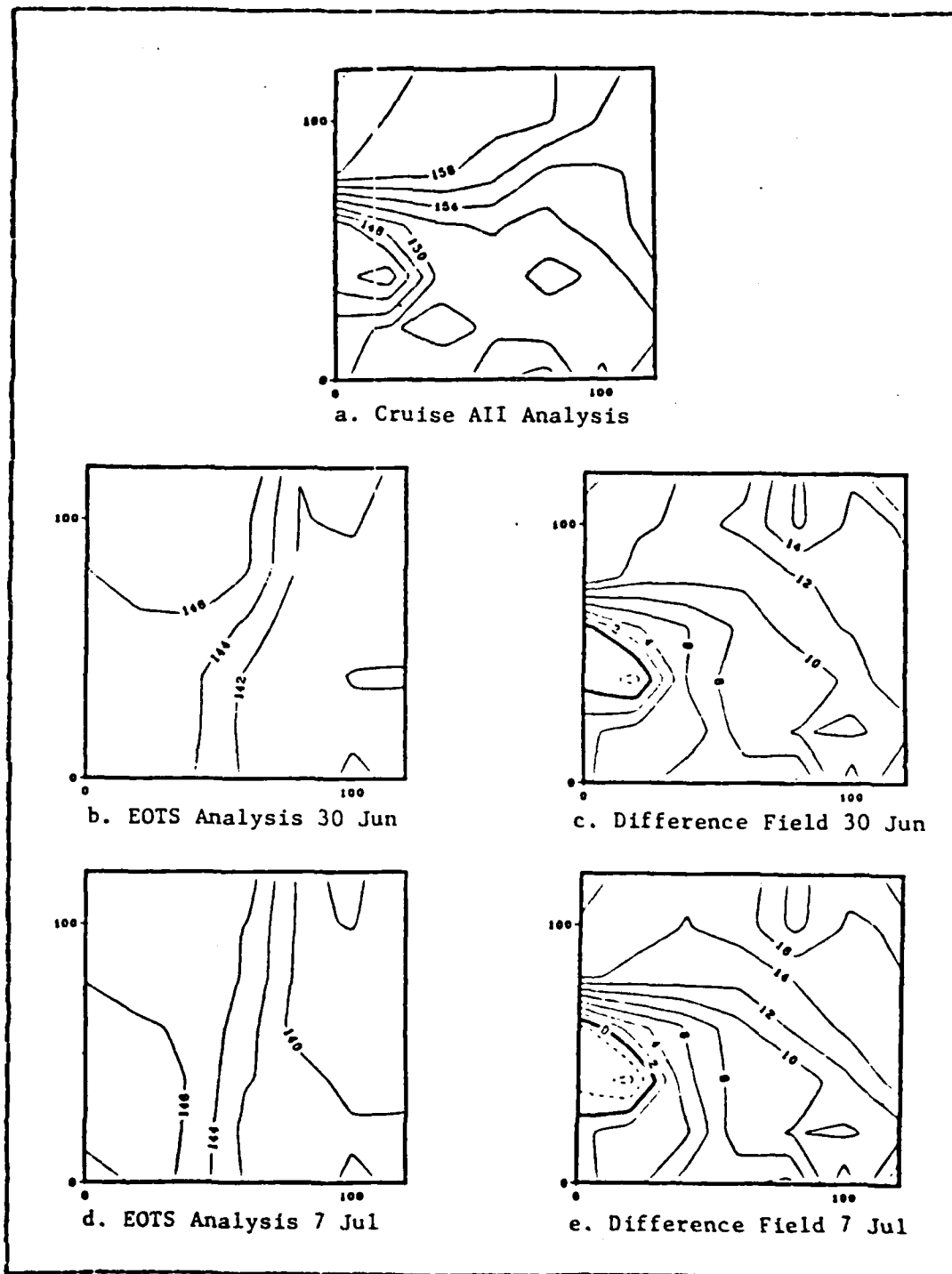
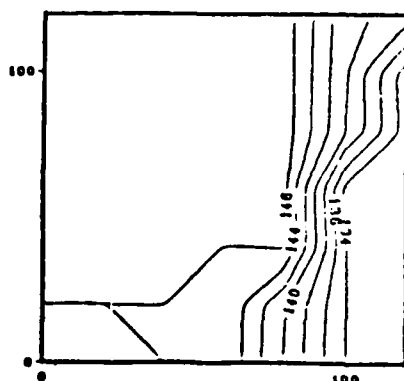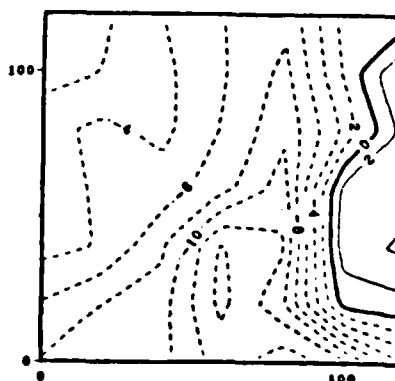Figure 5.9   Contoured SST Fields for EOTS/Cruise AII
(contour units °Cx10).

75

a. Cruise AII Analysis

b. EOTS Analysis 30 Jun

c. Difference Field 30 Jun

d. EOTS Analysis 7 Jul

e. Difference Field 7 Jul
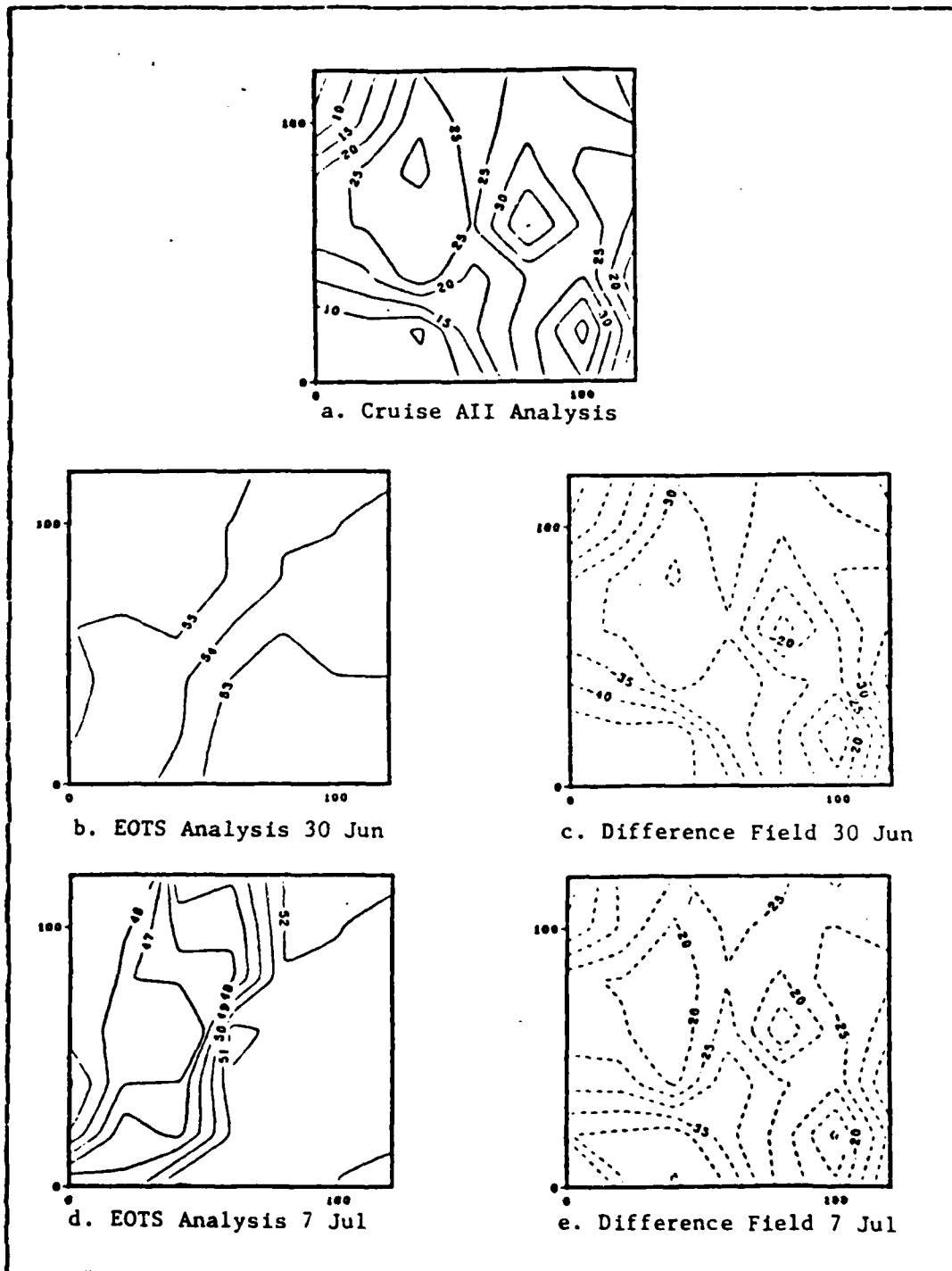
Figure 5.10   Contoured MLD Fields for EOTS/Cruise AII (contour units m).

76

a. Cruise AII Analysis

b. EOTS Analysis 30 Jun

c. Difference Field 30 Jun

d. EOTS Analysis 7 Jul

e. Difference Field 7 Jul
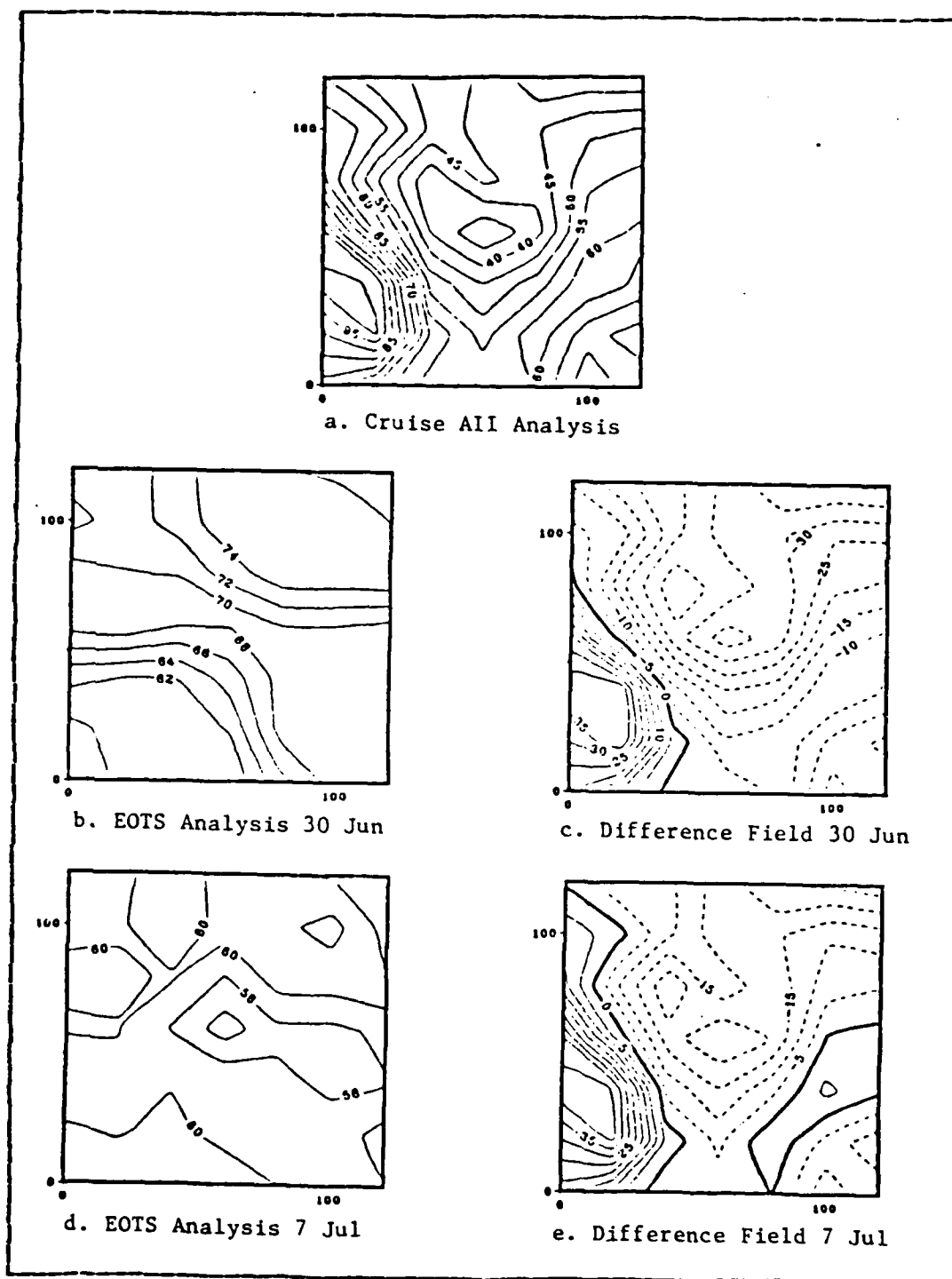
Figure 5.11   Contoured BLG Fields for EOTS/Cruise AII
(contour units °C/1000m).

77

a. Cruise AII Analysis
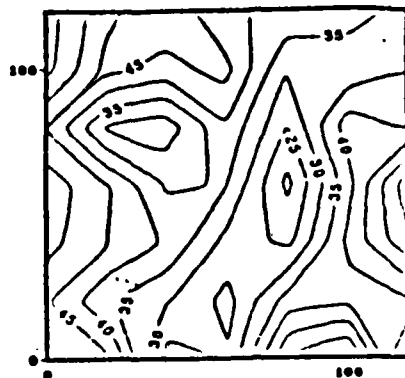
b. EOTS Analysis 30 Jun

c. Difference Field 30 Jun

d. EOTS Analysis 7 Jul

e. Difference Field 7 Jul
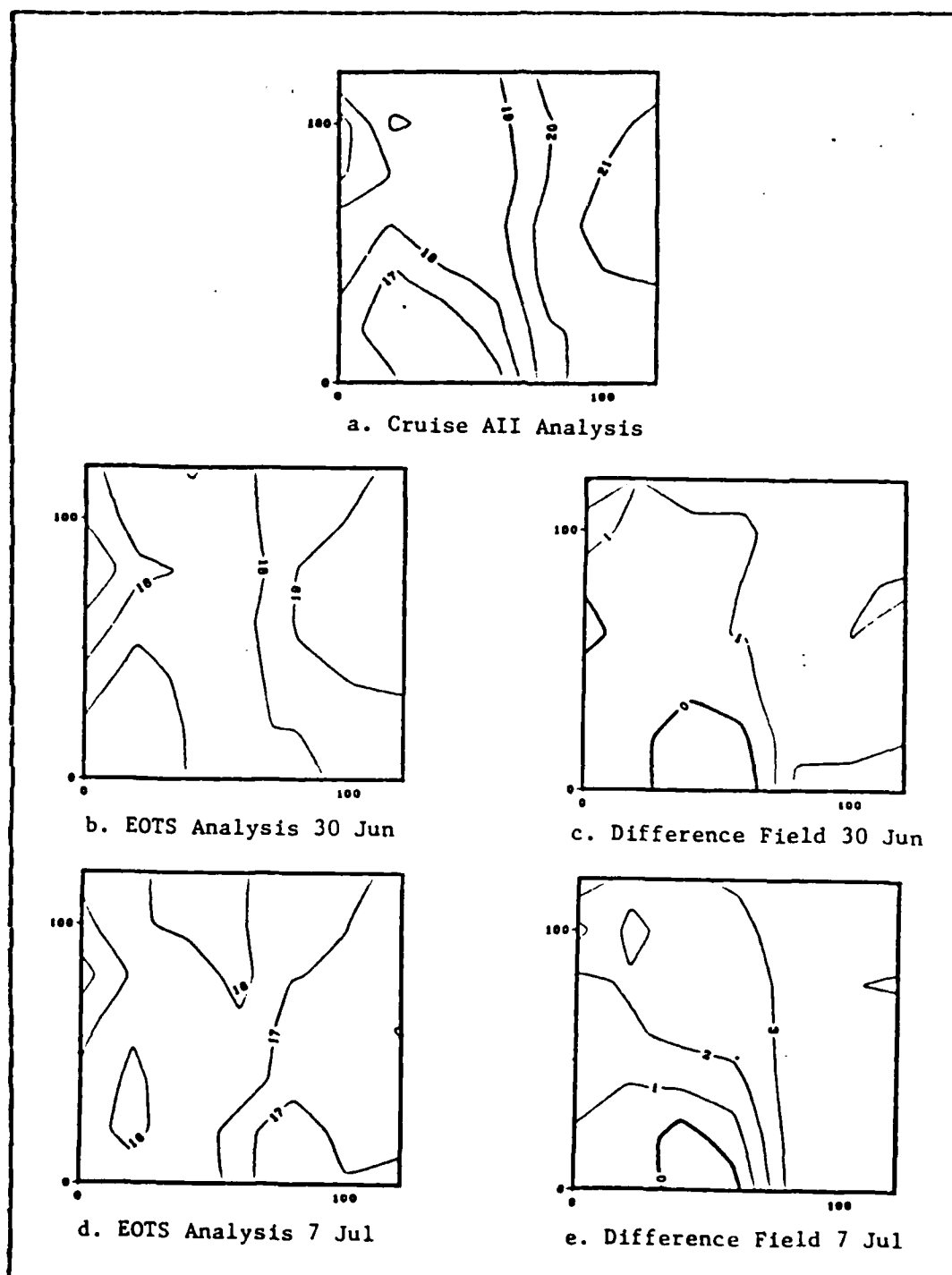
Figure 5.12   Contoured THG Fields for EOTS/Cruise AII
(contour units °C/1000m).

78

a. Cruise AII Analysis

b. TEOTS Analysis 30 Jun
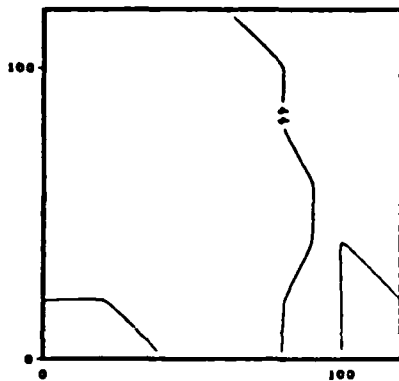
c. Difference Field 30 Jun
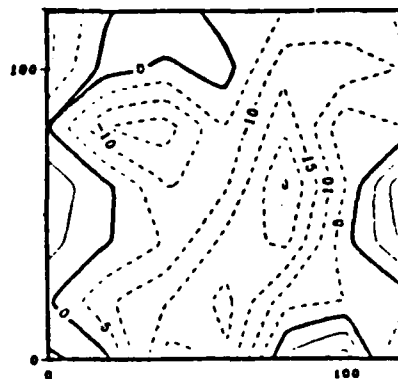
d. TEOTS Analysis 7 Jul

e. Difference Field 7 Jul

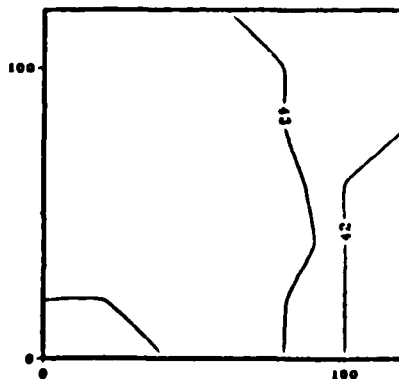Figure 5.13   Contoured SST Fields for TEOTS/Cruise AII
(contour units °Cx10).

79

a. Cruise AII Analysis

b. TEOTS Analysis 30 Jun

c. Difference Field 30 Jun

d. TEOTS Analysis 7 Jul

e. Difference Field 7 Jul
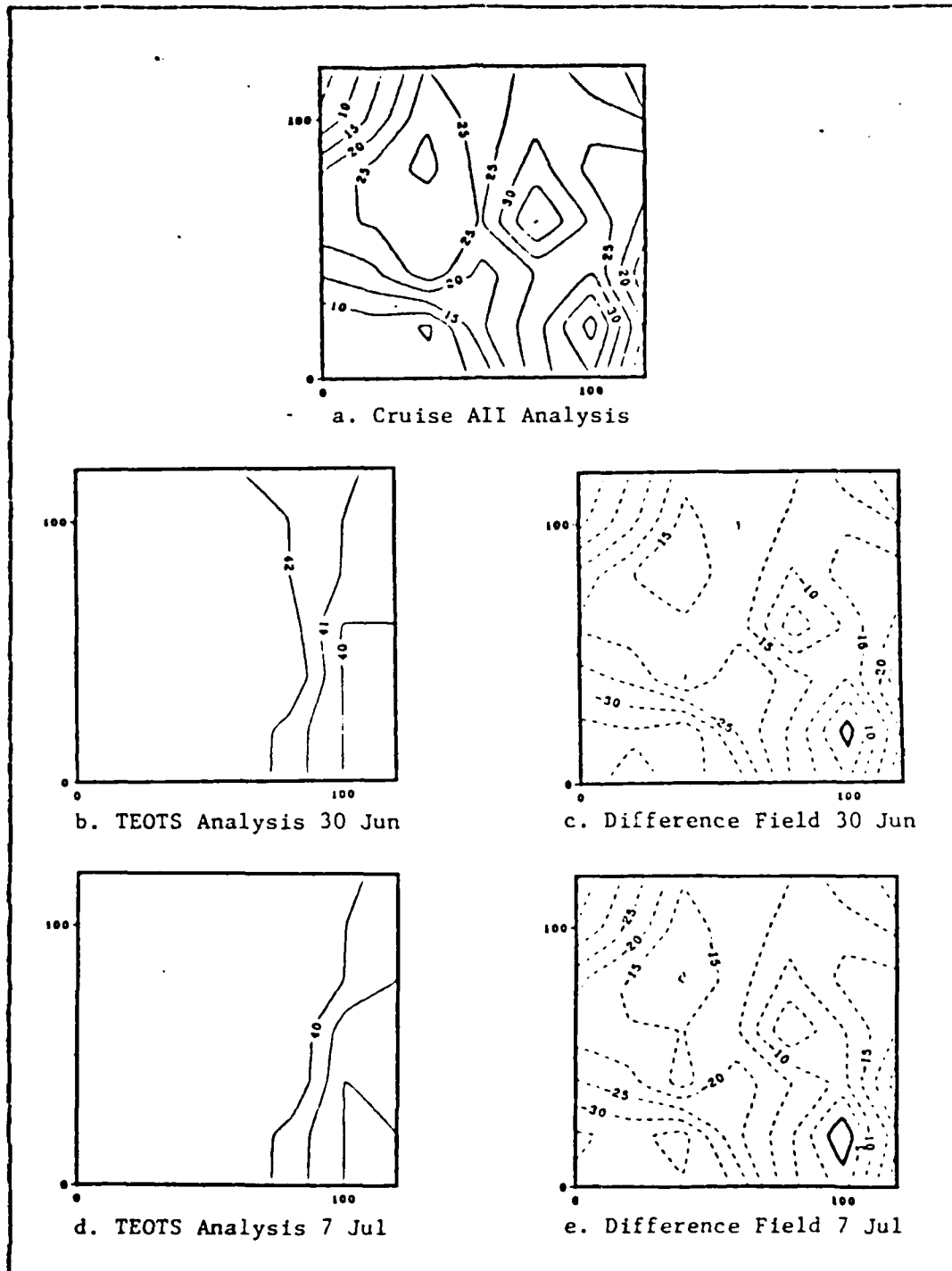
Figure 5.14   Contoured MLD Fields for TEOTS/Cruise AII
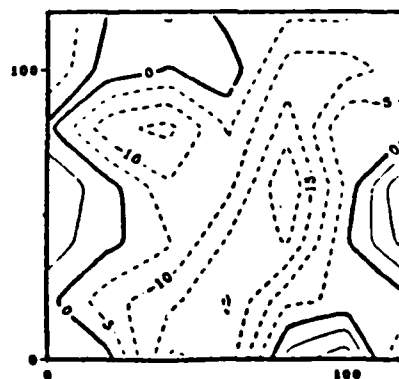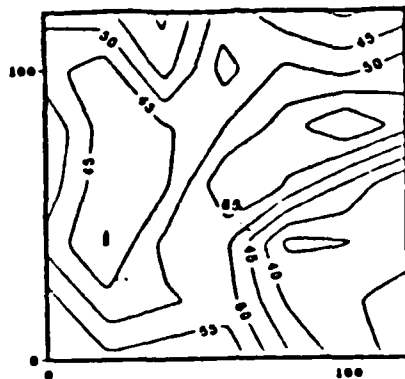(contour units m).

80

a. Cruise AII Analysis

b. TEOTS Analysis 30 Jun

c. Difference Field 30 Jun

d. TEOTS Analysis 7 Jul

e. Difference Field 7 Jul
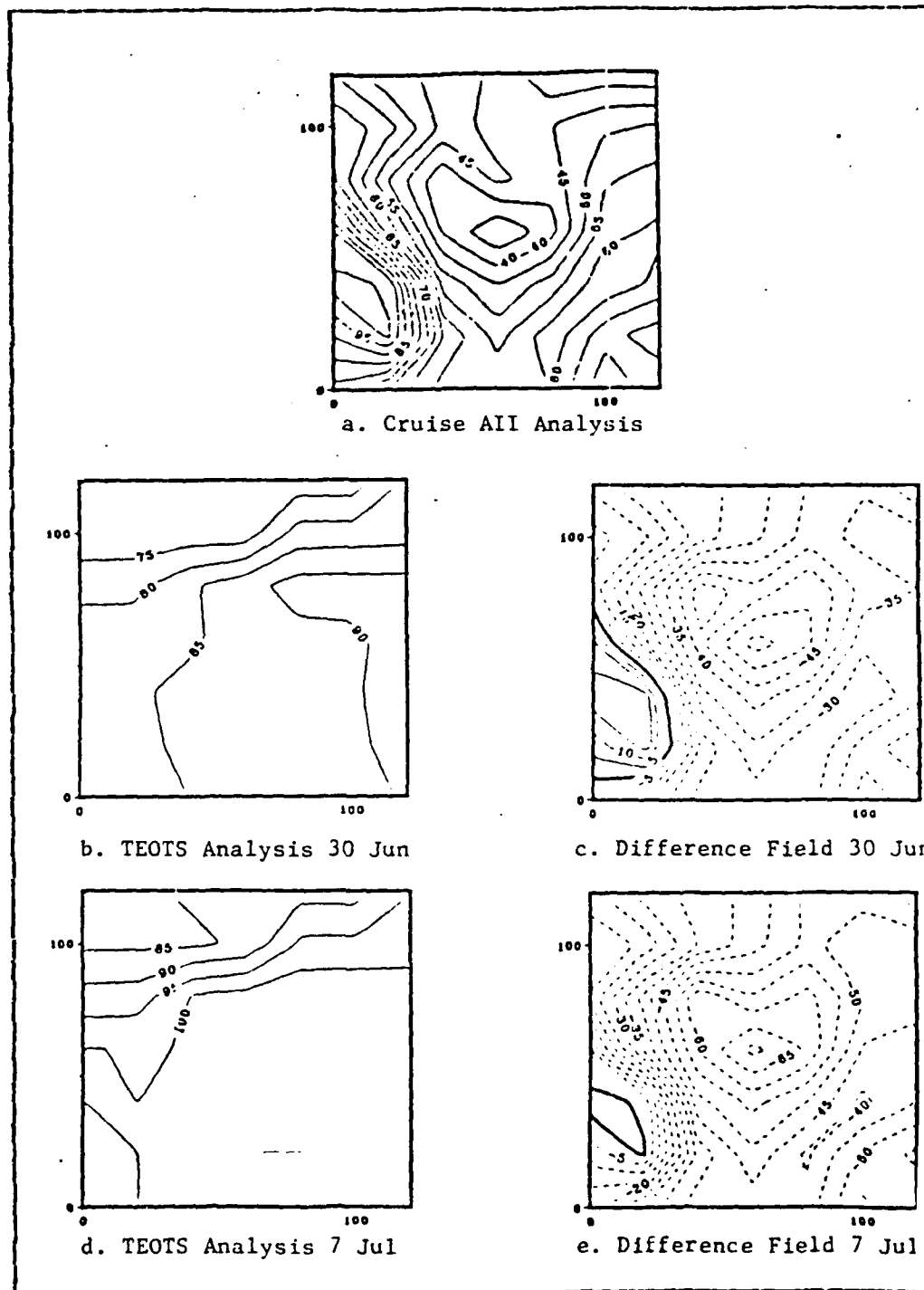
Figure 5.15   Contoured BLG Fields for TEOTS/Cruise A
(contour units °C/1000).

81

a. Cruise AII Analysis

b. TEOTS Analysis 30 Jun   c. Difference Field 30 Jun

d. TEOTS Analysis 7 Jul   e. Difference Field 7 Jul
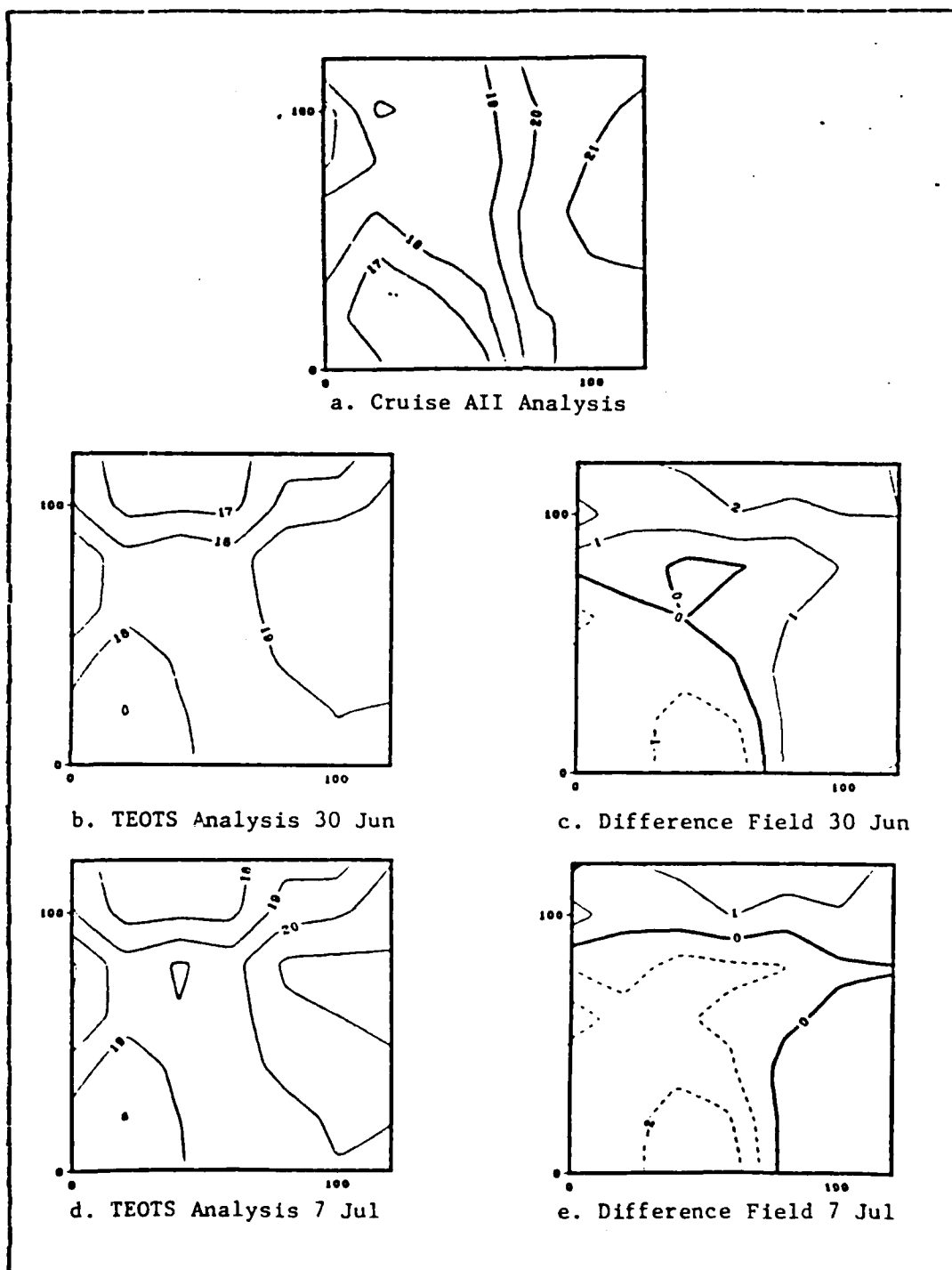
Figure 5.16   Contoured THG Fields for TEOTS/Cruise AII
(contour units °C/1000).

82
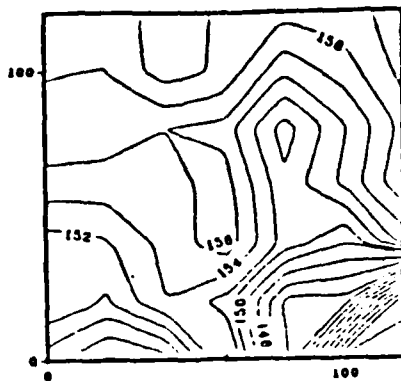
a. Cruise AIII Analysis

b. EOTS Analysis 10 Jul

c. Difference Field 10 Jul

Figure 5.17   Contoured SST Fields for EOTS/Cruise AIII
(contour units °Cx10).

83
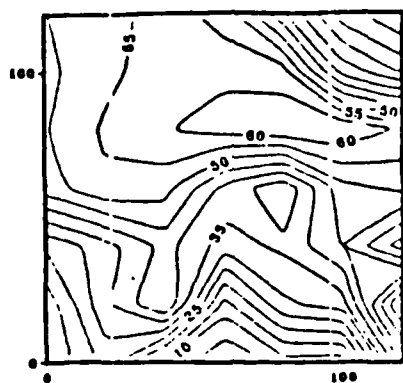
a. Cruise AIII Analysis
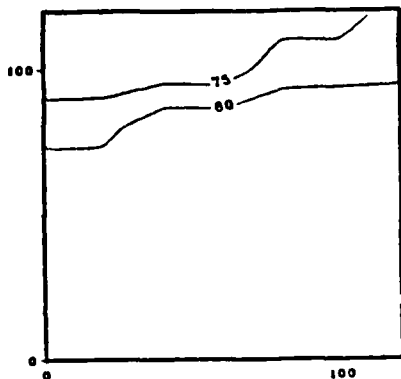

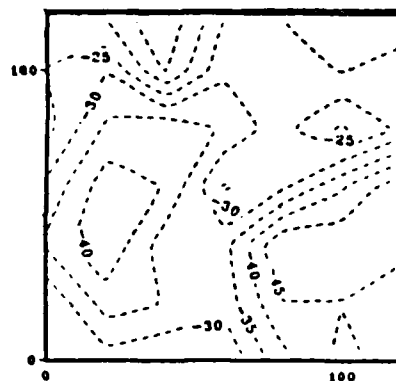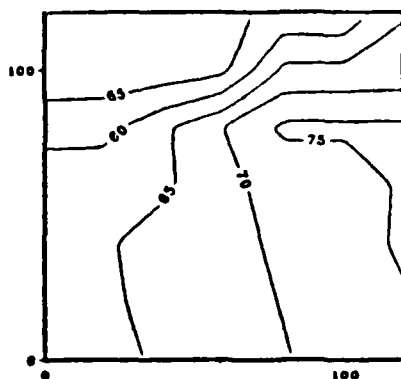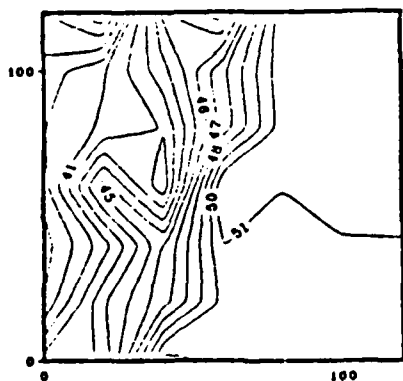b. EOTS Analysis 10 Jul
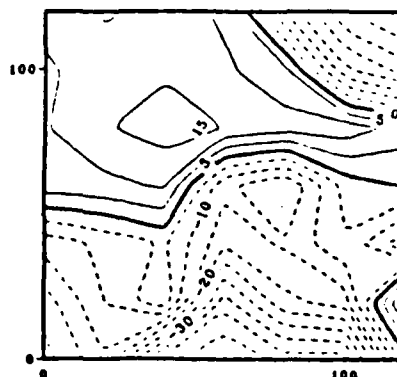
c. Difference Field 10 Jul

Figure 5.18   Contoured MLD Fields for EOTS/Cruise AIII
(contour units m).

84
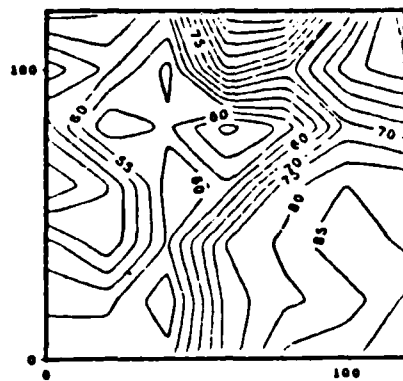
a. Cruise AIII Analysis
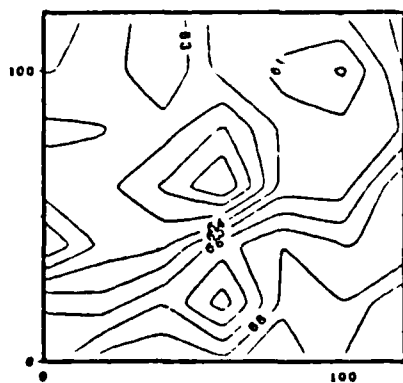
b. EOTS Analysis 10 Jul
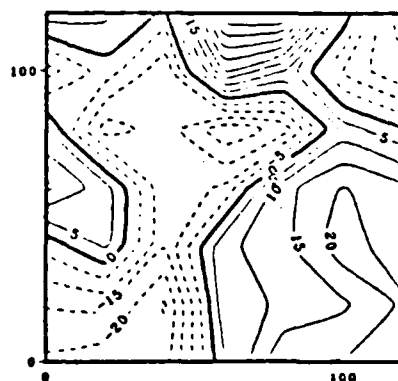
c. Difference Field 10 Jul

Figure 5.19   Contoured BLG Fields for EOTS/Cruise AIII
(contour units °C/1000).

85
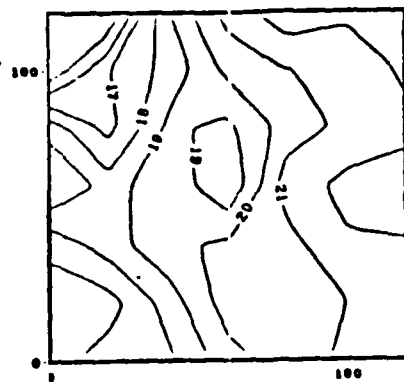
a. Cruise AIII Analysis

b. EOTS Analysis 10 Jul   c. Difference Field 10 Jul

Figure 5.20   Contoured TBG Fields for EOTS/Cruise AIII
                (contour units °C/1000).

86
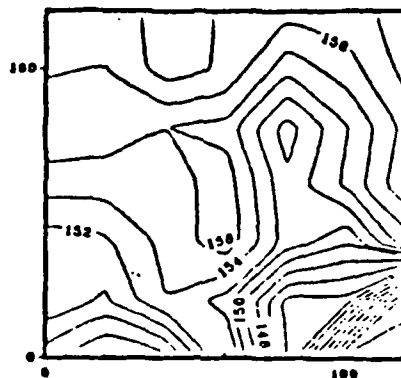
a. Cruise AIII Analysis

b. TEOTS Analysis 10 Jul

c. Difference Field 10 Jul

Figure 5.21   Contoured SST Fields for TEOTS/Cruise AIII
(contour units $^{\circ}$Cx10).

87
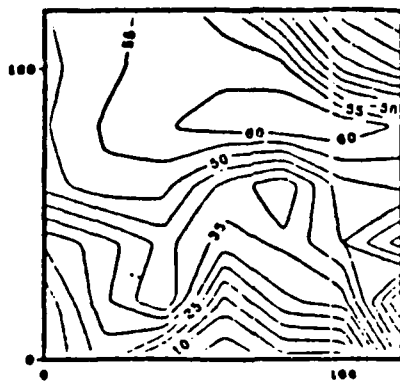
a. Cruise AIII Analysis
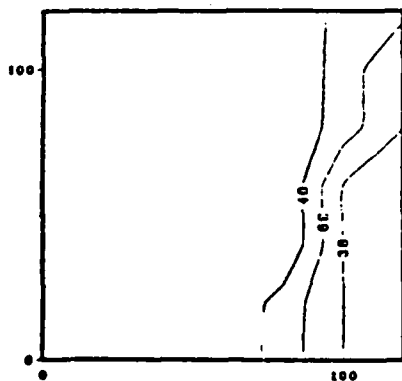
b. TEOTS Analysis 10 Jul
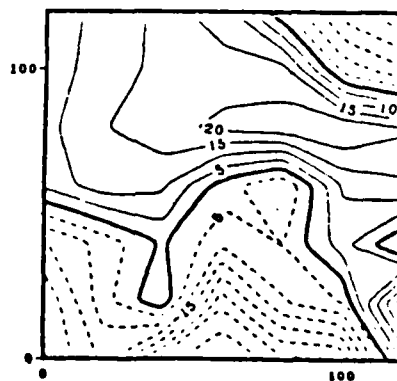
c. Difference Field 10 Jul

Figure 5.22   Contoured MLD Fields for TEOTS/Cruise AIII
(contour units m).

88
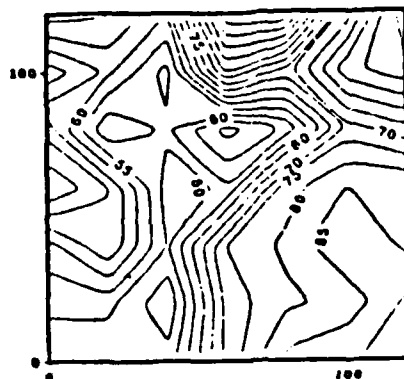
a. Cruise AIII Analysis
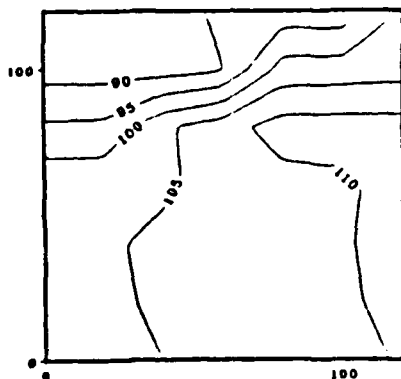
b. TEOTS Analysis 10 Jul
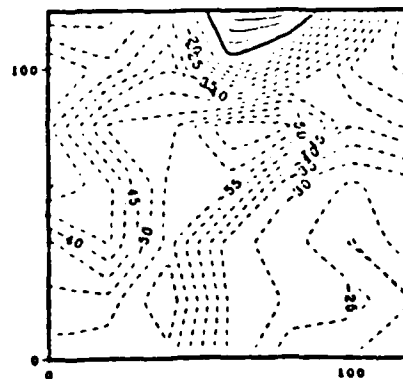
c. Difference Field 10 Jul

Figure 5.23   Contoured BLG Fields for TEOTS/Cruise AIII
(contour units °C/1000).
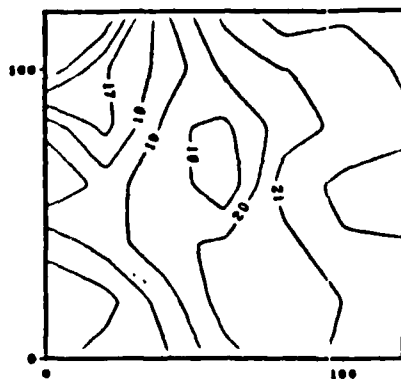
a. Cruise AIII Analysis
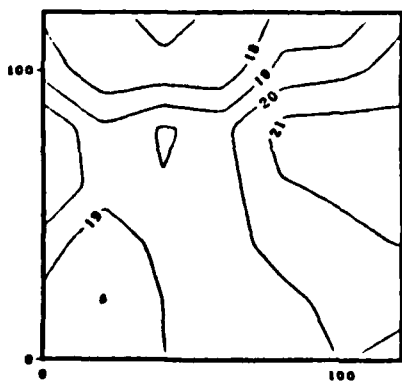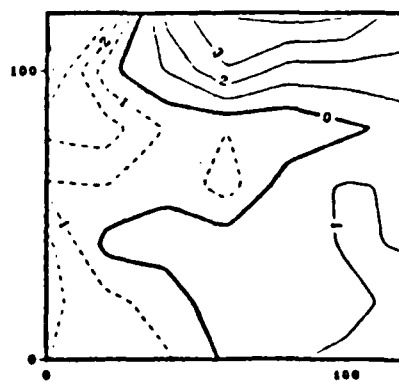
b. TEOTS Analysis 10 Jul   c. Difference Field 10 Jul

Figure 5.24   Contoured THG Fields for TEOTS/Cruise AIII
(contour units °C/1000).

90
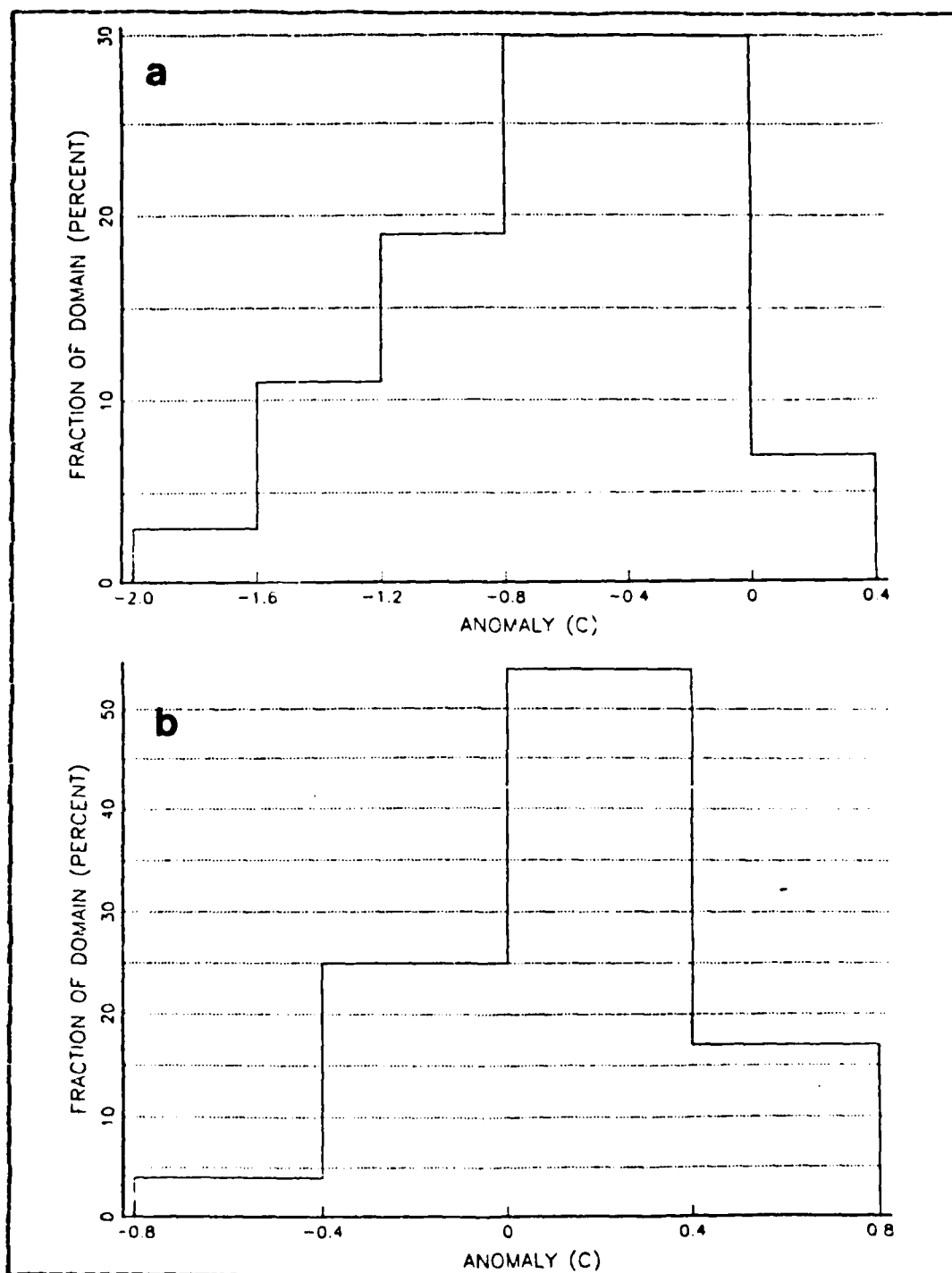
Figure 5.25   SST Difference Distribution EOTS/Cruise AI
a. 16 Jun Analysis b. 23 Jun Analysis.

91
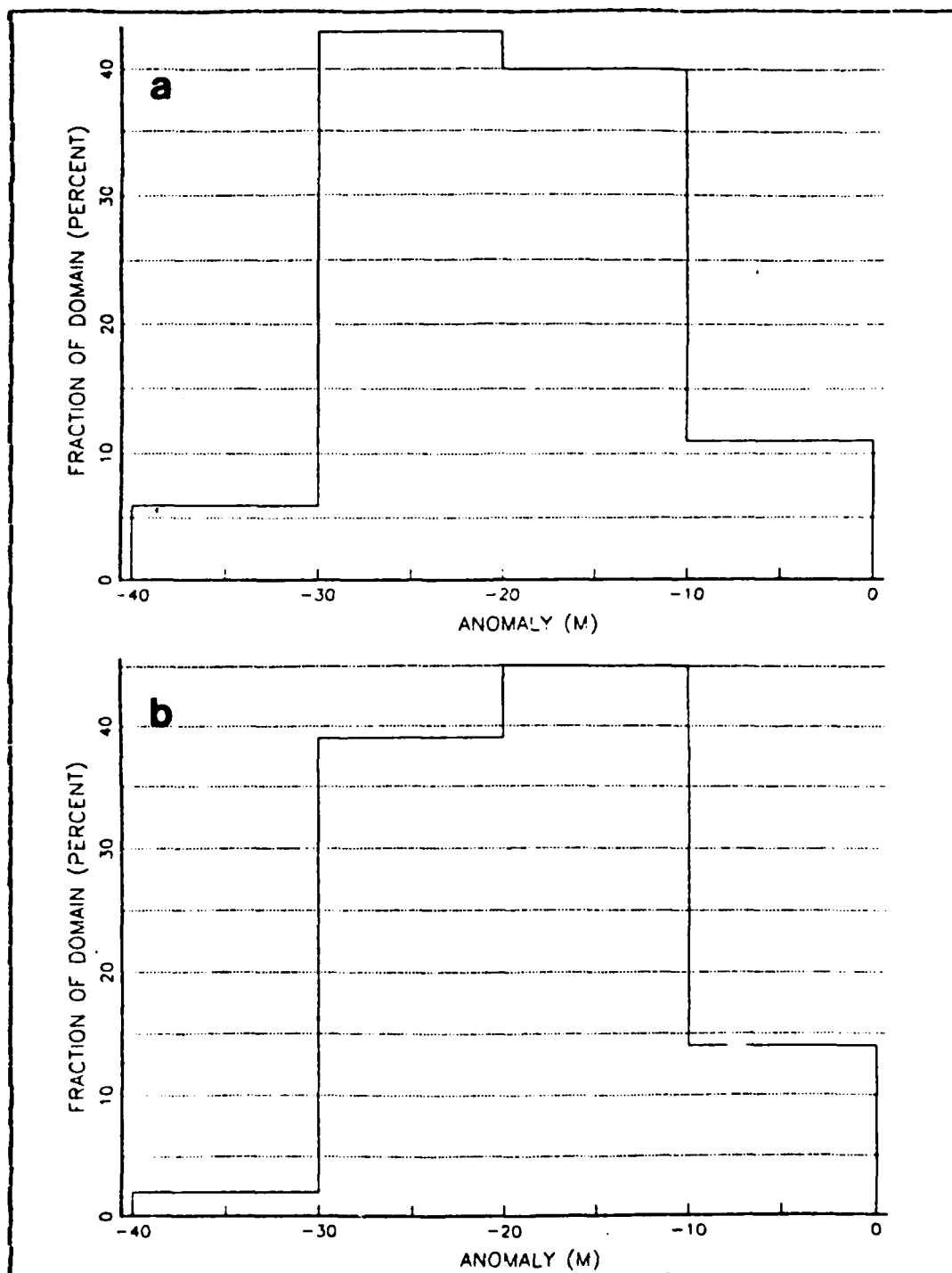
Figure 5.26   MLD Difference Distribution EOTS/Cruise AI
a. 16 Jun Analysis b. 23 Jun Analysis.

92
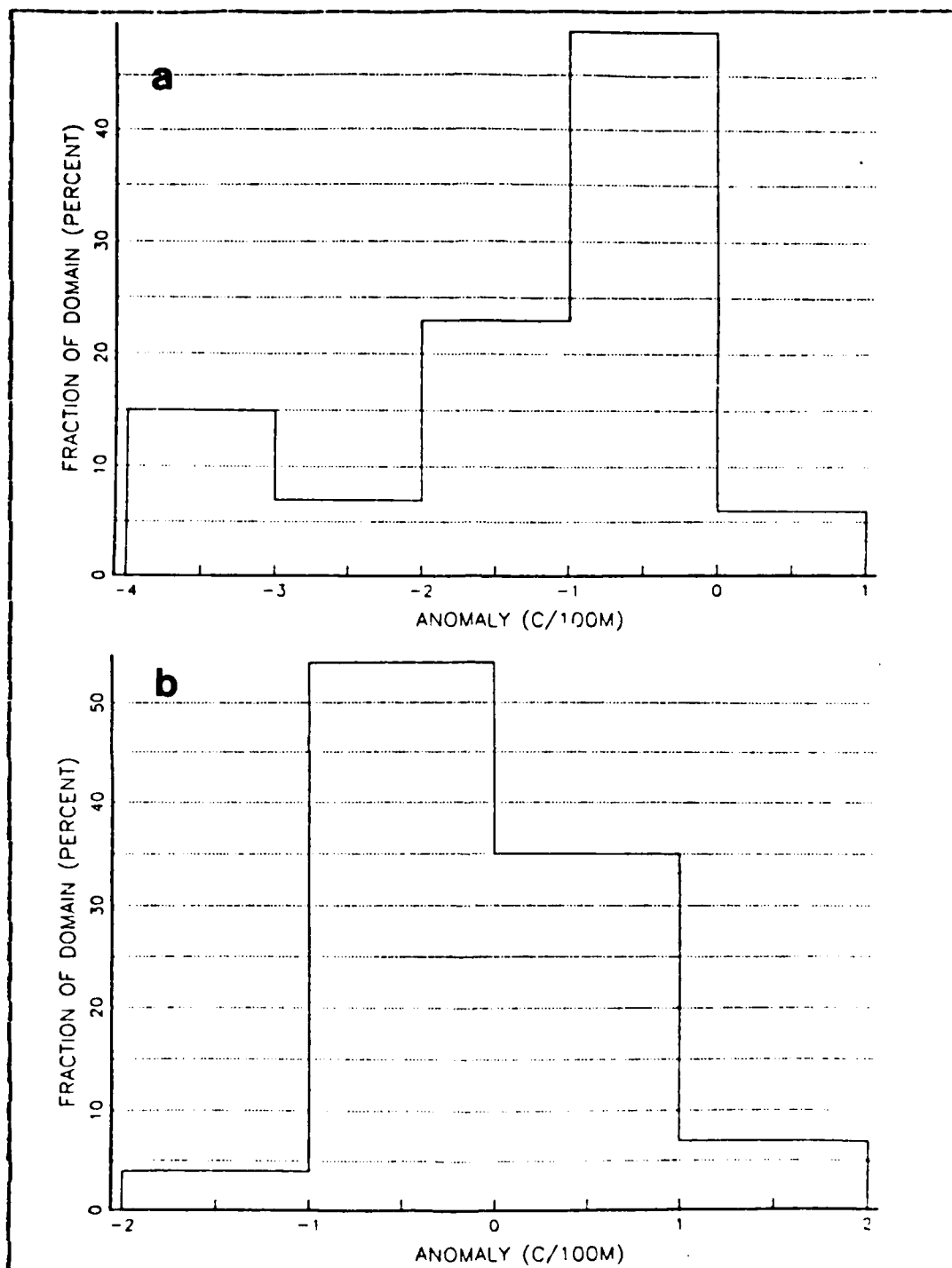
Figure 5.27   BLG Difference Distribution EOTS/Cruise AI
a. 16 Jun Analysis b. 23 Jun Analysis.

93
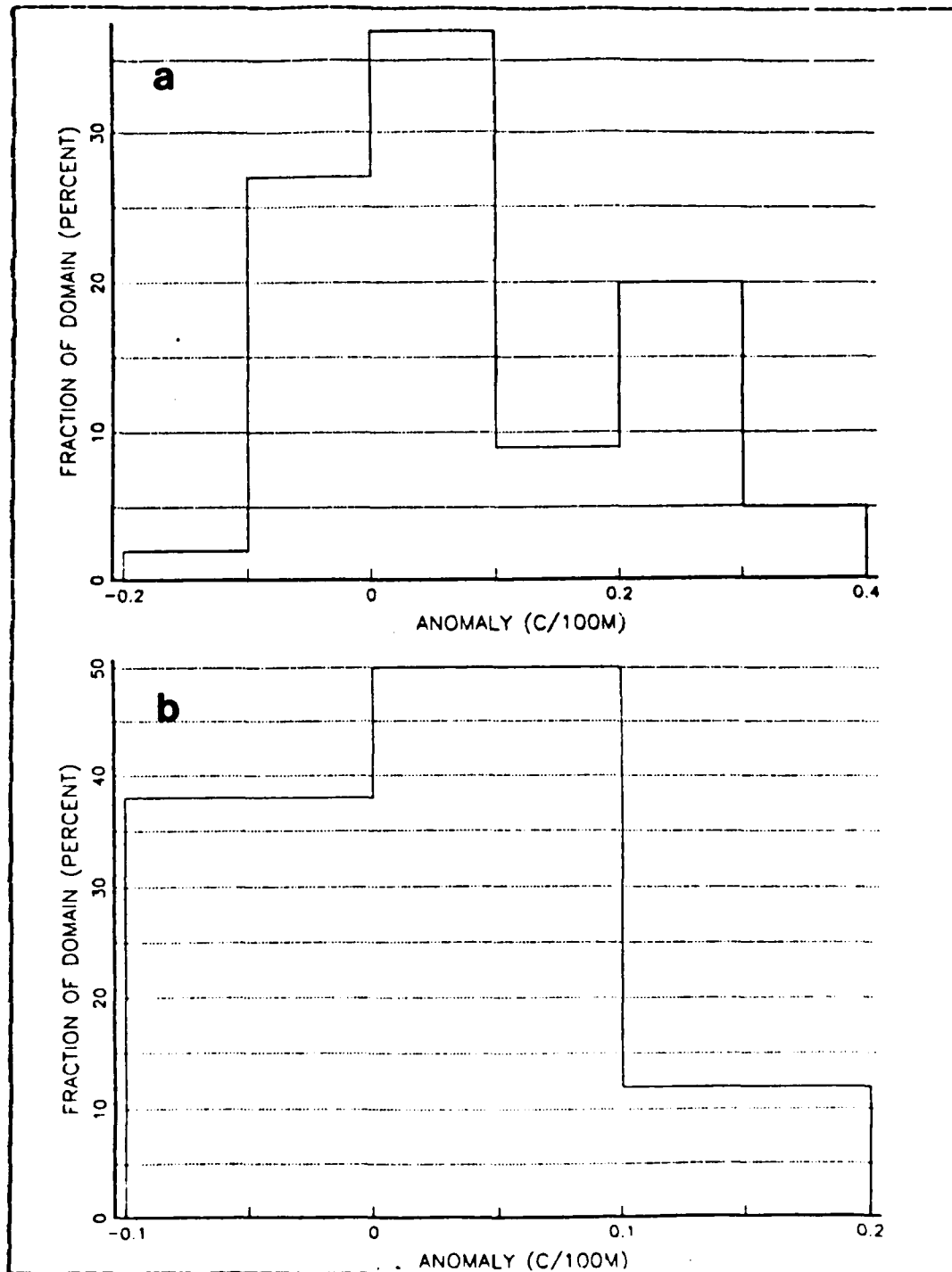
Figure 5.28   THG Difference Distribution EOTS/Cruise AI
a. 16 Jun Analysis b. 23 Jun Analysis.

94

END
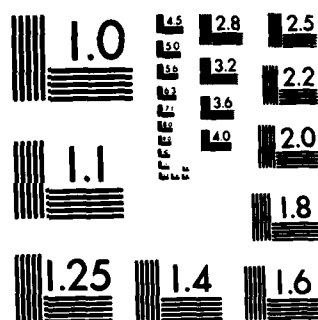
MICROCOPY RESOLUTION TEST CHART

NATIONAL BUREAU OF STANDARDS-1963-A
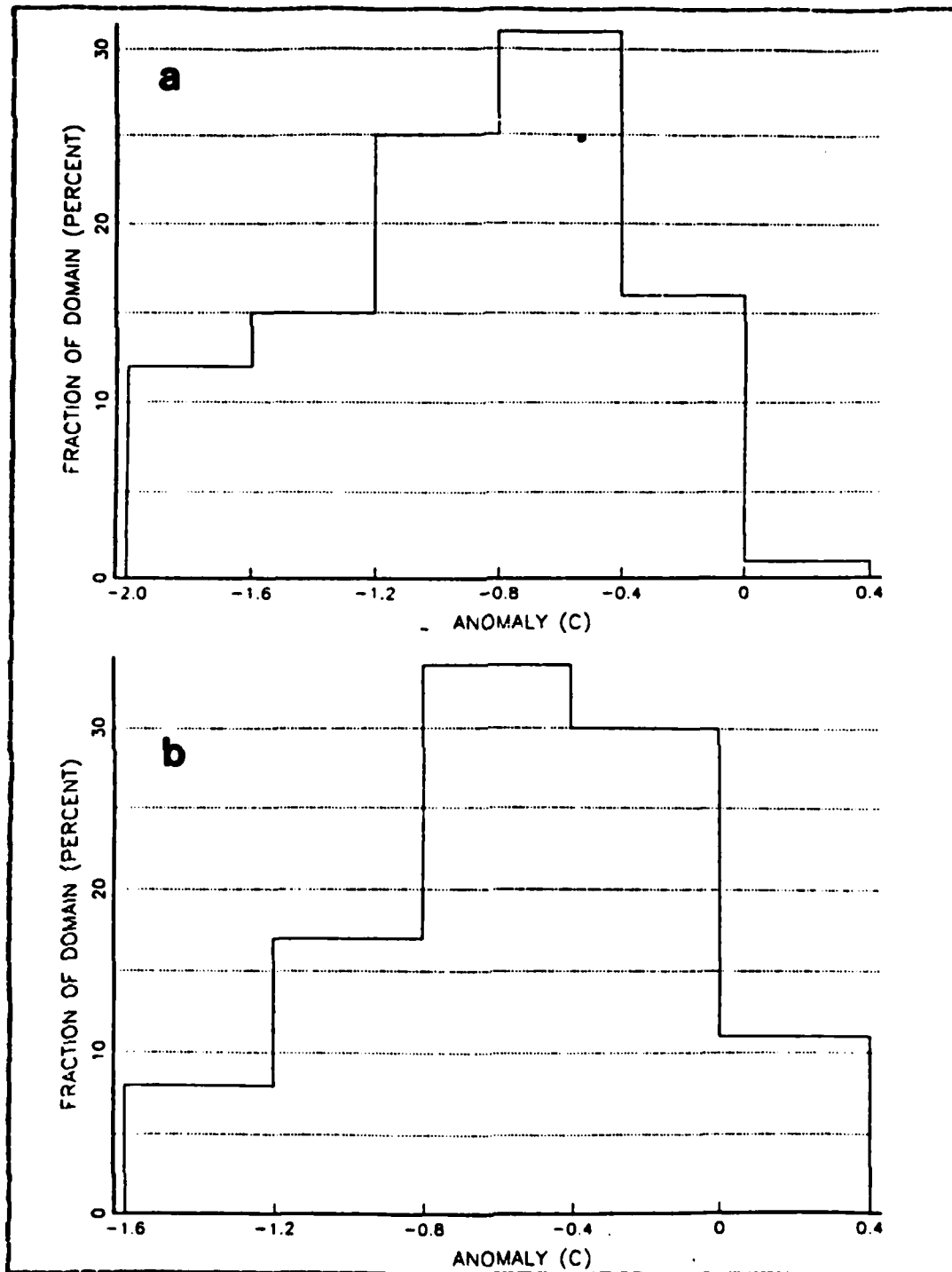
Figure 5.29   SST Difference Distribution TEOTS/Cruise AI
a. 16 Jun Analysis b. 23 Jun Analysis.
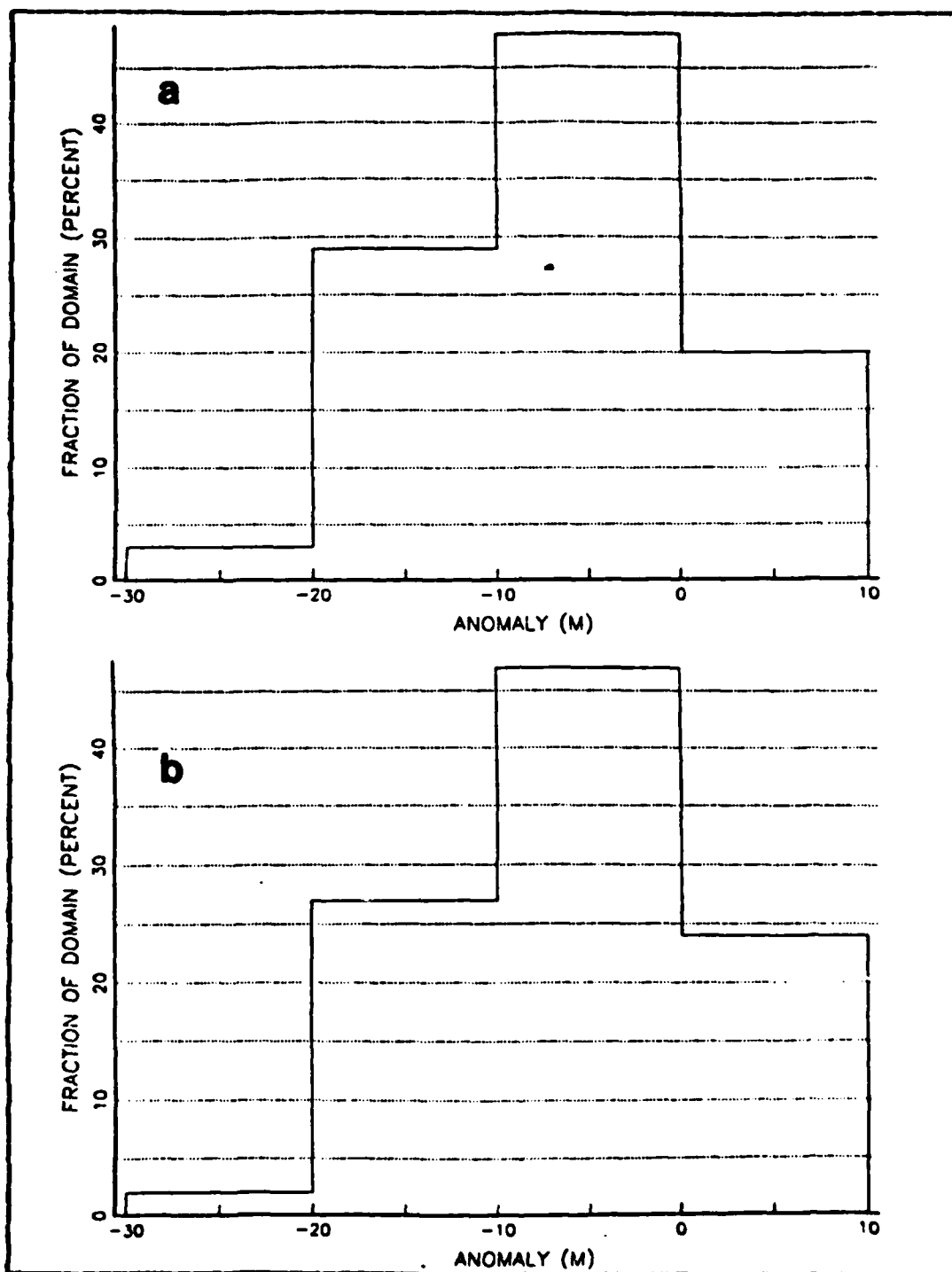
95

Figure 5.30 MLD Difference Distribution TEOTS/Cruise AI
a. 16 Jun Analysis b. 23 Jun Analysis.

96
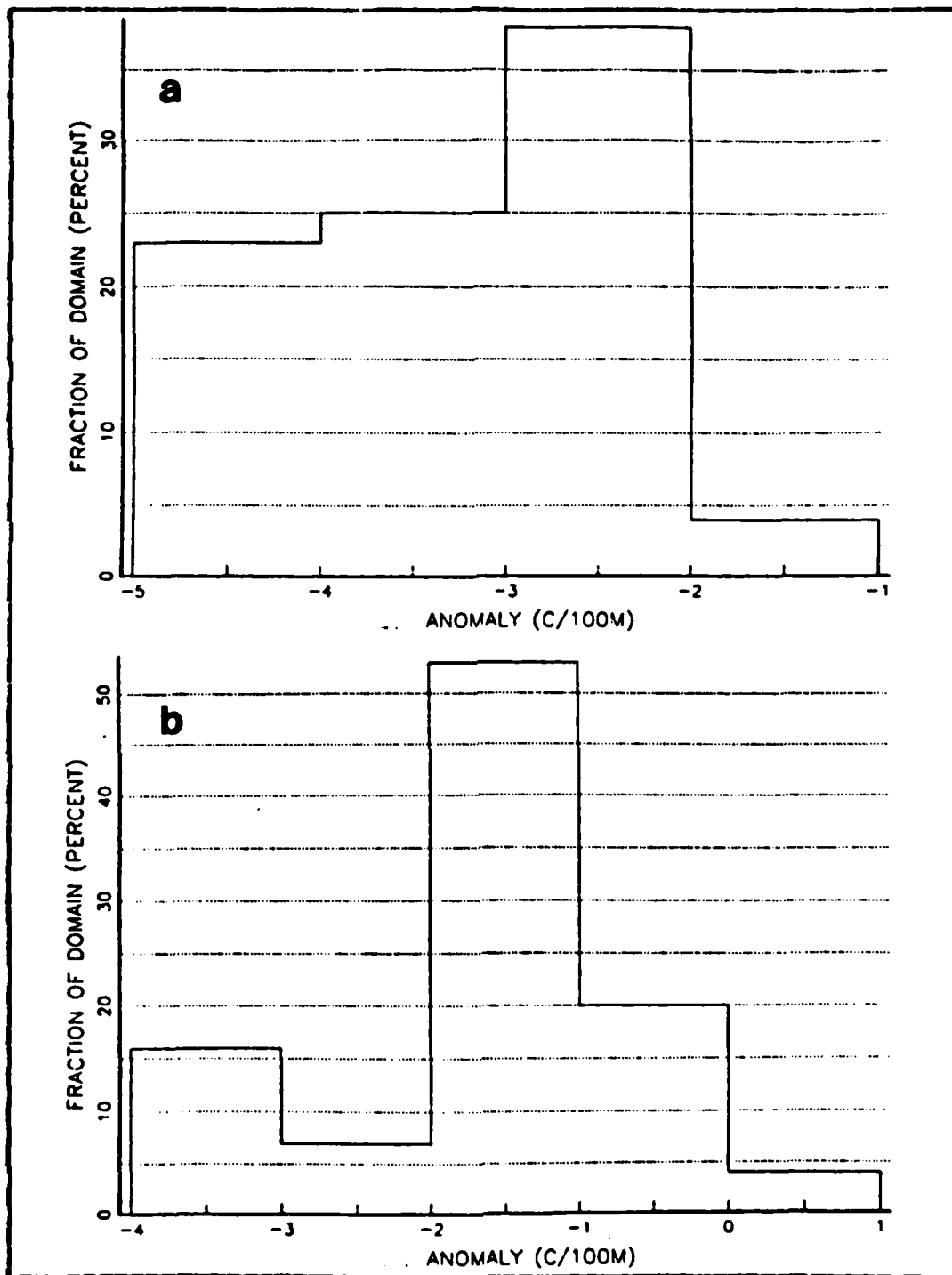
**Figure 5.31   BLG Difference Distribution TEOTS/Cruise AI
a. 16 Jun Analysis b. 23 Jun Analysis.**

97
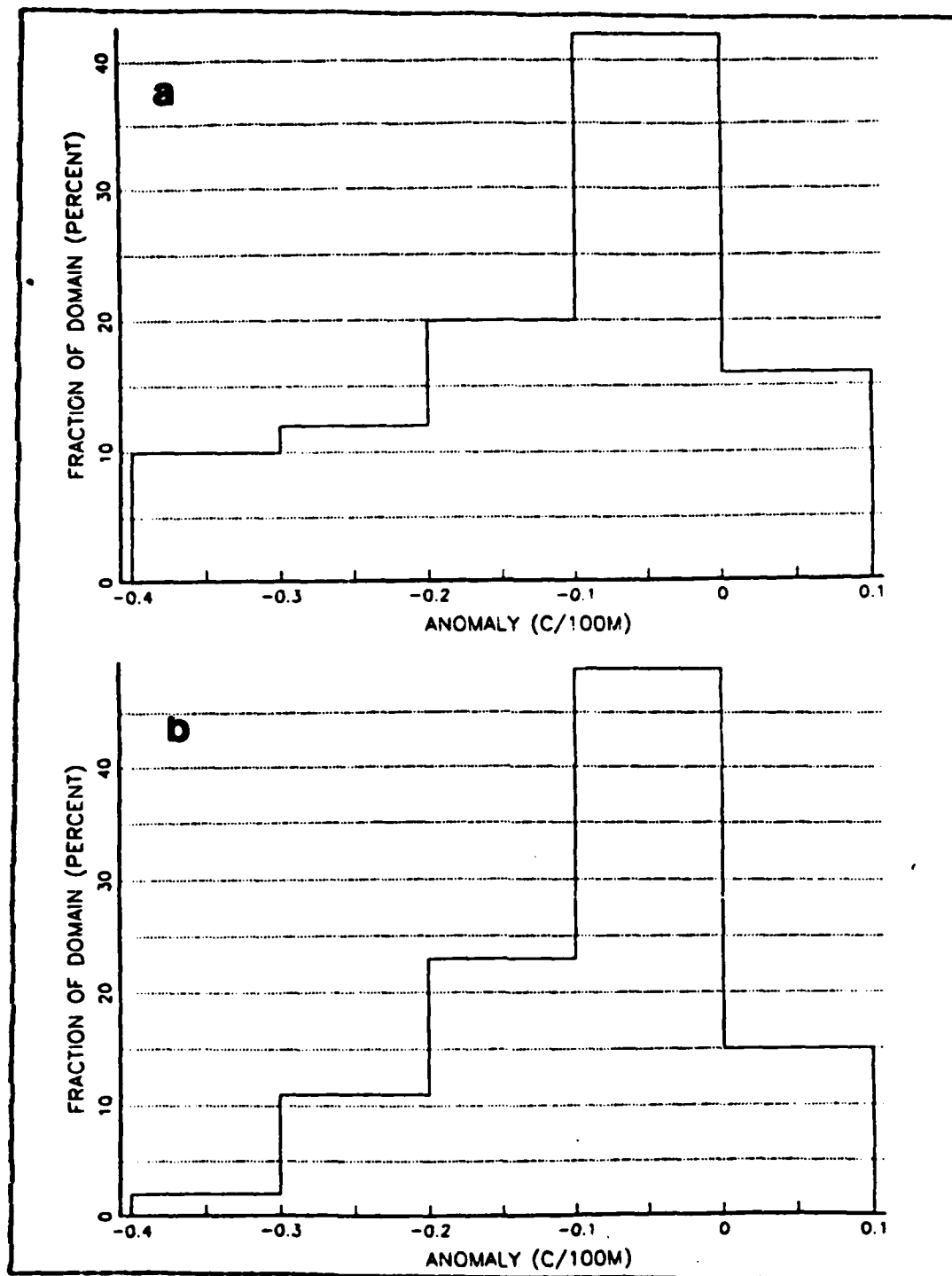
Figure 5.32   THG Difference Distribution TEOTS/Cruise AI
a. 16 Jun Analysis b. 23 Jun Analysis.

98
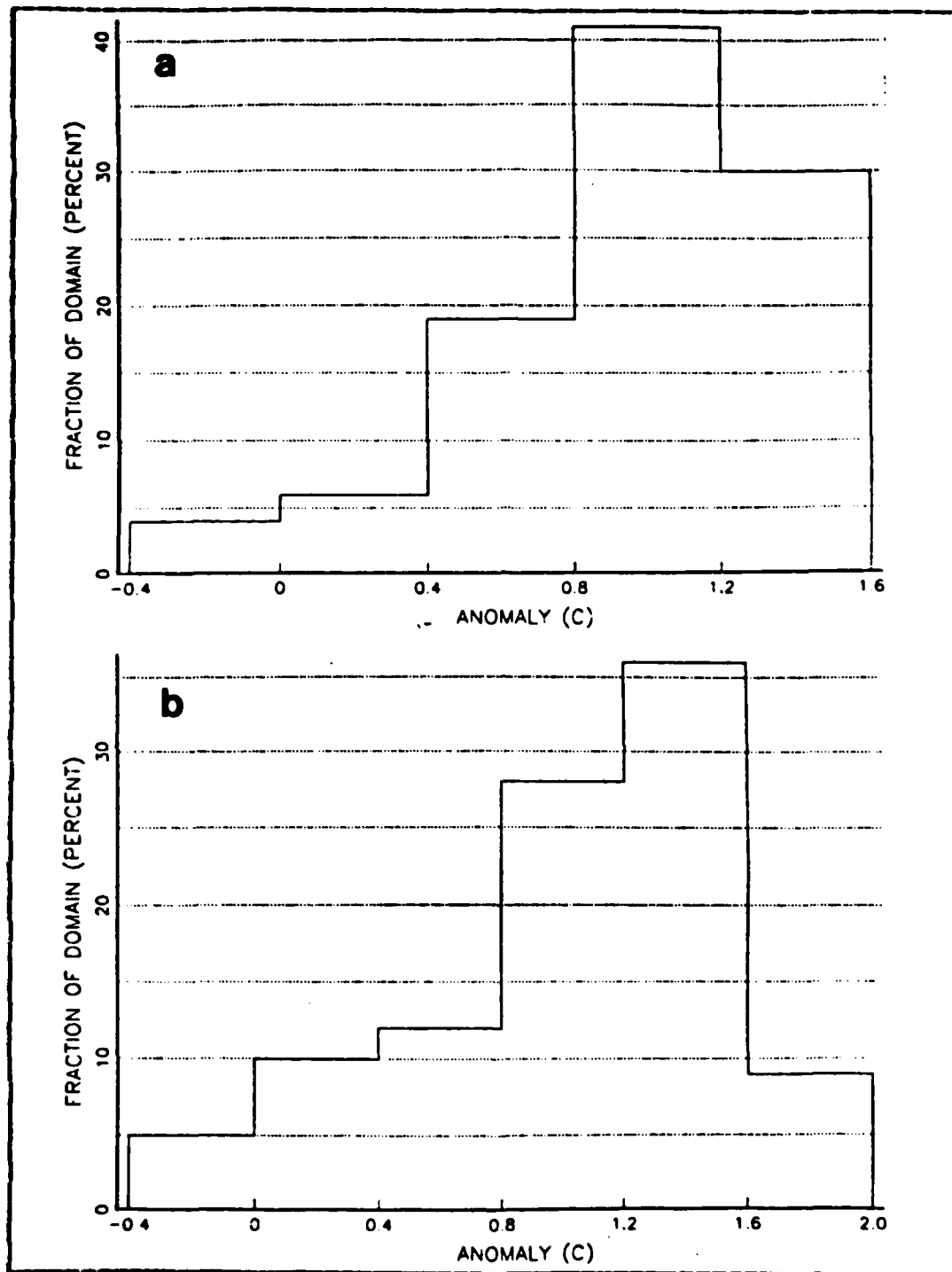
Figure 5.33 SST Difference Distribution EOTS/Cruise AII
a. 30 Jun Analysis b. 7 Jul Analysis.

99
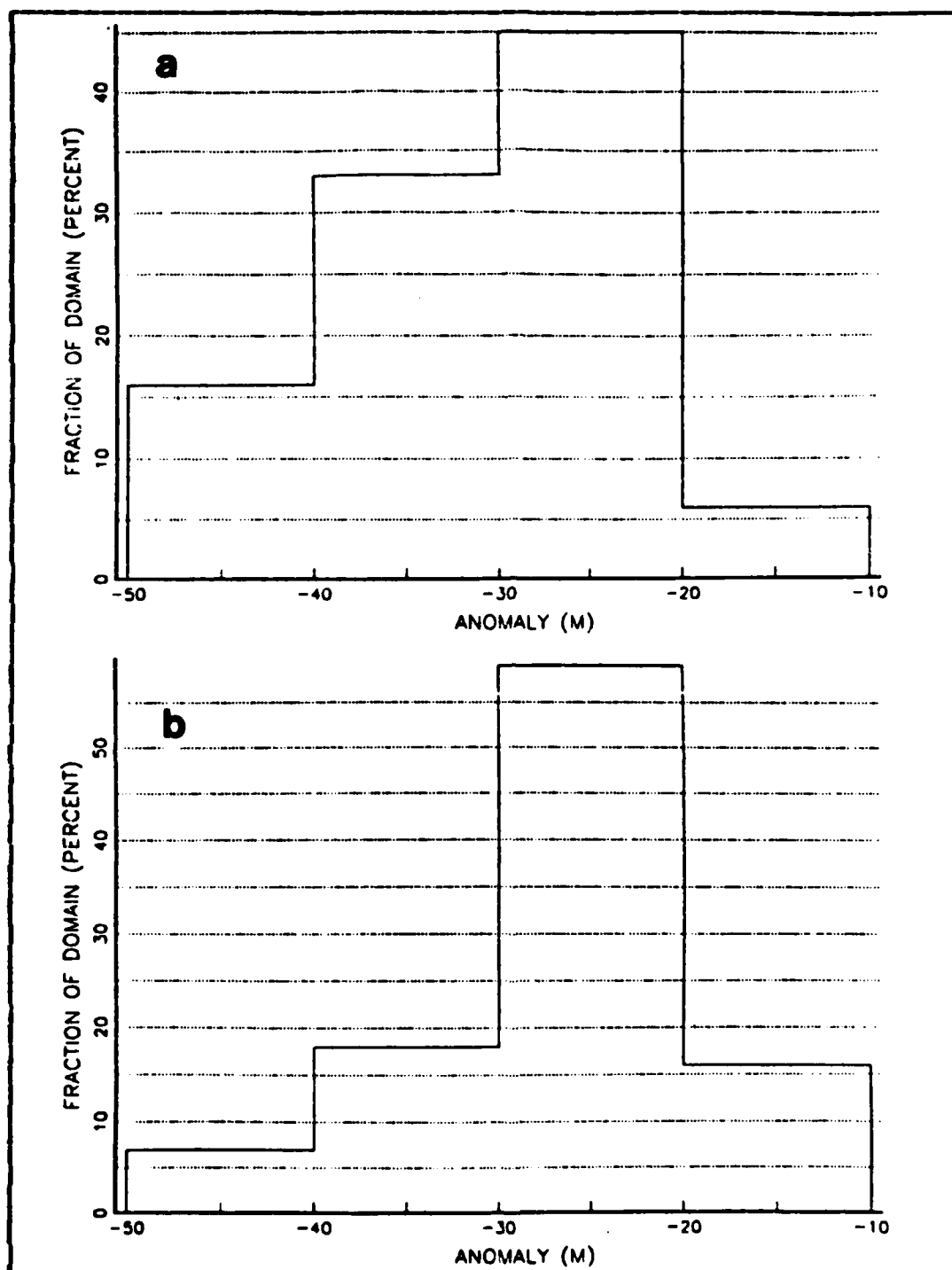
Figure 5.34   MLD Difference Distribution EOTS/Cruise AII
a. 30 Jun Analysis b. 7 Jul Analysis.

100
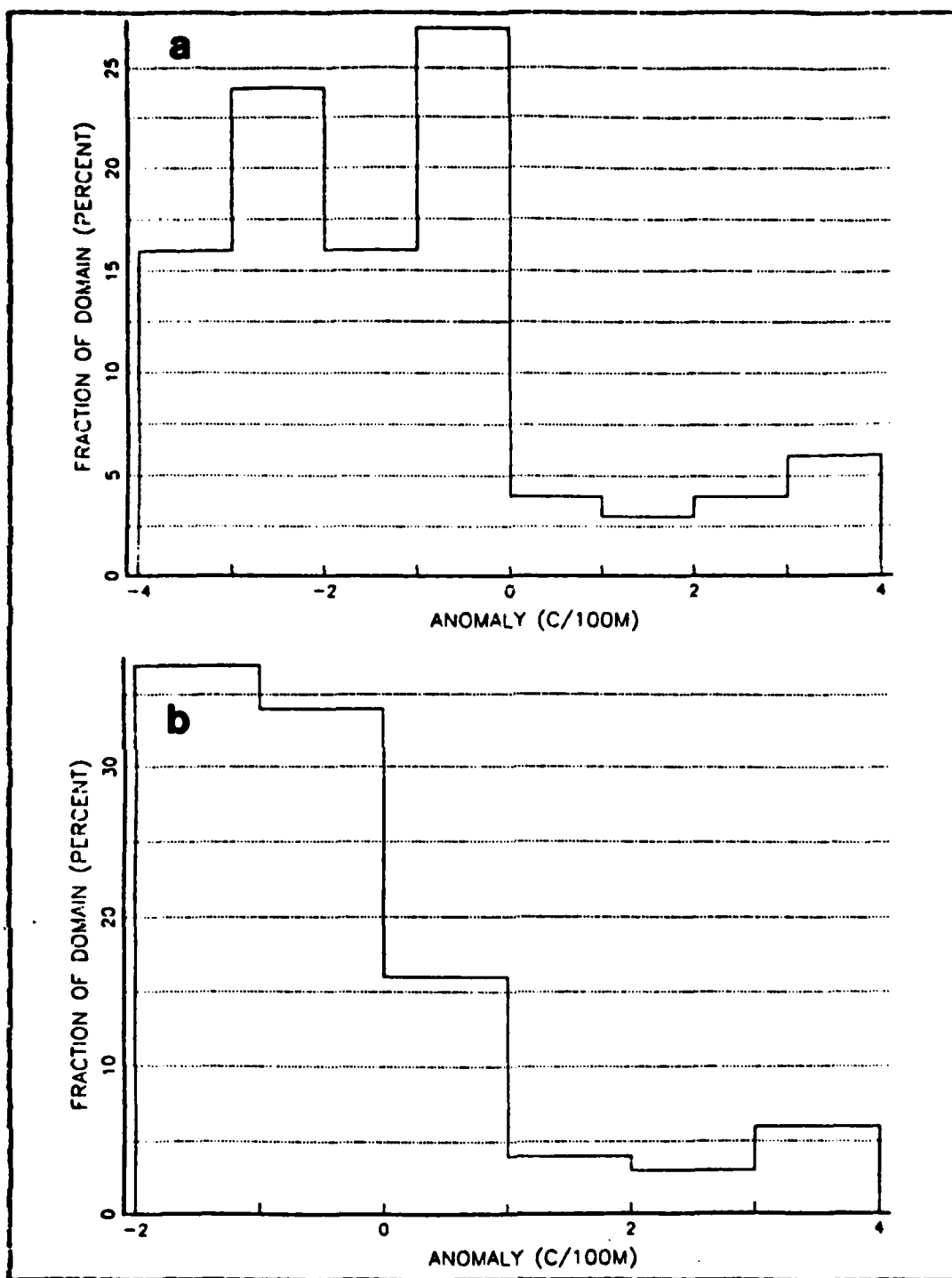
Figure 5.35   BLG Difference Distribution EOTS/Cruise AII
a. 30 Jun Analysis b. 7 Jul Analysis.

101
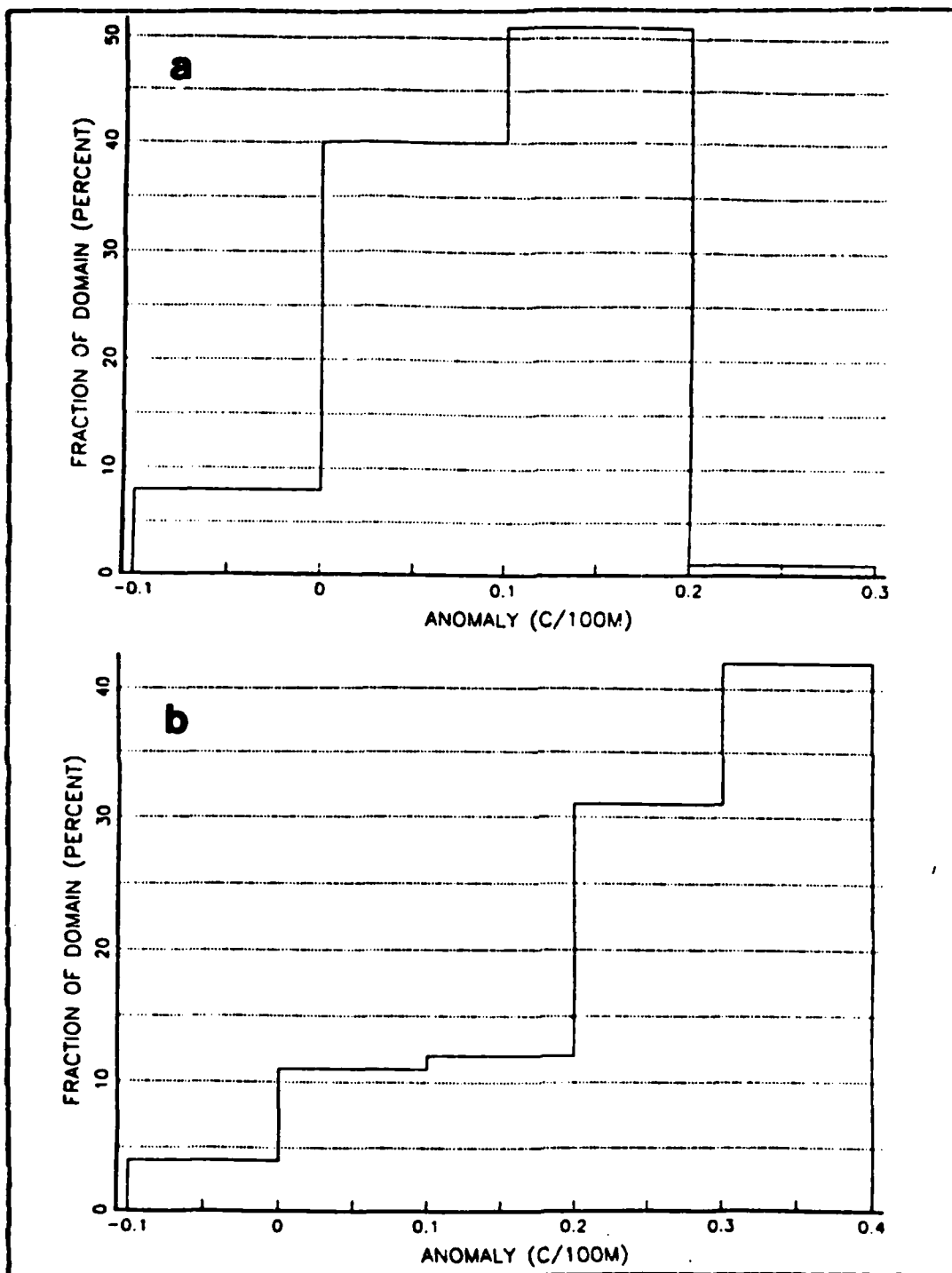
Figure 5.36   THG Difference Distribution EOTS/Cruise AII
a. 30 Jun Analysis b. 7 Jul Analysis.

102
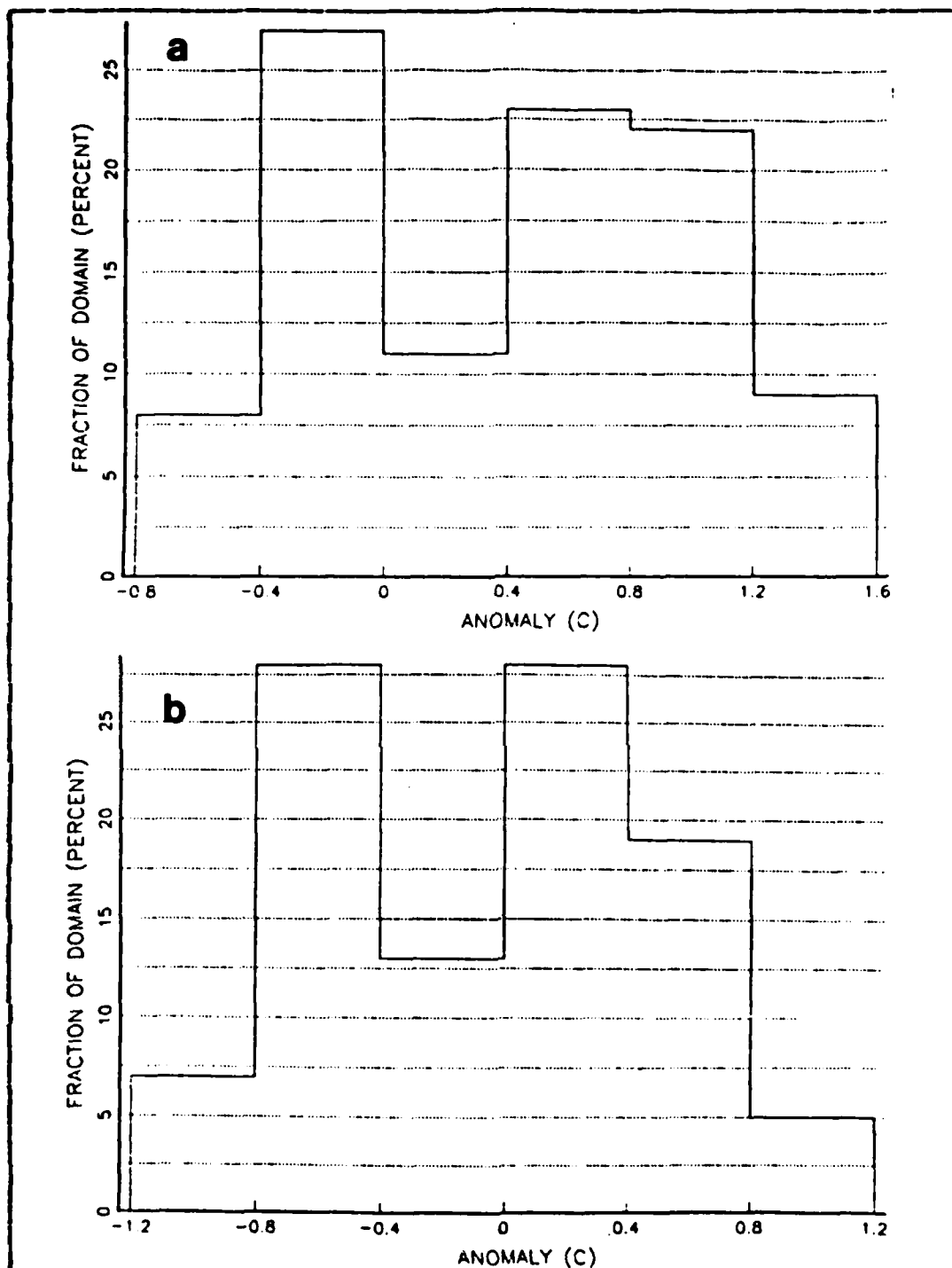
Figure 5.37 SST Difference Distribution TEOTS/Cruise AII
a. 30 Jun Analysis b. 7 Jul Analysis.

103
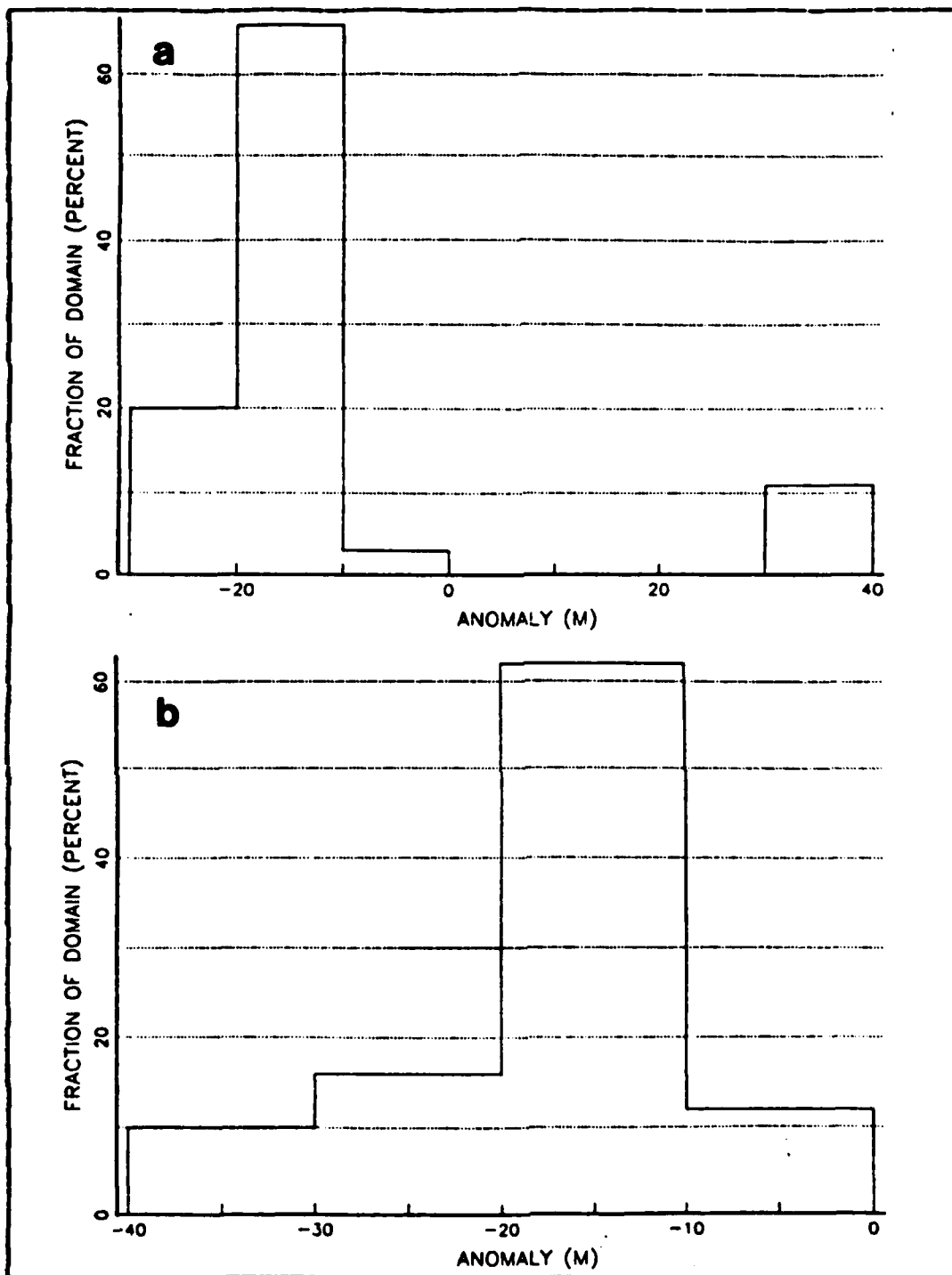
Figure 5.38   MLD Difference Distribution TEOTS/Cruise AII
a. 30 Jun Analysis b. 7 Jul Analysis.

104
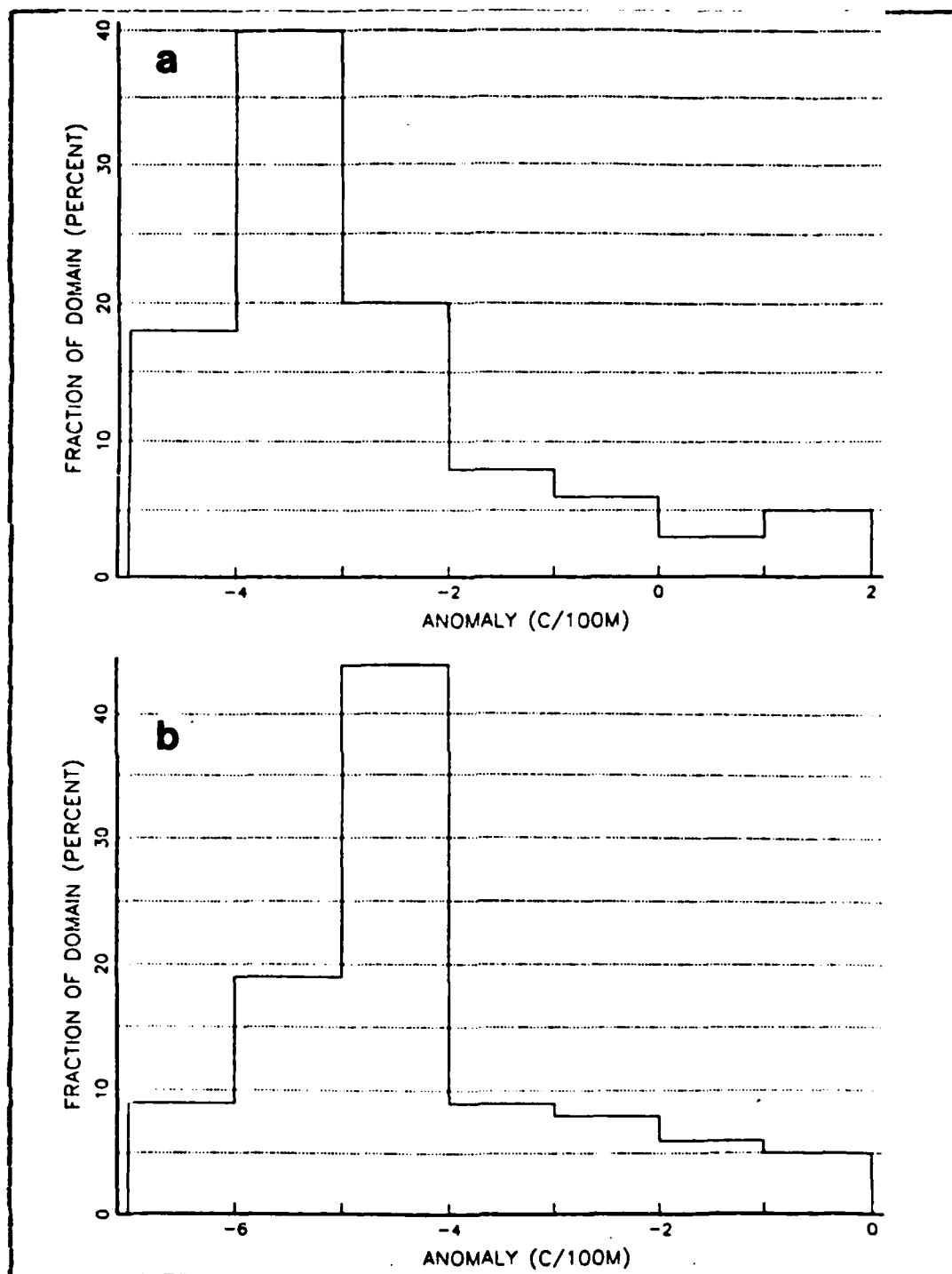
Figure 5.39   BLG Difference Distribution TEOTS/Cruise AII
a. 30 Jun Analysis b. 7 Jul Analysis.

105
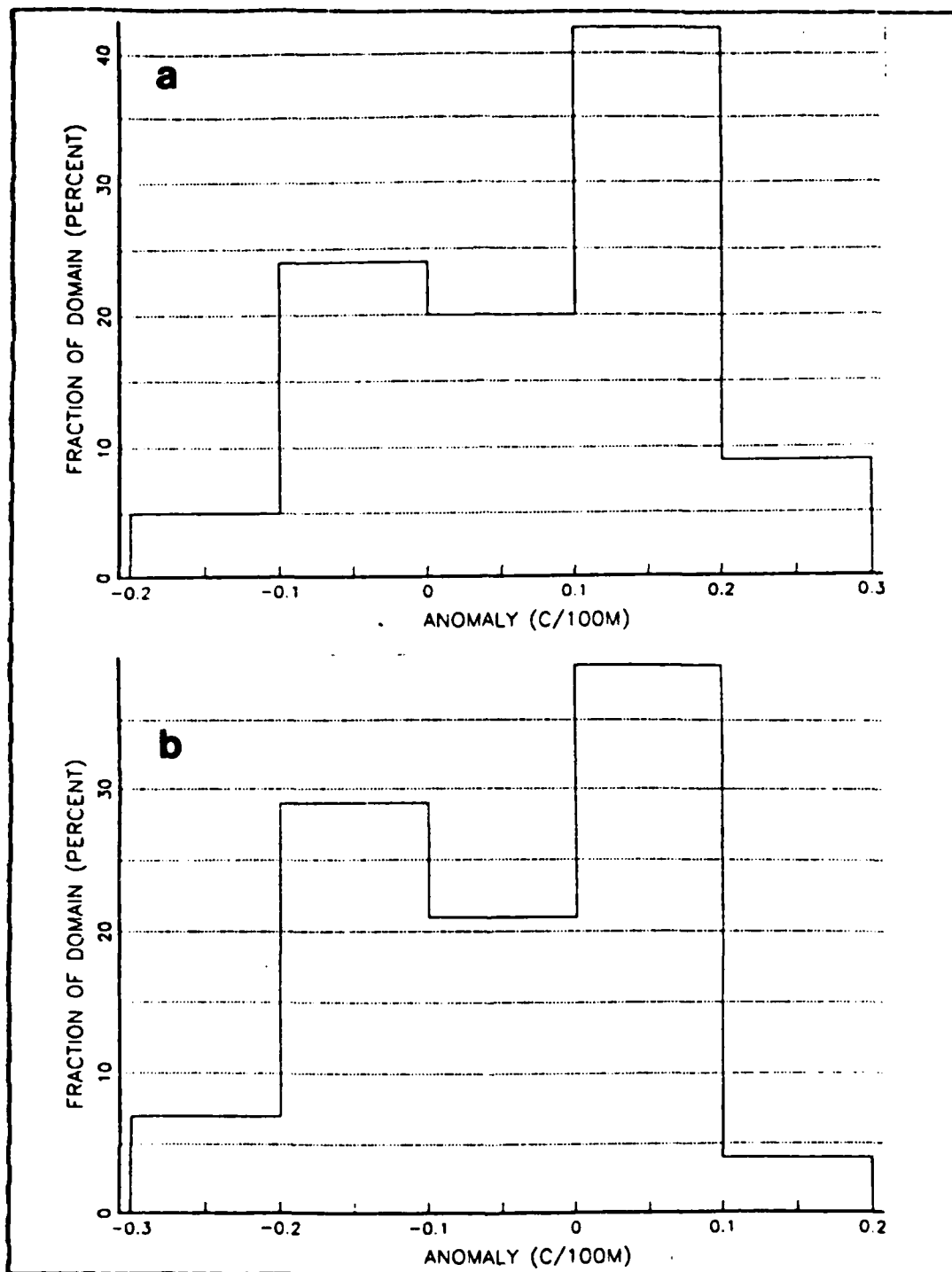
Figure 5.40   THG Difference Distribution TEOTS/Cruise AII
a. 30 Jun Analysis b. 7 Jul Analysis.

106
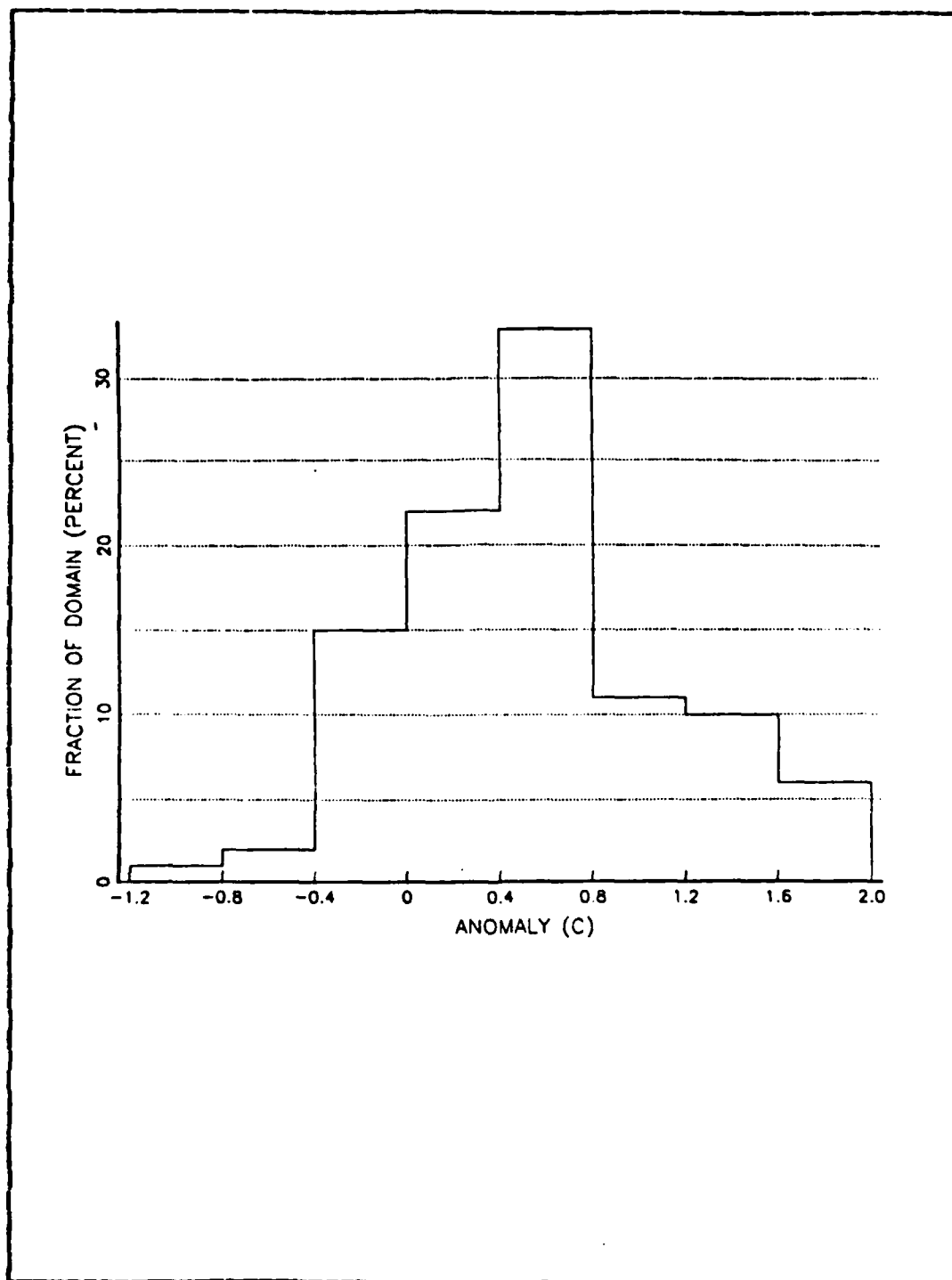
**Figure 5.41   SST Difference Distribution EOTS/Cruise AII
10 Jul Analysis.**

107
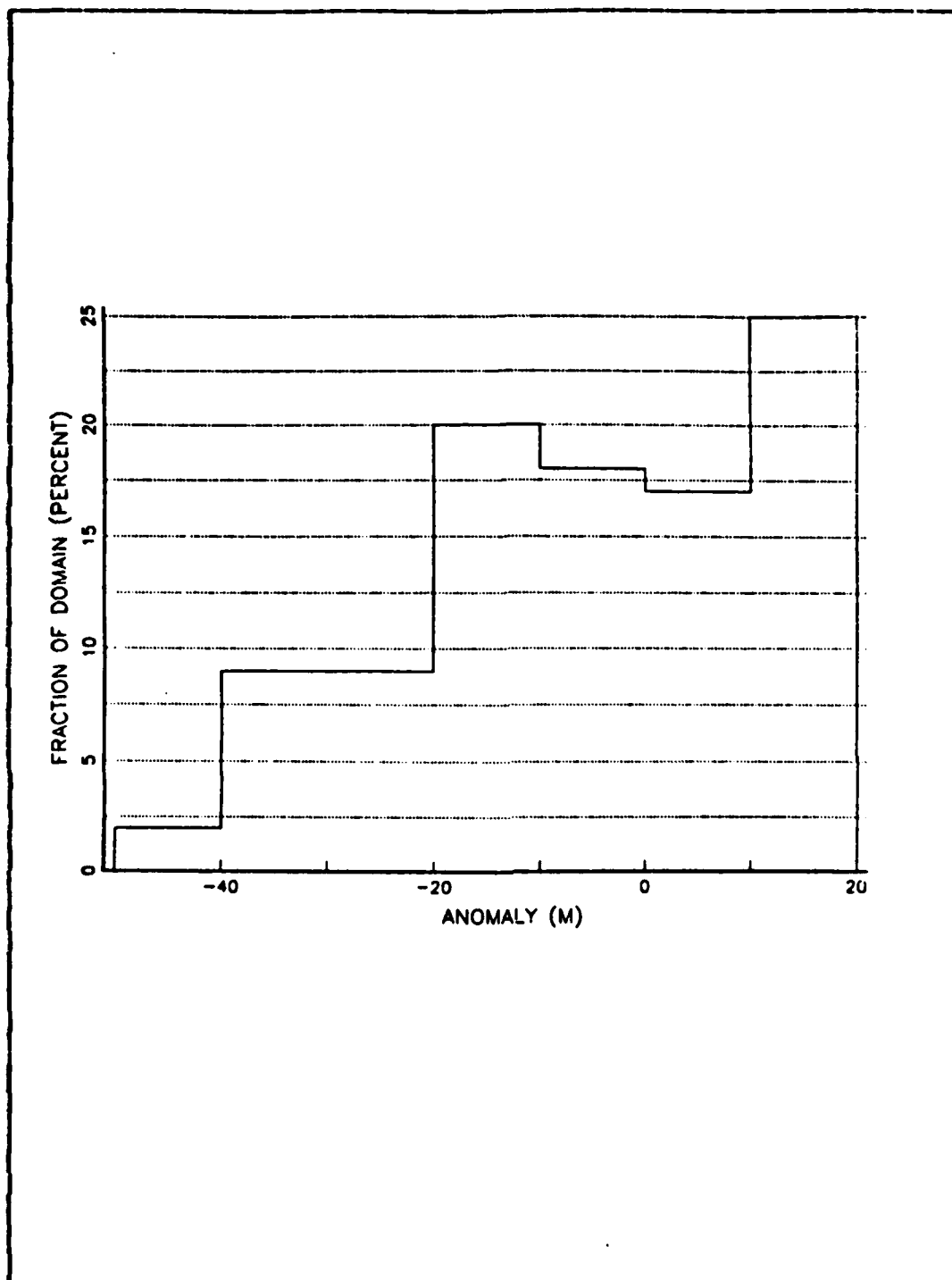
Figure 5.42   MLD Difference Distribution EOTS/Cruise AII 10 Jul Analysis.

108
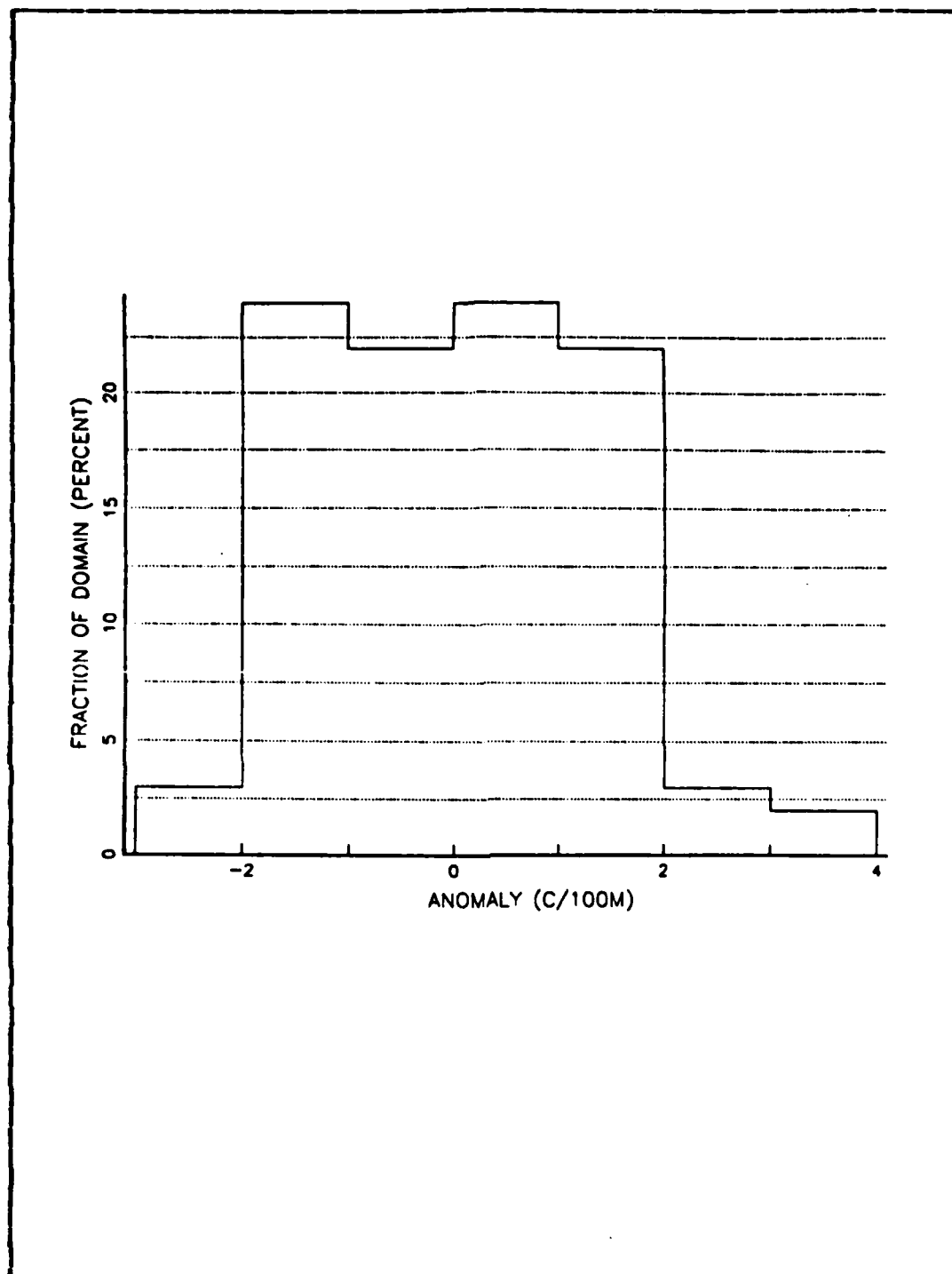
Figure 5.43   BLG Difference Distribution EOTS/Cruise AII
10 Jul Analysis.

109
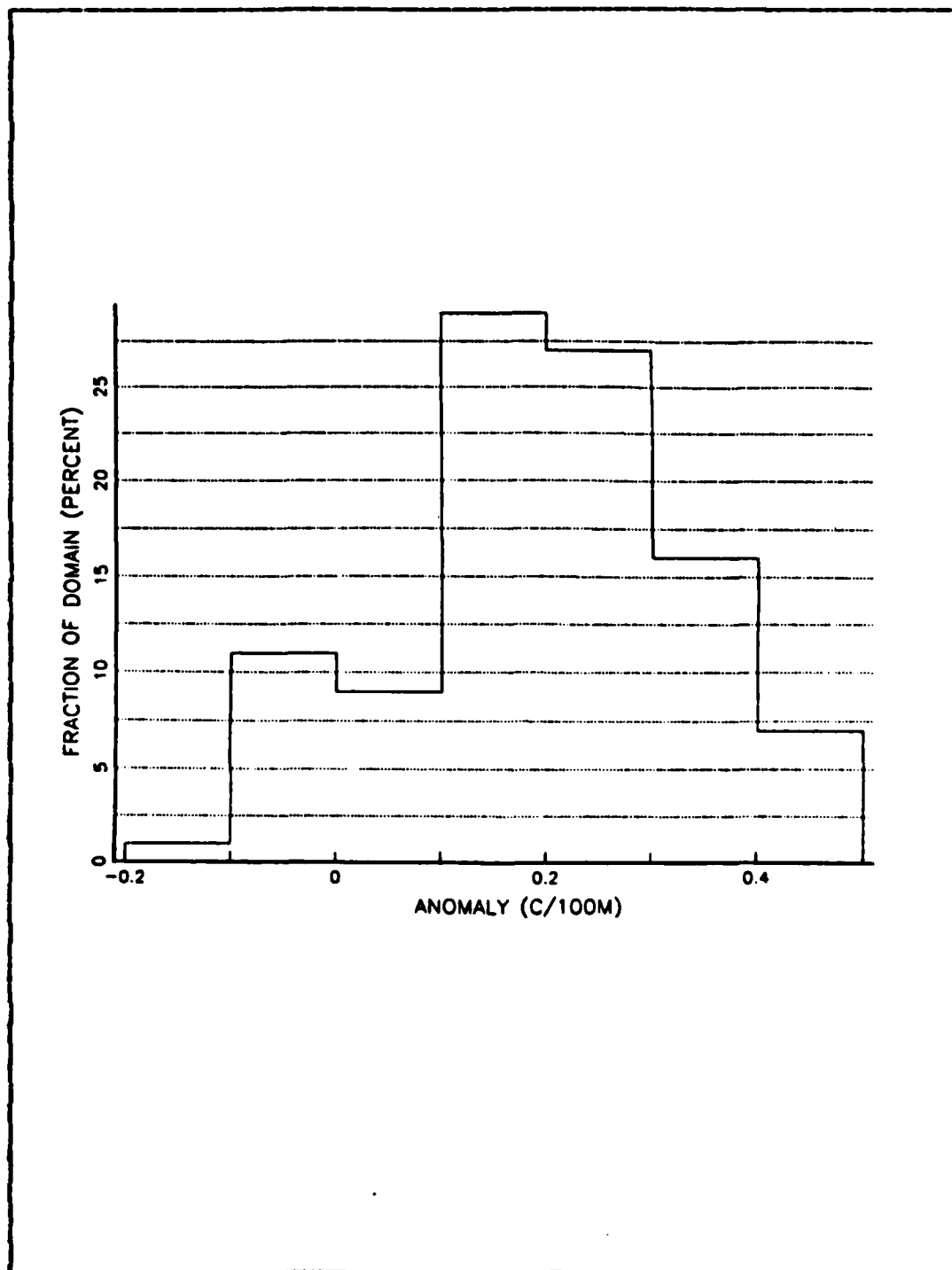
Figure 5.44   THG Difference Distribution EOTS/Cruise AII 10 Jul Analysis.

110
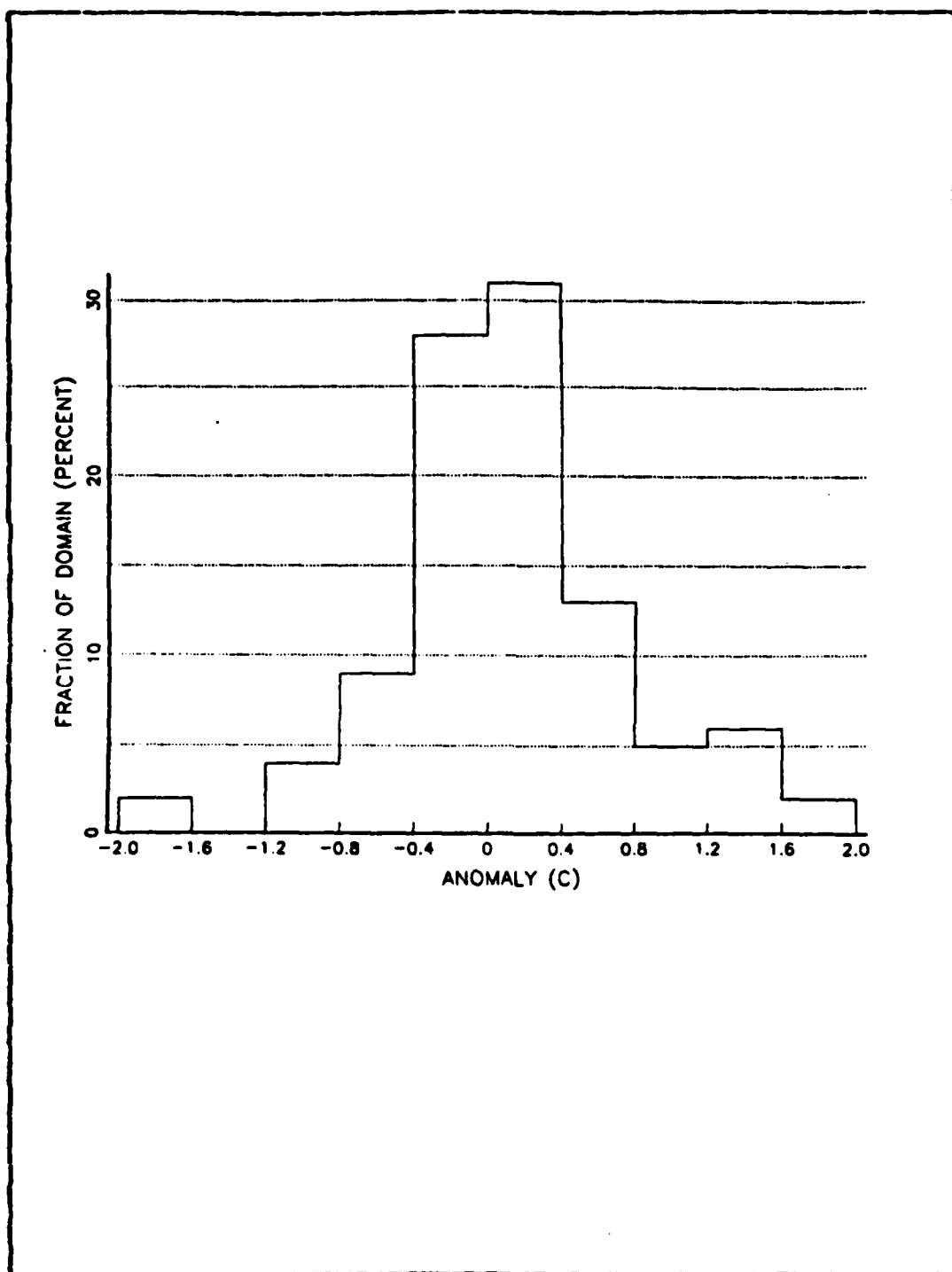
Figure 5.45 SST Difference Distribution TEOTS/Cruise AII 10 Jul Analysis.
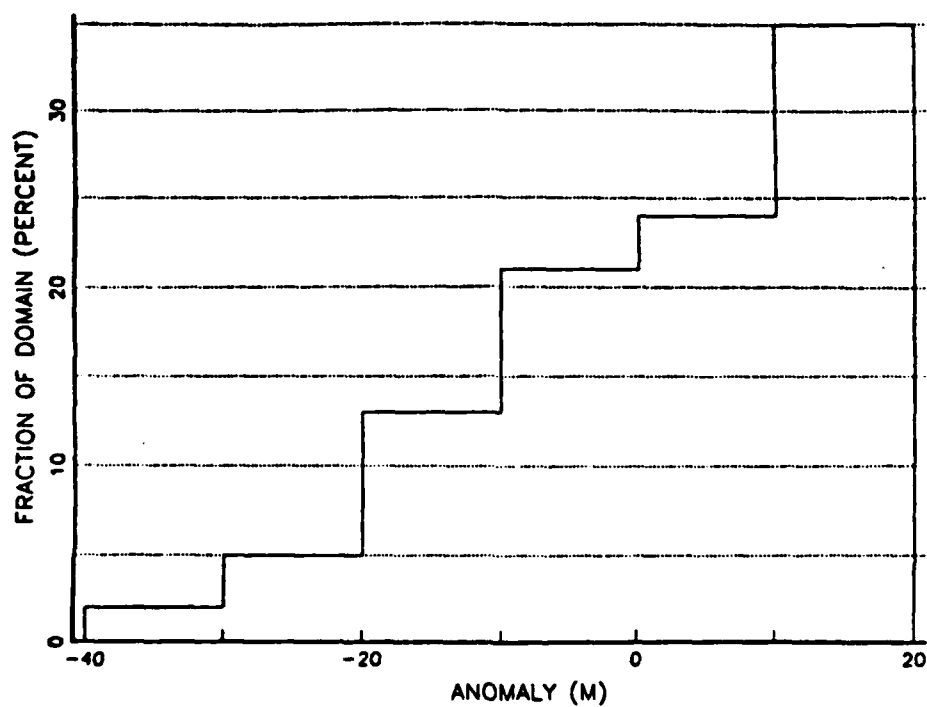
111

Figure 5.46   MLD Difference Distribution TEOTS/Cruise AII 10 Jul Analysis.

112
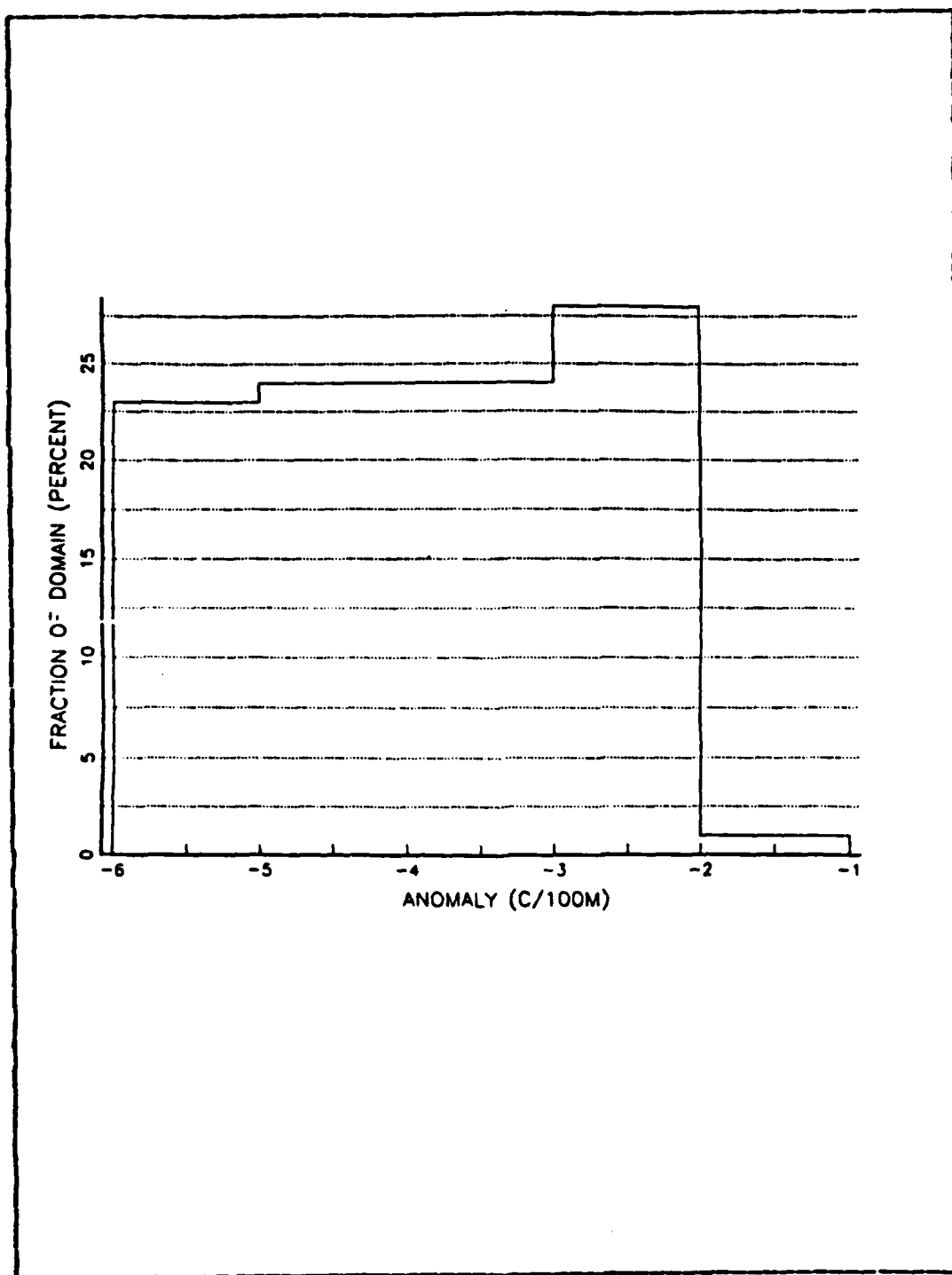
Figure 5.47   BLG Difference Distribution TEOTS/Cruise AII
10 Jul Analysis.

113
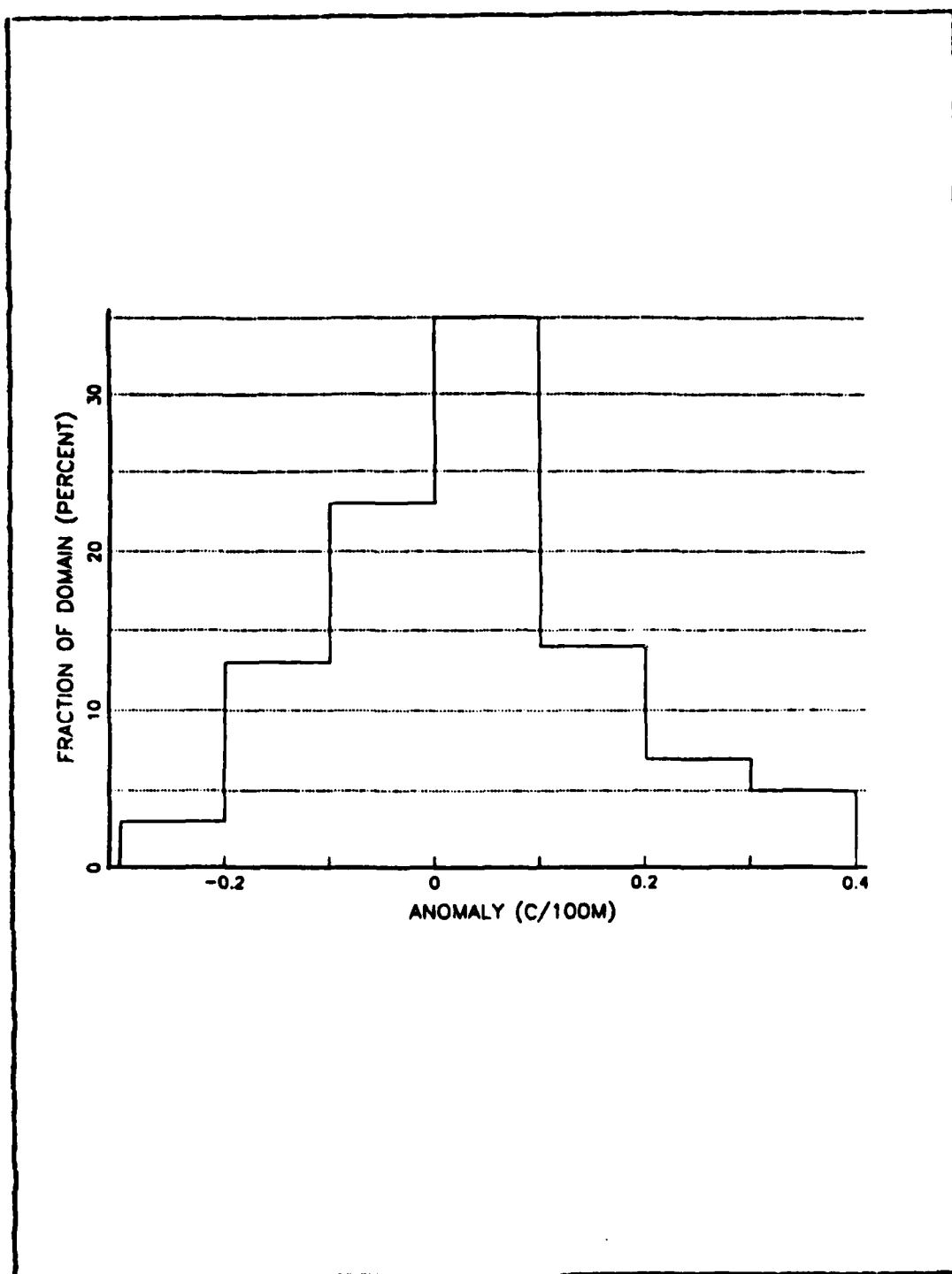
Figure 5.48   THG Difference Distribution TEOTS/Cruise AII
10 Jul Analysis.

114
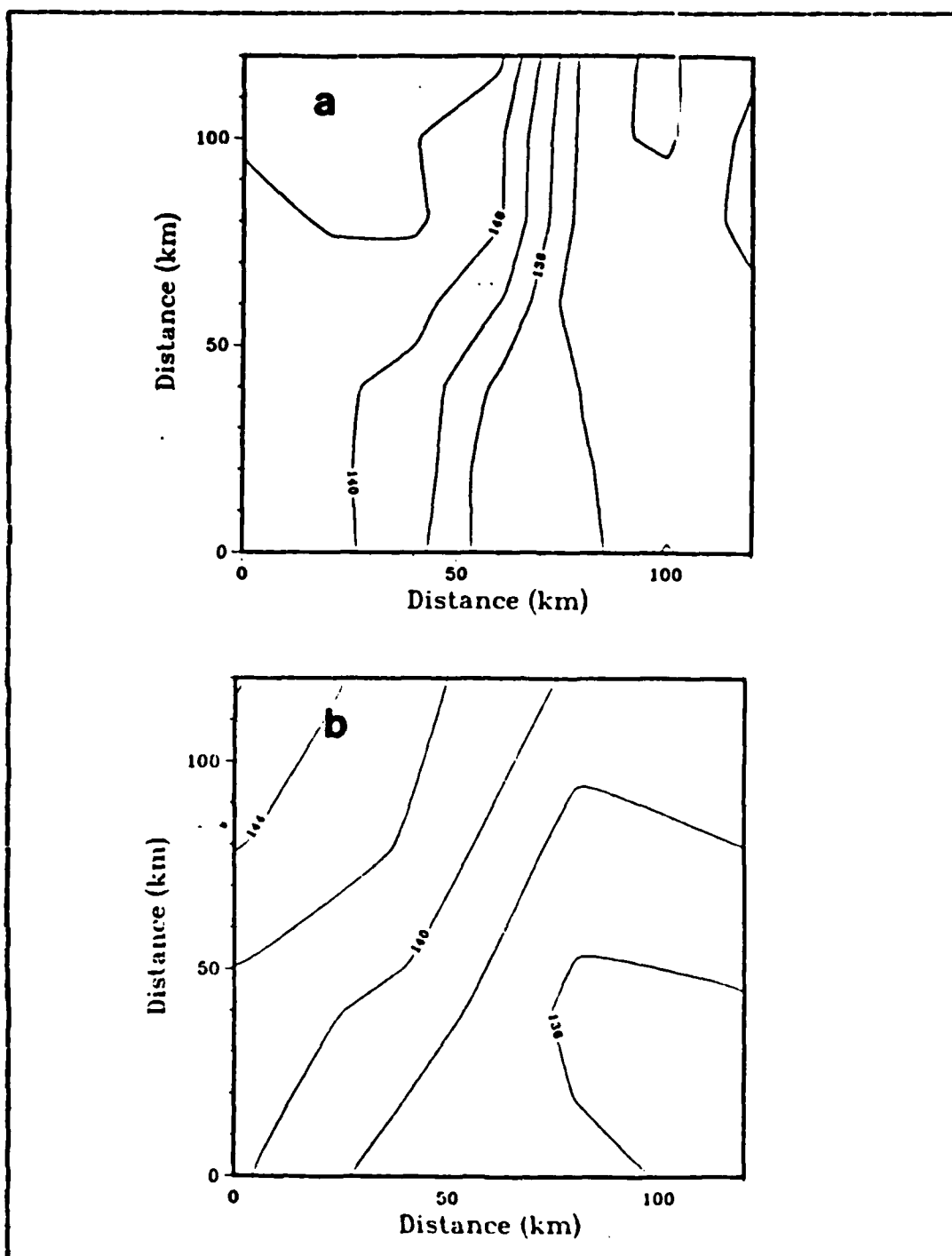
Figure 5.49   SST Contour Fields: (a) EOTS 23 Jun Analysis
(b) Author's Contouring Program
(same inputs as EOTS 23 Jun Analysis).

115
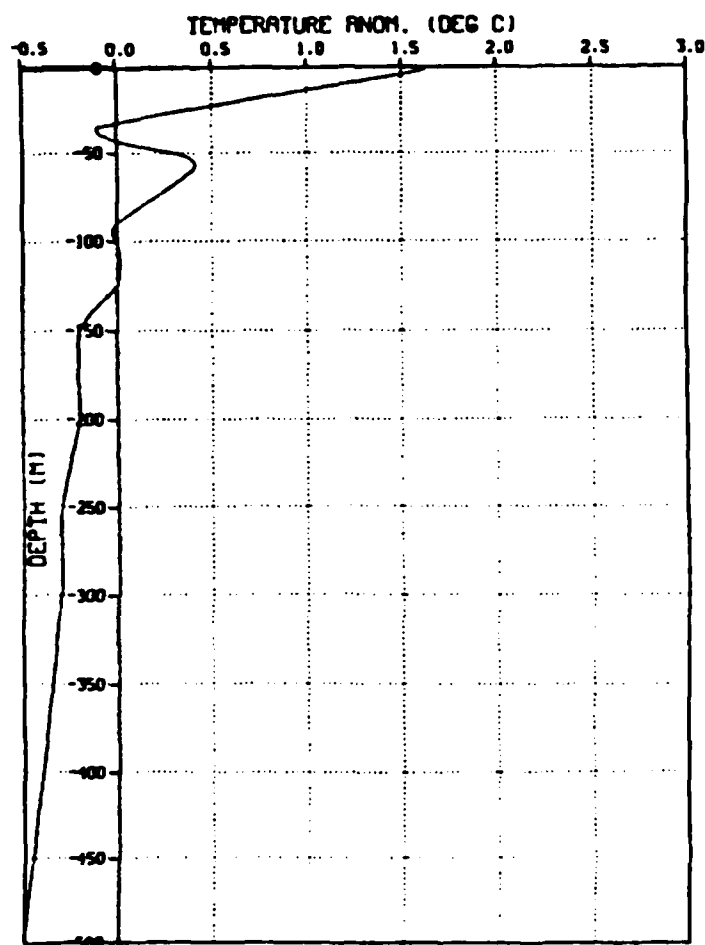
Figure 5.50   Temperature Anomaly vs. Depth
Jul 1982-FNOC Climatology.

116

TEMPERATURE ANOMALY (CCS5-CCS2)
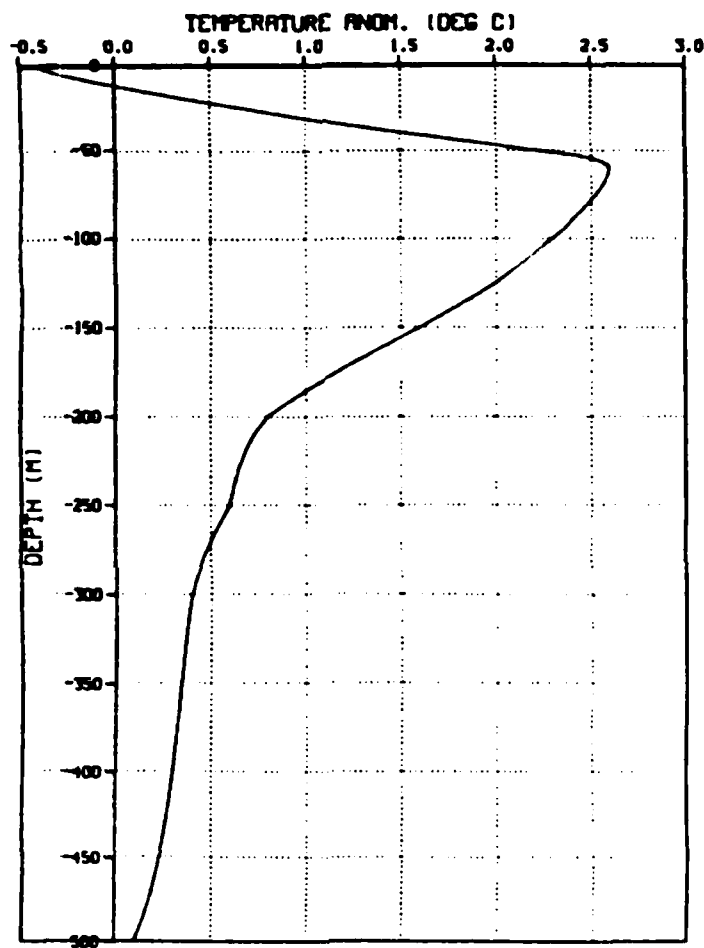
Figure 5.51   Temperature Anomaly vs. Depth
Jul 1983-Jul 1982.

117

Figure 5.52   Temperature Anomaly vs. Depth
Jul 1983-FNOC Climatology.

118

CLIMAT SSP JULY

SOURCE DEPTH 20.00 M, RECEIVER DEPTH 20.00 M, WATER DEPTH 4000.00 M
SLD 12.00 M., WAVE HEIGHT 1.0 M., USER DEF BTM
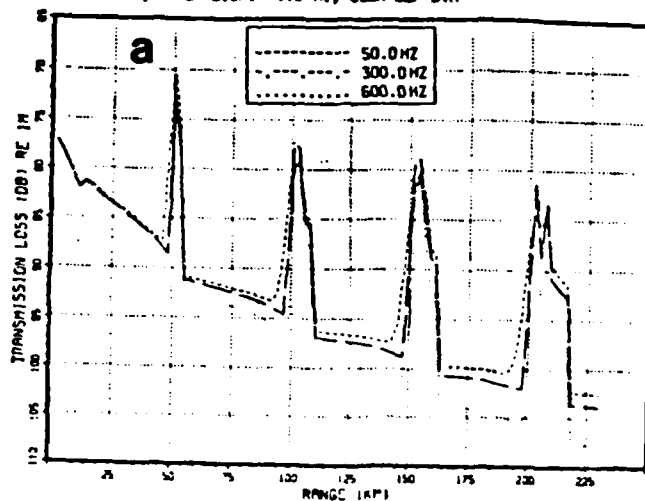
CCS5AV SSP 1983

SOURCE DEPTH 20.00 M, RECEIVER DEPTH 20.00 M, WATER DEPTH 4000.00 M
SLD 35.00 M., WAVE HEIGHT 1.0 M., USER DEF BTM
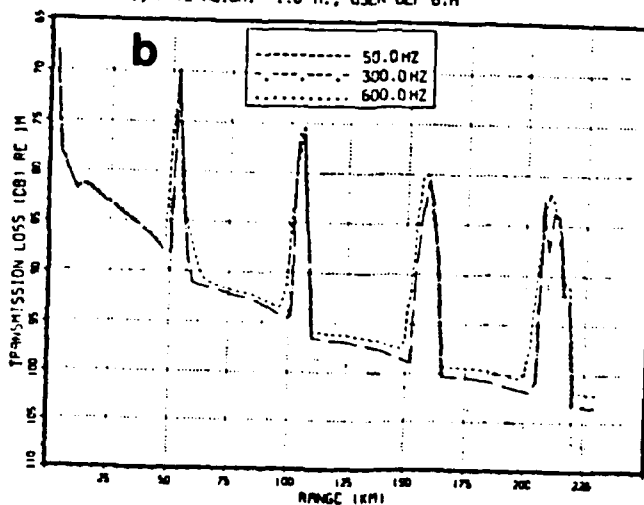
Figure 5.53   Transmission Loss Curves-S/S Disposition
   a. Climatology b. OPTOMA5 AIII (mean profile).

119

CLIMAT SSP JULY

SOURCE DEPTH 200.00 M, RECEIVER DEPTH 20.00 M, WATER DEPTH 4000.00 M
SLD 12.00 M., WAVE HEIGHT 1.0 M., USER DEF BTM
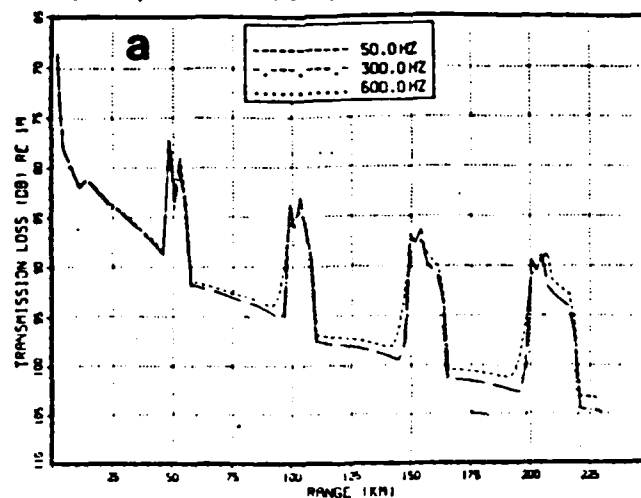
CCSSAV SSP 1983

SOURCE DEPTH 200.00 M, RECEIVER DEPTH 20.00 M, WATER DEPTH 4000.00 M
SLD 35.00 M., WAVE HEIGHT 1.0 M., USER DEF BTM
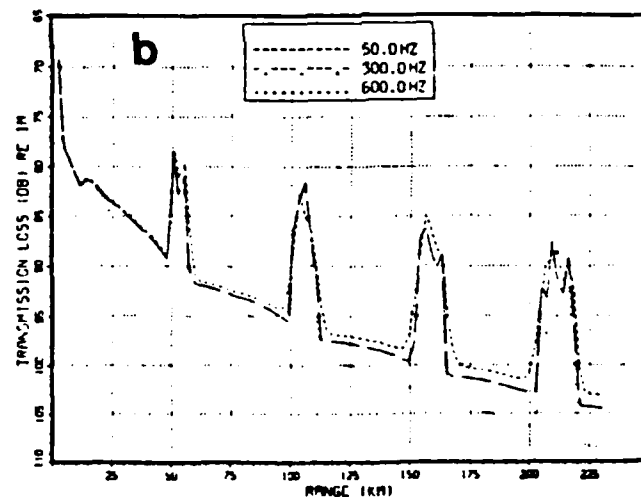
Figure 5.54   Transmission Loss Curves-S/D Disposition
a. Climatology b. OPTOMA5 AIII (mean profile).

120
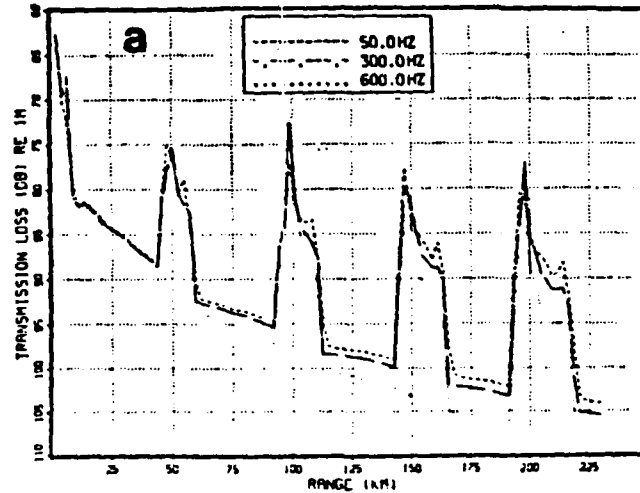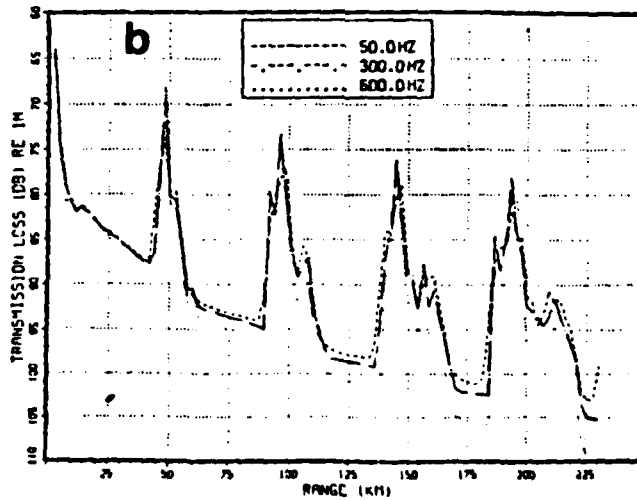
Figure 5.55   Transmission Loss Curves-D/D Disposition
a. Climatology b. OPTOMA5 AIII (mean profile).

121

TABLE II
Comparison Statistics Cruise AI

PARAMETER	MODEL	EOTS		TEOTS	
	ANALYSIS DATE	16 Jun	23 Jun	16 Jun	23 Jun
SST (° C)	mean	-0.80	0.10	-0.90	-0.50
	std. deviation	0.50	0.30	0.50	0.40
	median	-0.60	0.20	-1.00	-0.60
	skewness	-0.40	-0.30	-0.30	-0.20
MLD (m)	mean	-19.4	-17.9	-6.50	-5.70
	std. deviation	7.70	7.30	7.70	7.70
	median	-15.0	-15.0	-5.00	-5.00
	skewness	0.10	0.20	-0.10	-0.20
BLG (°C/100m)	mean	-1.26	-0.05	-3.24	-1.60
	std. deviation	1.16	0.70	0.90	1.00
	median	-0.50	-0.50	-3.50	-1.50
	skewness	-0.80	0.50	-0.10	-0.40
THG (°C/100m)	mean	0.08	0.02	-0.11	-0.09
	std. deviation	0.13	0.07	0.12	0.09
	median	0.05	0.05	-0.05	-0.05
	skewness	0.50	0.30	-0.60	-0.60

TABLE III
Comparison Statistics Cruise AII

PARAMETER	MODEL	EOTS		TEOTS	
	ANALYSIS DATE	30 Jun	07 Jul	30 Jun	07 Jul
SST (°C)	mean	0.90	1.03	0.40	-0.04
	std. deviation	0.40	0.50	0.60	0.60
	median	1.00	1.00	0.60	0.20
	skewness	-0.90	-0.70	-0.02	0.01
MLD (m)	mean	-30.9	-26.6	-11.2	-17.4
	std. deviation	8.30	7.70	16.8	7.89
	median	-25.0	-25.0	-15.0	-15.0
	skewness	-0.20	-0.60	2.16	-0.80
BLG (°C/100m)	mean	-1.20	-0.30	-2.80	-4.24
	std. deviation	1.90	1.40	1.60	1.49
	median	-1.50	-0.50	-3.50	-4.50
	skewness	0.90	1.40	1.20	0.90
THG (°C/100m)	mean	0.09	0.25	0.08	-0.04
	std. deviation	0.07	0.12	0.11	0.11
	median	0.20	0.30	0.15	-0.05
	skewness	-0.60	-1.00	-0.30	-0.20

123

TABLE IV
Comparison Statistics Cruise AIII

PARAMETER	MODEL	EOTS		TEOTS	
	ANALYSIS DATE	10 Jul	21 Jul	10 Jul	21 Jul
SST (°C)	mean	0.50		0.12	
	std. deviation	0.60		0.60	
	median	0.60		0.20	
	skewness	0.20		0.10	
MLD (m)	mean	-5.60		1.50	
	std. deviation	16.90		13.10	
	median	-5.00		5.00	
	skewness	-0.40		-0.70	
BLG (°C/100m)	mean	0.05		-3.90	
	std. deviation	1.33		1.15	
	median	0.50		-3.50	
	skewness	0.20		-0.05	
THG (°C/100m)	mean	0.20		0.04	
	std. deviation	0.14		0.14	
	median	0.20		0.05	
	skewness	-0.20		0.30	

124

VI. ACOUSTIC IMPACT OF ERRORS IN FNOC OCEAN THERMAL STRUCTURE ANALYSIS

A. DEFINITION OF ACOUSTIC TERMS

• Convergence Zone (CZ) - Region of focussing or convergence of sound.

• Direct Range - The shortest distance from the receiver at which the transmission loss exceeds the Figure of Merit.

• Figure of Merit (FOM) - The maximum allowable one way transmission loss (passive sonars) for which a 50% probability of detection is possible for a particular sonar.

• Leakage - Loss of energy from a surface duct to the main sound channel.

• Low-Frequency Cut-Off - Frequency below which no trapped normal mode may exist for a given channel or duct.

• Sound-Speed Profile (SSP) - Depth/sound-speed combinations defining the vertical variation in sound speed.

• Transmission Loss (TL) - Acoustic parameter which quantitatively describes the weakening of sound intensity between a point 1m from the source and a point at a distance in the ocean.

• Vertical Beam-Width - Included angle between the maximum upward and downward propagating rays.

B. ASSUMPTIONS

The only variable in the range calculations was to be the SSP. To achieve this goal certain representative, acoustic parameters were assumed constant throughout and were used as standard inputs to all transmission loss calculations.

• The ocean bottom was assumed flat.

• A standard bottom-loss/grazing angle curve applied to all frequencies.

• A flat sea surface (sea state 1) input to the FACT models (assumed flat in the FE model)

• The FOM's used in the range calculations were 80db and 90db. These figures are representative of the range of FOM's encountered in operational systems.

• Source/receiver dispositions used were:

20m/20m-shallow/shallow (S/S)

20m/200m-shallow/deep (S/D)

200m/200m-deep/deep (D/D)

The S/S disposition was intended to give a measure of the surface duct acoustic propagation; S/D of cross-layer propagation and D/D of deep sound channel propagation. All three combinations can be utilized by presently operational, shipborne systems.

C. DERIVATION OF SOUND-SPEED PROFILES

Depth/temperature profiles were constructed for both the EOTS and OPTOMA5 analyses at the positions of maximum error, between the two analyses, for SST, MLD, BLG and THG. The position of the maximum error was obtained from the difference field discussed in Chapter V and the depth/temperature profiles were generated by utilizing the contour fields derived as described in Chapter IV.

SSP's were computed from the temperature profiles using Wilson's Equation. The depth/salinity information was obtained from the DE STEIGUR, deep CTD data (Chapter II)

Only the data relevant to cruises AI and AII were utilized. Long range prediction (CZ) comparisons were made between profiles based on the OPTOMA5, EOTS and TEOTS analyses. Direct range comparisons were limited to profiles based on the OPTOMA5 and EOTS analyses only.

126

The SSP's derived for each model analysis (and all subsequent acoustic calculations based on those SSP's) were designated according to the parameter, and analysis date eg. SST1 refers to a profiles derived at the position of maximum difference between modeled and OPTOMA5 SST for the initial model analysis of the particular OPTOMA5 cruise being studied; MLD2 refers to the profile derived at the position of maximum difference in MLD's for the final model analysis of the cruise, etc.

D. TRANSMISSION LOSS MODEL COMPARISONS

Differences in model physics made direct comparisons between FACT9H and the PE Models unwieldy, as did limitations in the model computer programs. One of the major differences was that the PE model has a vertical beamwidth limitation which causes a program termination if exceeded. The limitation is a function of the SSP and, for the profiles utilized in this study, the maximum vertical beamwidth which could be maintained was 20°. No such limitation exists for the FACT9H model which sums acoustic intensities from all forward directions, equivalent to a vertical beamwidth of 180°. The effect of this beamwidth limitation is that the PE model will predict consistantly greater transmission loss for a given range than will the FACT9H model, assuming all other inputs to each model are identical. However, the effect of SSP changes relating to temperature profile differences between modeled and OPTOMA5 ocean thermal structures were computed on a model-by-model basis and the results compared, Table V. An example of the transmission loss curves computed from the two models for the same SSP, Fig. 6.1, clearly shows the effect of the differing model physics.

Table V shows the Parameter Error (difference between OPTOMA5 and EOTS values for the parameter, expressed as a percentage of the OPTCMA5 value); the Range(R) (direct range (km) computed from the transmission loss curve based on the OPTOMA5 data); Range Error (E) (difference between direct range obtained utilizing OPTOMA5 data and that utilizing EOTS analysis data, expressed as a percentage of R). A negative sign indicates that the model analysis had produced an overestimate of that particular parameter. The comparisons shown in Table V are for a 600Hz frequency.

The lack of agreement between the two transmission loss models was apparent with the PE model predicting significantly shorter ranges than the FACT9H model. The PE model was also far more sensitive to variations in the input SSP, particularly when both source and receiver were shallow, and showed a dependence on the SSP for the S/D and D/D dispositions, which, as discussed in later sections, was not the case for the FACT9H model. Convergence zone ranges computed by both FACT9H and the PE model were in good agreement. However, the gain in acoustic energy at the convergence zones was approximately 5db lower in the PE model computations than those of FACT9H.

The remaining comparisons discussed in this chapter were based on the FACT9H transmission loss computations.

E. SUMMARY OF ACOUSTIC COMPUTATIONS

When comparing ranges predicted utilizing measured and modeled profiles, an error of less than 20% was assumed operationally insignificant. This assumption was believed reasonable when the uncertainties associated with the FACT9H acoustic model accuracy (eg., the lack of attenuation due to absorption and volumetric scattering) are considered.

128

1. Long Range (CZ) Predictions

Comparisons of CZ ranges computed using SSP's derived from OPTOMA5, EOTS and TEOTS data, Tables VI to IX revealed a relative lack of sensitivity of the CZ range to thermal structure variations of the order of magnitude present between modeled and sea truth analyses. The average CZ range computed from sea truth data was 50km, varying between 44km and 62km. Ranges computed utilizing SSP's derived from FNOC model analyses were within 10% of those computed utilizing sea truth data. The maximum errors were observed when both source and receiver were shallow.

2. Direct Range Comparisons

Subjective analysis of the transmission loss curves computed for the long range comparisons discussed above, combined with an understanding of ray-theory physics, led to the direct range comparisons being concentrated on the surface duct propagation paths (i.e., shallow source and receiver). A limited number of comparisons were made between direct ranges obtained from the transmission loss curves computed utilizing OPTOMA5 and those utilizing EOTS derived profiles for cross-layer and below layer propagation paths. The results from these comparisons, Tables X and XI confirm the supposition that the FACT9H computed transmission losses for the S/D and D/D propagation paths are relatively insensitive to SSP variations of the order of magnitude present between profiles derived from OPTOMA5 data and those from the EOTS analyses. In the remainder of this discussion 'range error' will refer to the difference between ranges calculated from transmission loss curves computed from sea truth profiles and those computed from EOTS profiles.

The maximum range error for the cross-layer propagation path was 18% on a range of 8km, with the majority of

the range errors within 10% of a sea truth range of 8km at
the 50Hz frequency. However, a weak frequency dependence was
observed and errors cf the order of 15% on a range of 8km
were measured at 600Hz, associated with the lower FOM. The
maximum error also cccurred at this frequency, associated
with the lower FOM, Table X .

The range errors measured for the below layer propa-
gation paths were generally negligible (<5%) and independent
of frequency and FOM, Table XI . However, for profiles
SST1and SST2 errors of the order of 15% on a range of 18km
for the lower FOM and 15% on a range of 77km for the higher
FOM, were measured. The presence of a weak shallow sound
channel in the sea truth SSP is believed to be the cause of
these significantly higher range errors and would also
explain the longer direct ranges associated with the sea
truth profile (i.e., 18km compared to the average of 8km for
the remaining profiles)

For the surface duct propagation paths (S/S), trans-
mission loss curves were computed at frequencies of 50, 300
600 and 1000Hz for profiles associated with cruise AI and at
300, 600 and 1000Hz for those associated with cruise AII.
The 50Hz frequency was removed from the comparisons in
cruise AII, Table XIII, once the range errors were shown to
be negligible at this frequency for the cruise AI compari-
sons, Table XII .

From the range comparisons, Table XII and XIII it
can be seen that at the higher FOM and for frequencies below
1000Hz, the transmission loss is insensitive to SSP varia-
tions of the order of magnitude observed with a range error
of less than 10% on a mean range of 55km.

For range calculations based on the lower FOM,
significant range errors were observed for frequencies of
300Hz and above. The range error was also observed to be a
function of frequency. Plots of range error versus parameter

130

error for the four parameters being studied revealed a strong dependence of the range error on the MLD error, Fig. 6.2 . The curves shown in Fig. 6.2 were fitted to the points in an RMS manner and do not imply a functional relationship between MLD and range error but are intended to show a general trend. The scatter of the points in Fig. 6.2 indicate the complex interaction between the various parameters. From the curves it can be seen that the range error increased with increasing MLD error and frequency, for frequecies above approximately 300Hz. The presence cf a non-zero range error for a zero MLD error was a further indication of the effect of the other parameters. Plcts of range error versus errors in the remaining three parameters were also generated, Figs. 6.3 to 6.5 These curves appeared to indicate a marked dependence of range error on each parameter. However, plots of MLD error versus the errors in the remaining parameters, Figs. 6.6 to 6.8 revealed that the major range error dependence was indeed on MLD error; e.g. the trend in range error when compared to SST error is in the same general sense as the trend in MLD error when that too is compared to SST error.
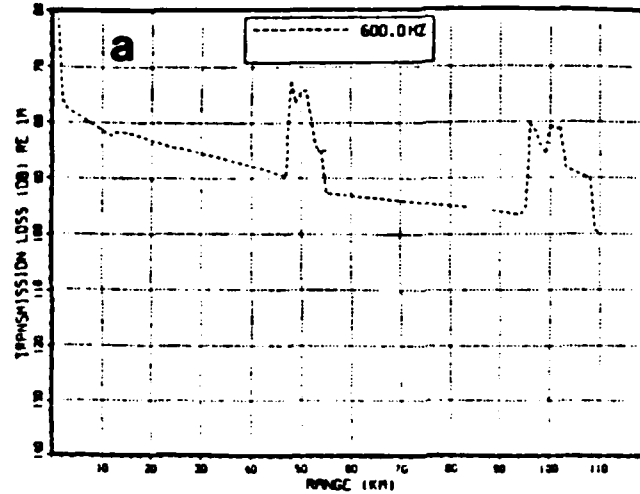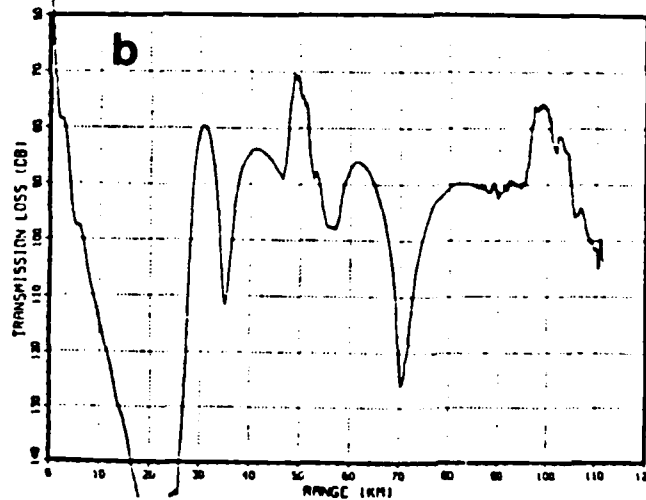
Figure 6.1   Example of Transmission Loss Curves
a. FACT9H Model b. PE Model.

132
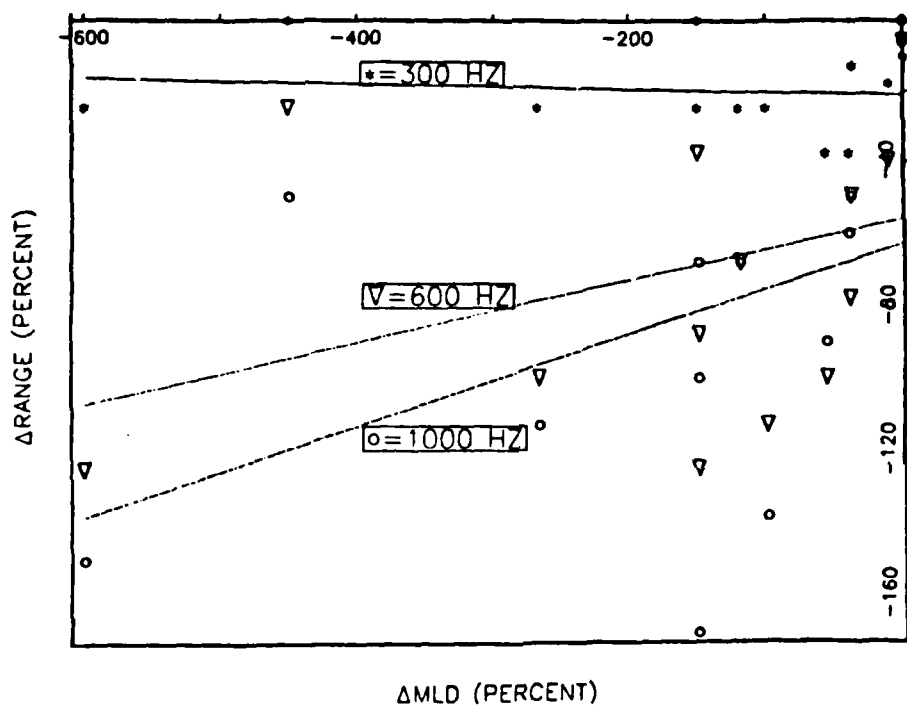
Figure 6.2   Plot of MLD Error vs. Range Error.

133
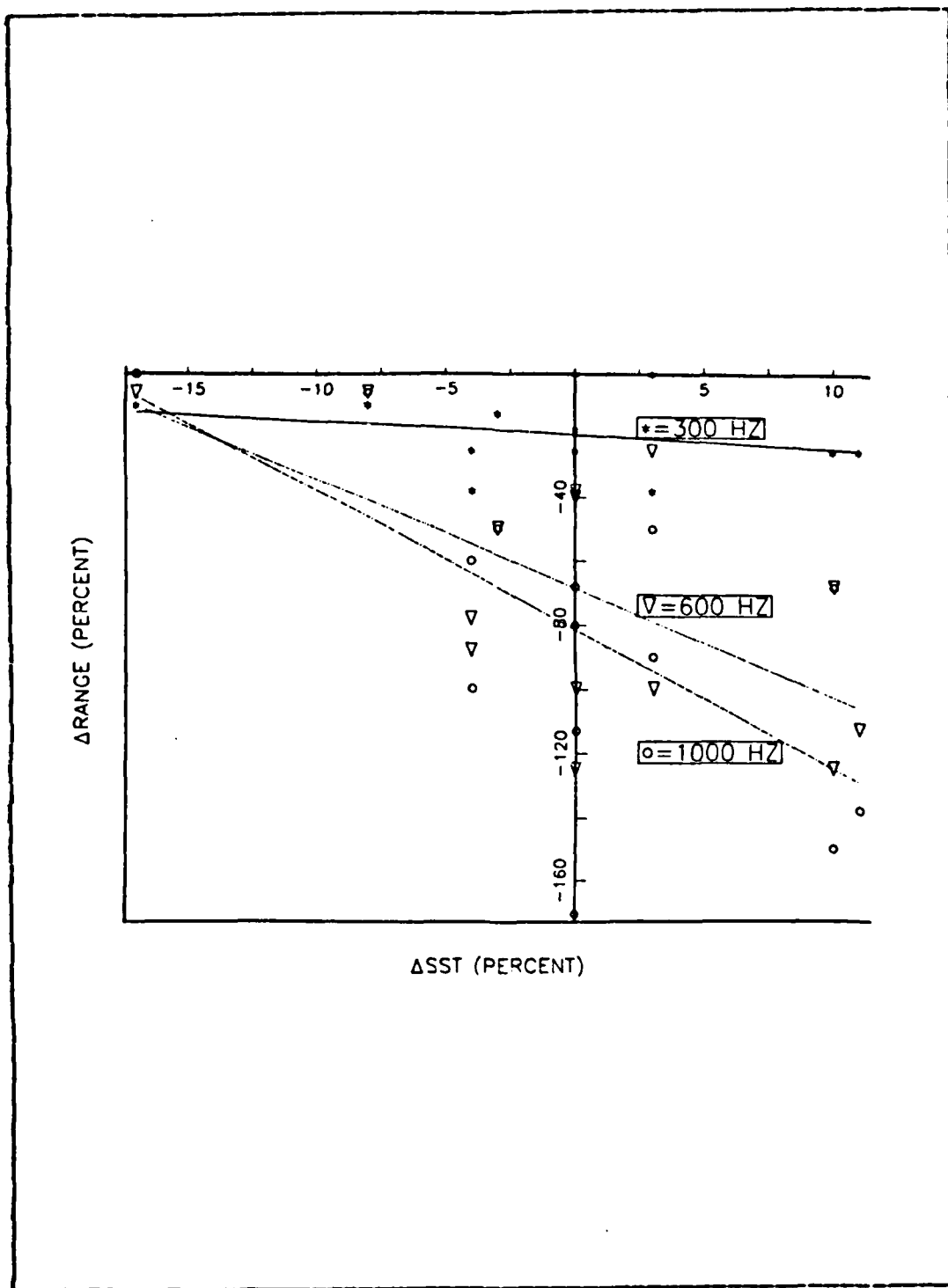
Figure 6.3   Plot of SST Error vs. Range Error.

134
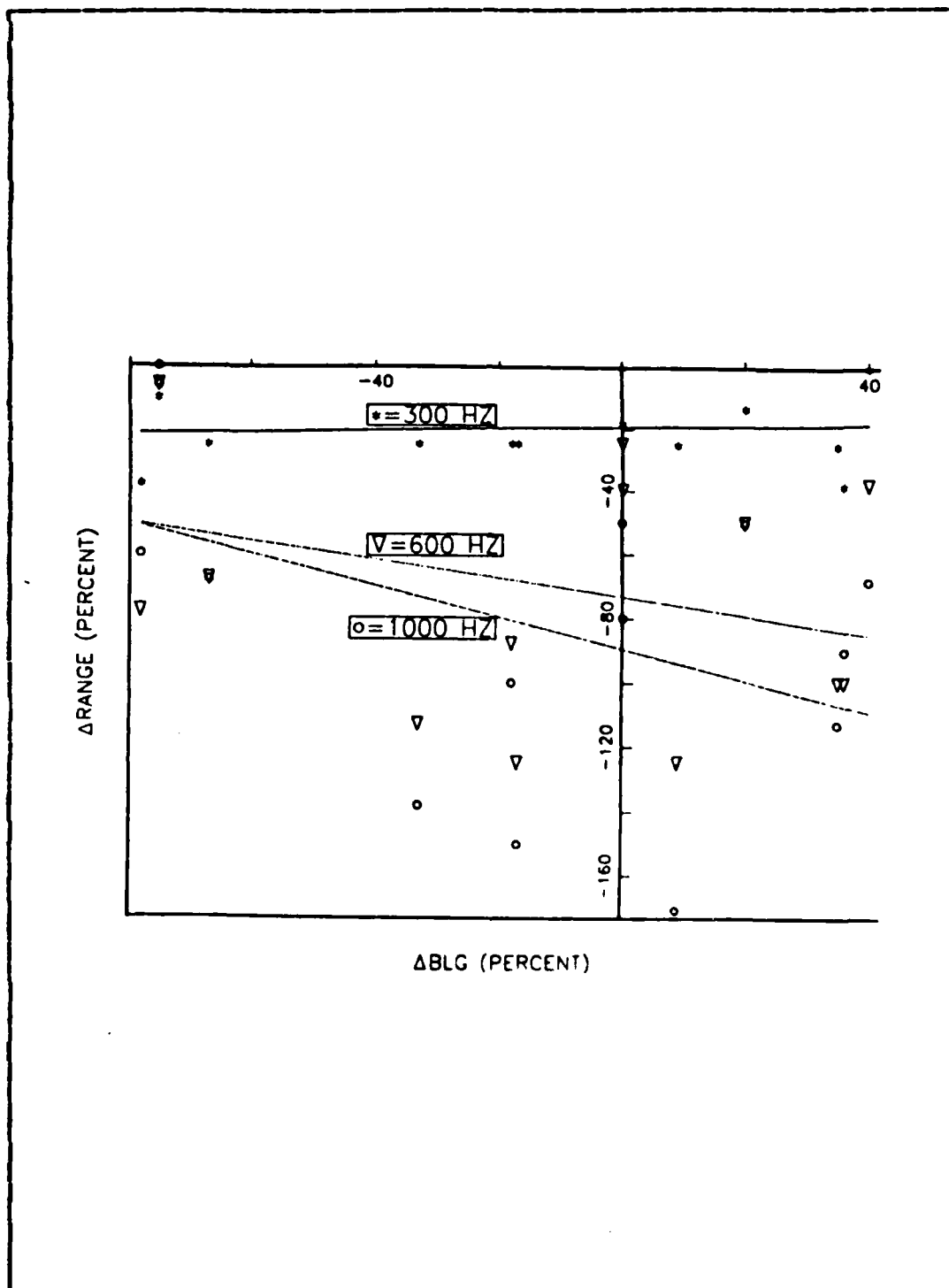
Figure 6.4 Plot of BLG Error vs. Range Error.

135
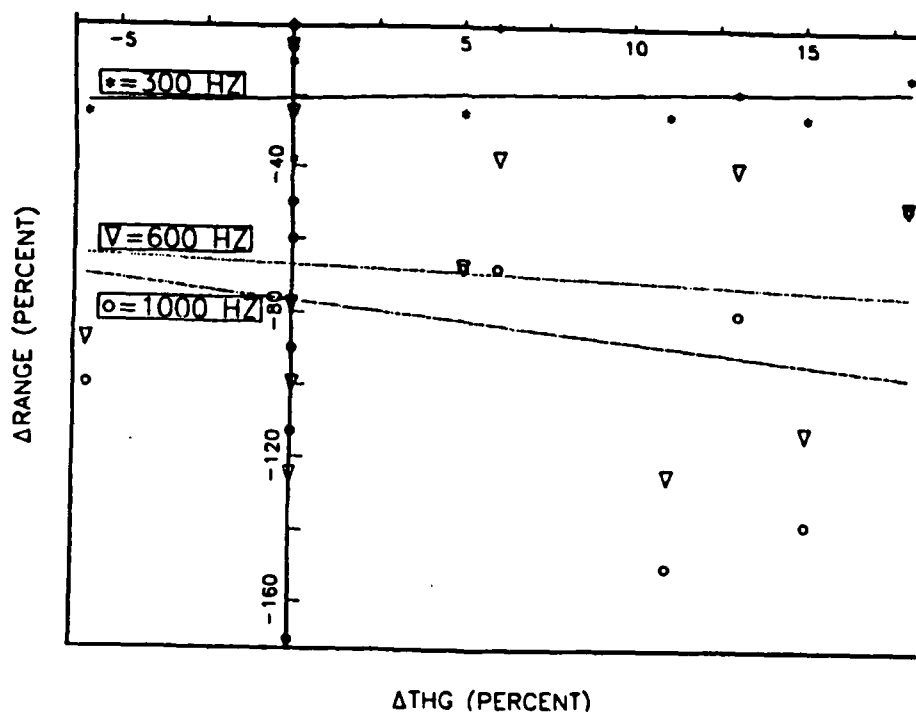
Figure 6.5   Plot of THG Error vs. Range Error.

136
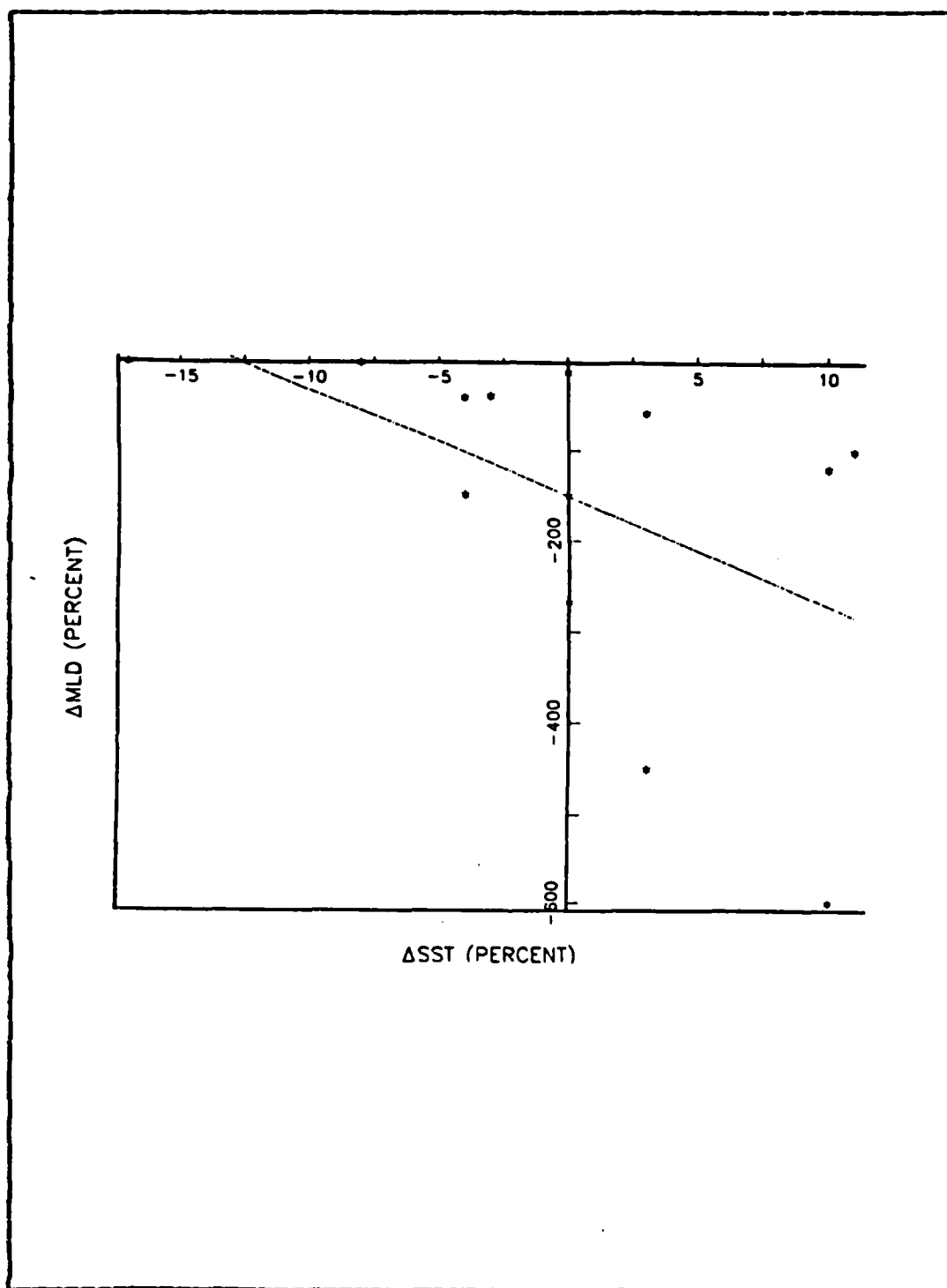
Figure 6.6   Plot of SST Error vs. MLD Error.

137
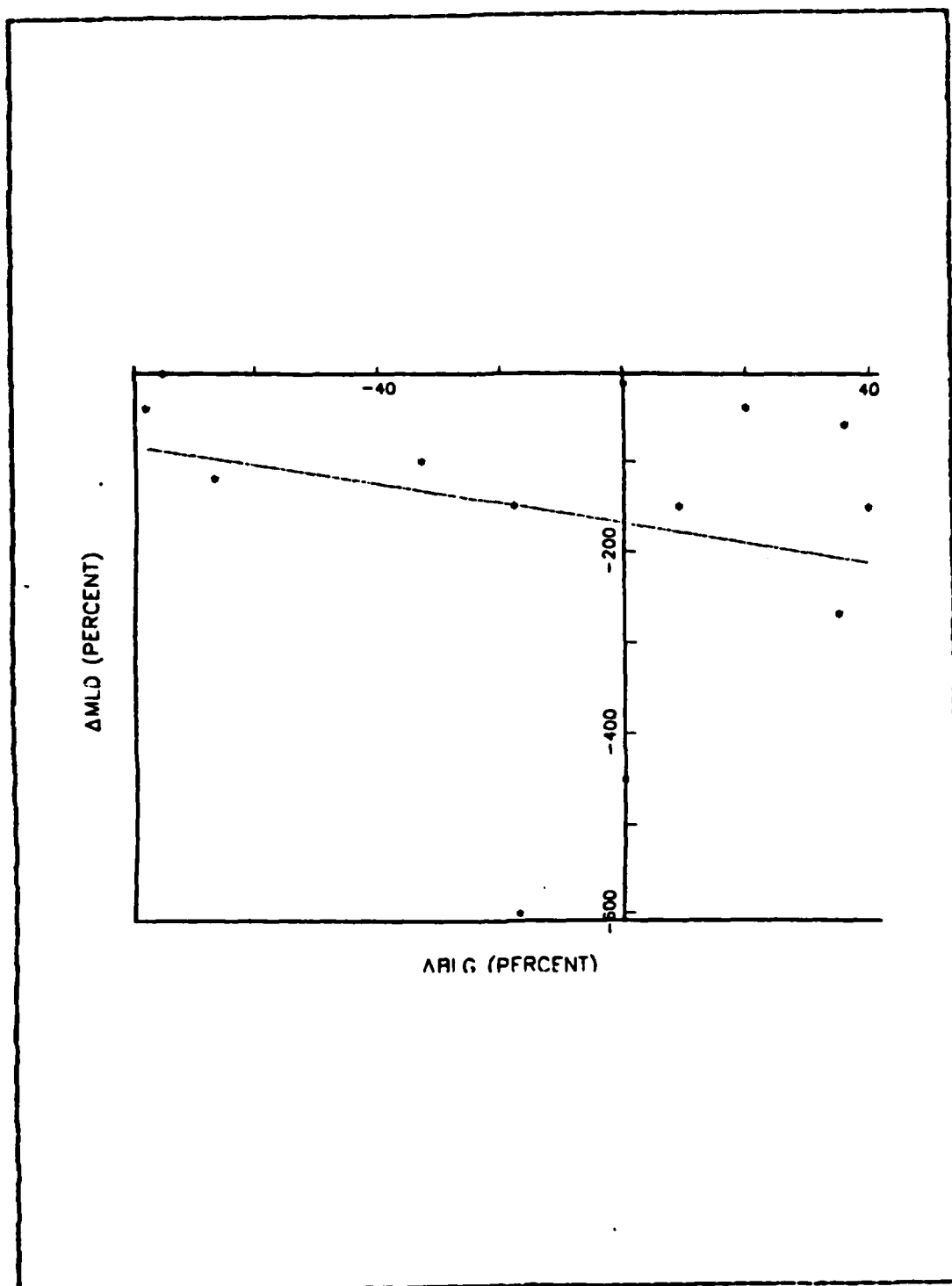
Figure 6.7   Plot of BLG Error vs. MLD Error.

138
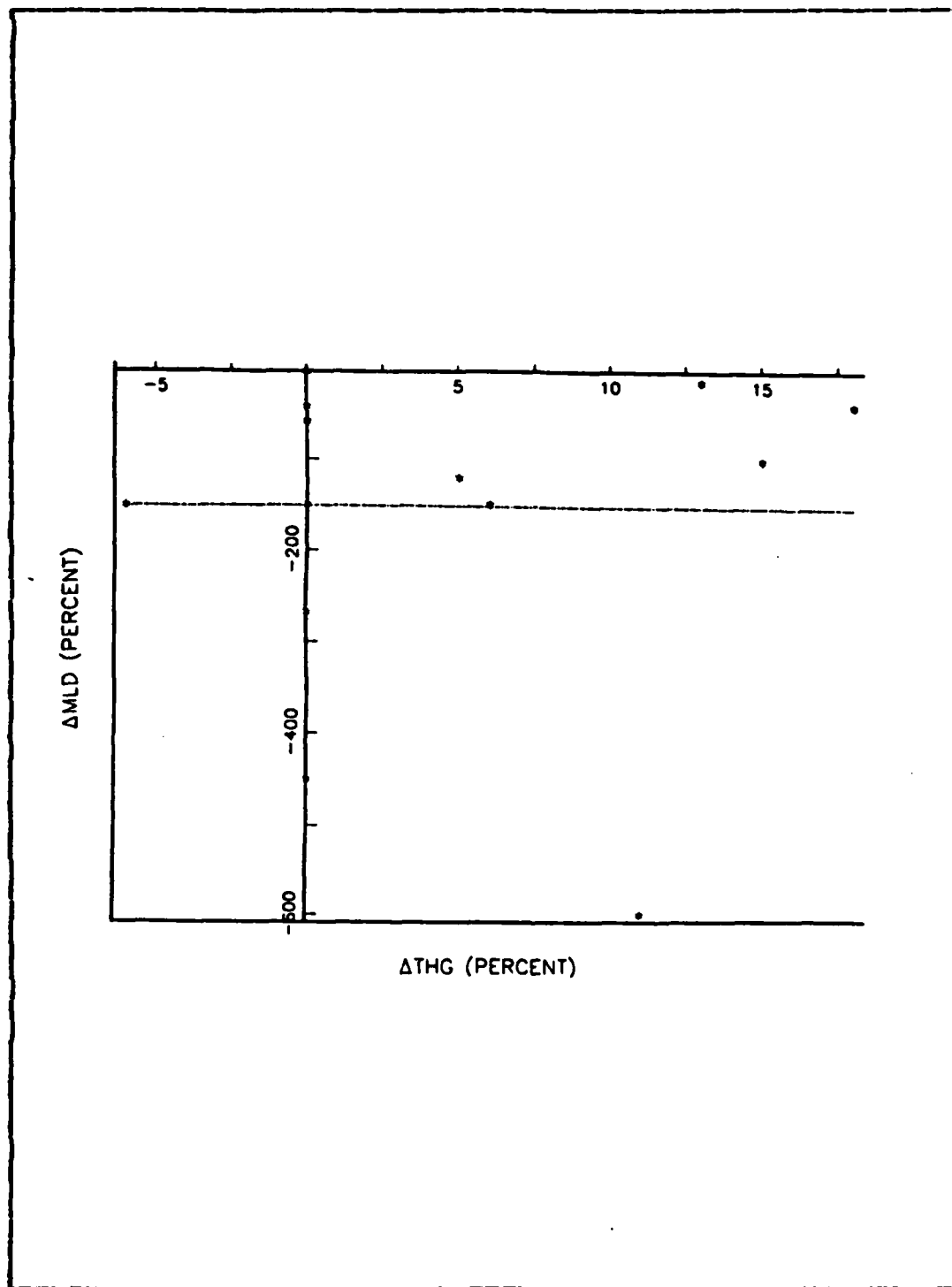
Figure 6.8   Plot of THG Error vs. MLD Error.

139

TABLE V
FACT9H-PE Model Comparisons

PARAMETER	PARAMETER ERROR (Z)				MODEL DISPN	RANGE / RANGE ERROR (Z)											
						FACT9H						PE					
						S/S		S/D		D/D		S/S		S/D		D/D	
	SST	MLD	BLG	THG	FOM	R	E	R	E	R	E	R	E	R	E	R	F
SST1	-17	0	-75	0	80	16	-6	10	0	18	16	3	-600	3	0	8	50
					90	54	0	55	0	77	15	4	-900	6	-130	10	20
MLD1	-4	-150	-18	-6	80	8	-88	7	-12	8	0	1	-1100	2	-50	4	0
					90	57	0	57	0	57	0	3	-600	3	-300	6	0
BLG1	-4	-40	-78	0	80	9	-78	8	-15	9	0	3	-500	4	0	4	0
					90	55	0	56	0	58	2	5	-450	6	-100	6	0
THG1	-3	-38	20	18	80	8	-50	8	0	8	0	4	-75	4	0	3	-200
					90	62	8	60	0	57	0	6	-90	6	-50	6	-200

140

TABLE VI

EOTS/Cruise AI CZ Range Comparisons

PARAMETER	PARAMETER ERROR (%)				CZ RANGE ERROR (%)					
					50 Hz			600 Hz		
	SST	MLD	BLG	THG	S/S	S/D	D/D	S/S	S/D	D/D
SST1	-17	0	-75	0	-6	-13	4	-6	-4	6
SST2	-8	0	-75	0	-4	0	4	-4	0	6
MLD1	-4	-150	-18	-6	6	0	-4	-6	-2	0
MLD2	0	-150	9	0	4	4	0	-4	-2	0
BLG1	-4	-40	-78	0	6	0	0	-6	-2	2
BLG2	3	-57	36	0	-2	-2	0	-2	-4	0
THG1	-3	-38	20	18	0	-2	-6	0	-2	-9
THG2	0	-11	0	13	-2	-4	2	-2	-4	-2

TABLE VII

TROTS/Cruise AI CZ Range Comparisons

PARAMETER	PARAMETER ERROR (Z)				CZ RANGE ERROR (Z)					
					50 Hz			600 Hz		
	SST	MLD	BLG	THG	S/S	S/D	D/D	S/S	S/D	D/D
SST1	-17	-20	-113	0	-2	-2	0	-6	-2	0
SST2	-10	-20	-75	0	-10	-2	4	-2	-2	4
MLD1	-9	-100	-51	-6	0	-2	0	-2	0	0
MLD2	-6	-100	-27	-6	-6	-4	0	-2	-4	0
BLG1	-3	0	-100	0	4	0	2	-2	0	-2
BLG2	0	0	-78	0	-4	-2	2	-2	-3	2
THG1	-3	-20	-50	-27	4	-2	0	4	-2	0
THG2	-1	-10	-10	-20	0	0	0	-1	0	0

142

TABLE VIII

EOTS/Cruise AII Cz Range Comparisons

PARAMETER	PARAMETER ERROR (%)				CZ RANGE ERROR (%)					
					50 Hz			600 Hz		
	SST	MLD	BLG	THG	S/S	S/D	D/D	S/S	S/D	D/D
SST1	10	-120	-67	5	0	0	0	0	0	0
SST2	11	-100	-33	15	4	-4	-2	4	-4	-2
MLD1	10	-600	-17	11	2	0	0	2	0	0
MLD2	3	-450	0	0	-8	-4	2	-6	-4	-2
BLG1	0	-270	35	0	-8	-2	2	-6	-2	2
BLG2	0	-150	40	6	-4	-4	-4	-2	-2	-4
THG1										
THG2										

143

TABLE IX

TEOTS/Cruise AII CZ Range Comparisons

PARAMETER	PARAMETER ERROR (%)				CZ RANGE ERROR (%)					
					50 Hz			600 Hz		
	SST	MLD	BLG	THG	S/S	S/D	D/D	S/S	S/D	D/D
SST1	10	-60	-70	10	4	2	-4	4	2	-4
SST2	8	-167	0	-6	-8	-6	0	-2	0	0
MLD1	-1	-400	-14	-6	-10	-2	-2	-6	0	-4
MLD2	4	-700	-33	0	-2	0	-7	0	0	-2
BLG1	0	-60	-157	0	0	0	2	-2	-2	2
BLG2	-3	-60	-200	-5	-2	0	4	0	0	4
THG1										
THG2										

144

TABLE X

Cross-Layer Propagation Comparisons (S/D)

PARAMETER	PARAMETER ERROR (%)				FOM	RANGE / RANGE ERROR (%)							
						50		300		600		1000	
	SST	MLD	BLG	THG	FREQ.	R	E	R	E	R	E	R	E
SST1	-17	0	-75	0	80	8	0			10	0		
					90	55	0			55	0		
SST2	-8	0	-75	0	80	8	0			10	-10		
					90	55	-7			55	-7		
MLD1	-4	-150	-18	-6	80	7	0			7	-12		
					90	56	-5			56	-2		
MLD2	0	-150	9	0	80	7	-12			7	-14		
					90	56	-2			56	-2		
BLG1	-4	-40	-78	0	80	8	13			8	-15		
					90	56	-2			56	0		
BLG2	3	-57	36	0	80	7	-14			7	-15		
					90	57	1			57	1		
THG1	-3	-38	20	18	80	8	0			8	0		
					90	60	0			60	0		
THG2	0	-11	0	13	80	8	0			8	-18		
					90	57	1			57	1		

145

TABLE XI

Below-Layer Propagation Comparisons (D/D)

| PARAMETER | PARAMETER ERROR (%) | | | | FOM | RANGE / RANGE ERROR (%) | | | | | | | |
	SST	MLD	BLG	THG	FREQ.	50 R	50 E	300 R	300 E	600 R	600 E	1000 R	1000 E
SST1	-17	0	-75	0	80	18	16			18	16		
					90	77	12			77	15		
SST2	-8	0	-75	0	80	18	16			18	16		
					90	77	15			77	15		
MLD1	-4	-150	-18	-6	80	8	0			8	0		
					90	57	0			57	0		
MLD2	0	-150	9	0	80	8	0			8	0		
					90	58	0			58	0		
BLG1	-4	-40	-78	0	80	9	0			9	0		
					90	60	3			58	2		
BLG2	3	-57	36	0	80	8	0			8	0		
					90	58	0			58	0		
THG1	-3	-38	20	18	80	8	0			8	0		
					90	57	0			57	0		
THG2	0	-11	0	13	80	8	0			8	0		
					90	60	0			58	0		

146

TABLE XII

Surface Duct Propagation Comparisons (S/S)-Cruise AI

PARAMETER	PARAMETER ERROR (%)				FOM	RANGE	RANGE ERROR (%)							
	SST	MLD	BLG	THG	FREQ.	50		300		600		1000		
						R	E	R	E	R	E	R	E	
SST1	-17	0	-75	0	80	8	0	10	-10	16	-6	18	0	
					90	55	2	55	0	54	0	42	-7	
SST2	-8	0	-75	0	80	8	0	10	-10	16	-6	18	-6	
					90	55	-10	54	-11	54	-10	42	0	
MLD1	-4	-150	-18	-6	80	8	0	8	-25	8	-88	7	-100	
					90	57	0	57	0	57	0	43	0	
MLD2	0	-150	9	0	80	8	0	8	-25	8	-125	7	-171	
					90	57	0	57	0	57	0	42	0	
BLG1	-4	-40	-78	0	80	8	10	8	-38	9	-78	10	-60	
					90	55	0	55	0	55	0	43	0	
BLG2	3	-57	36	0	80	8	-13	8	-38	8	-100	10	-90	
					90	56	3	57	5	56	3	43	0	
THG1	-3	-38	20	18	80	8	0	8	-13	8	-50	10	-50	
					90	62	8	62	8	62	8	44	0	
THG2	0	-11	0	13	80	8	0	8	-18	10	-40	10	-80	
					90	56	3	56	3	56	3	44	0	

147

TABLE XIII

Surface Duct Propagation Comparisons (S/S)-Cruise AII

PARAMETER	PARAMETER ERROR (%)				FOM	RANGE RANGE ERROR (%)							
	SST	MLD	BLG	THG	FREQ.	50 R	50 E	300 R	300 E	600 R	600 E	1000 R	1000 E
SST1	10	-120	-67	5	80			8	-25	8	-68	8	-68
					90			55	-13	55	-13	45	2
SST2	11	-100	-33	15	80			8	-25	8	-113	8	-138
					90			55	0	55	0	45	4
MLD1	10	-600	-17	11	80			8	-25	8	-125	8	-150
					90			56	-9	56	-9	46	-12
MLD2	3	-450	0	0	80			8	0	8	-25	8	-50
					90			55	-2	55	-2	43	0
BLC1	0	-270	35	0	80			8	-25	8	-100	8	-113
					90			55	-3	55	-3	44	0
BLC2	0	-150	40	6	80			8	0	8	-38	8	-62
					90			55	0	55	0	44	0
THG1					80								
					90								
THG2					80								
					90								

148

VII. SUMMARY AND CONCLUSIONS

The grid spacing used in the FNOC ocean thermal analysis models (i.e., 40km for EOTS and 320km for TEOTS) made it extremely unlikely that they would be capable of recovering the mesoscale, horizontal variability (of the order of 30 to 40km) dominating the study domain.

Within the limitations of the grid spacing used, the EOTS SST analysis responded well to input data. However, the analysis methodology is believed to have smoothed the input field to the extent that significant detail was lost.

The hemispherical TEOTS SST analysis responded to data input in magnitude but was totally insensitive to the horizontal shape information provided by the input data. This lack of response is believed to be a function of the coarse grid spacing of the TEOTS analysis field.

Both EOTS and TEOTS were insensitive to input mixed layer depth (MLD) information. The EOTS MLD analysis remained almost constant throughout the study period in both magnitude and shape. The TEOTS MLD analyses did change over the study period and were, on average, in closer agreement with the measured MLD magnitudes, but had an almost constant shape field. The lack of detail in both EOTS and TEOTS MLD analyses was in marked contrast to the complex and variable measured MLD shape fields. The improved performance of the TEOTS analysis over the EOTS analysis is believed to be the result of the influence of the TOPS element on the analysis.

The response of the models to data input for depths below the MLD was inconclusive since the parameters tested (BLG and THG) were functions of the MLD and, thus, errors in the MLD analysis would propagate into these remaining fields.

The FNOC procedure of using a single climatological depth/temperature profile for areas such as the study domain was shown to be inaccurate. The study domain was shown to vary on a secular time scale (El Nino effect) with a 2 to 3°C thermal anomaly, compared to FNOC climatology, measured at depths of 50 to 100m during the study period. The effect of a poor climatology would be reflected in the model analyses in the absence of input data.

For acoustic frequencies below 1000Hz and based on results from the FACT9H Transmission Loss model, the errors in the EOTS and TEOTS analyses were insignificant for (a) long range (convergence zone) predictions, (b) direct range predictions for sonar systems with a figure of merit of 90db or greater, and (c) direct range predictions for cross layer and below layer source/receiver dispositions. The errors in the model analyses were found to be significant for sonar systems with a figure of merit of 80db or less when both source and receiver were shallow.

The errors in modeled mixed layer depth were found to have the greatest effect on acoustic prediction errors, and the effect was found to be directly proportional to acoustic frequency.

A comparison between the FACT9H and PE Transmission Loss models revealed significant differences between the outputs of the two models.

The PE model appeared far more sensitive to errors in the temperature profile than did the FACT9H model. The direct range errors obtained from the PE model outputs, based on modeled and measured temperature profiles, showed no dependence on the figure of merit and less dependence on the source/receiver disposition than did those based on the FACT9H model outputs.

The disparity between FACT9H and PE model sensitivities made an absolute determination of the operational

150

significance of errors in the EOTS and TEOTS analyses impossible. However, the maximum effect of depth/temperature profile differences on direct range predictions was significant, whichever transmission loss model was used, when both source and receiver were shallow.

VIII. RECOMMENDATIONS

The staff at FNOC are presently restructuring the ocean thermal analysis model algorithms to enable the models to respond more readily to input data, particularly the PLD segment of the analysis. The physics of the TEOTS analysis are also being incorporated into the finer grid, regional analyses. The effectiveness of such changes should be tested in a similar areal manner to that of the present study, and for many more areas of the world's ocean, to establish the operational value of such an analysis system. The minimum data input required to give a representative analysis under varying conditions should also be established, in order that assets may be deployed effectively and economically.

For regions where anomalous events are known to occur, the feasability of utilizing a quasi-dynamic climatology, based on hindcasting, should be studied, i.e., climatology could be updated when a persistent anomalous event is known to be present. This would give a more representative analysis, at depths below those influenced by the TOPS elements of the TEOTS analysis, in the absence of input data.

Satellite IR imagery could be a powerful asset in data-sparse areas of the oceans, providing a necessary input to ocean thermal analysis models. However, the results of the present study have shown that the relationship between SST and sub-surface features is not always an obvious one. Studies should be undertaken to relate surface features with sub-surface structure, either through direct correlations or modeling. Such relationships would also assist the planning of sampling strategies aimed at achieving the most economical and efficient use of assets whilst providing sufficient input to the ocean thermal analysis model to achieve the desired accuracy.

The effect on the higher frequency;i.e., greater than 1Khz, active sonar performance of errors in the model analysis fields should be examined. The loss of vertical structure could prove important. In particular, areas where significant vertical features are present; e.g., shallow sound channels, should be examined and the feasibility of an additional floating level in the analysis, to represent the depth of such features, should be addressed.

The effect of mesoscale variations, on scales such as those observed in the present study, on the other parameters in the sonar equation should be examined; e.g., ambient noise changes due to changes in the marine ecosystem in the region of the weak ocean fronts associated with upwelling regions.

Operationally important areas are, in general, the more densely sampled regions of the ocean. However, the present fixed regional boundaries utilized in the FNOC analysis models are only broadly representative of these operational areas and generally extend beyond the limits of prime interest. As a consequence, the shape field used in the analysis is influenced by possibly less well sampled areas outside the region of interest with possible erroneous smoothing effects on the horizontal and vertical thermal structure that the analysis would otherwise produce. To remove such a possibility, the utilization of a flexible regional boundary, fitted to the area of interest , and with a grid spacing reprasentative of the horizontal variability of the region, should be studied. Such an approach as the one outlined above would also facilitate the incorporation of a more detailed, possibly dynamic, climatology into the analysis.

LIST OF REFERENCES

1. Clancy, R. M. and Pollack, K. D., "A Real-Time Synoptic Ocean Thermal Analysis/Forecast System," *Prog. Oceanog.* v. 12, pp.383-424, 1983.

2. *The AESD Parabolic Equation Model,* by H. K. Brock, 1978

3. Mooers, C. K. N. and Robinson, A. R., "Turbulent Jets and Eddies in the California Current and Inferred Cross-Shore Transports," *Science,* v. 223, pp. 51-53, 1984.

4. Reid, J. L., Roden, G. I. and Wyllie, J. G., *Studies of the California Current System,* Progress Reports of the California Cooperative Ocean Fisheries Investigations, pp. 136-174, 1958.

5. Sverdrup, H. U., Johnson, M. W. and Fleming, R. H., *The Oceans,* Prentice Hall, Inc., Englewood Cliffs, N. J., 1942

6. Breaker, L. C., *The Space-Time Scales of Variability in Oceanic Thermal Structure off the Central California Coast,* Phd Thesis, Naval Postgraduate School, Monterey, Ca., 1983.

7. Meteorology International Incorporated Report M-232, *The Expanded Ocean Thermal-Structure Analysis System User's Manual,* by B. R. Mendenhall, M.J. Cumming and M. M. Holl, pp. 110, 1978.

8. Meteorology International Incorporated Report M-167, *Fields by Information Blending, Sea-Level Pressure Version,* by M. M. Holl and B. R. Mendenhall, pp. 77, 1971.

9. *FACT9H: Version Description Document,* by G. Jacobs, 1982.

10. Naval Ocean Research and Development Activity Report NPS61-83-002, *An Introduction to the Parabolic Equation for Acoustic Propagation,* by A. B. Coppens, 1982.

11. Clay, C. S., *Sound Transmission in a Half-Channel and Surface Duct. Technical Note on Sound Propagation in the Sea, vol 2,* Meteorology International Incorporated, Monterey, Ca., 1968.

12. Marsh, H. W. and Schulkin, M., *Report on the Status of*

           Project AMOS, Naval Underwater Sound Laboratory, New London, Conn., 1967.

13.   Urick, F. J., Principles of Underwater Sound, McGraw-Hill., 1983.

14.   Podeszoa, E. M., Sound Speed Profiles for the North Pacific Ocean, pp. 6-7, Naval Underwater Systems Center, New London Laboratory, 1976.

BIBLIOGRAPHY

Allen, J. S., "Upwelling and Coastal JETS IN A Continuously Stratified Ocean," _Journal Phys. Oceanogr._, v. 3(3), 1973.

Bakun, A., "Climatology of Upwelling off California," _EOS_, v. 52(11), 1971.

Bakun, A., Mclain, Mayo, "The Mean Annual Cycle of Coastal Upwelling off Western North America as Observed from Surface Measurements," _Fish. Bull._, v. 72(3), 1974.

Barkley, R. A., _Oceanographic Atlas of the Pacific Ocean_, University of Hawaii Press, 1978.

Bathen, K. H., "On Seasonal Changes in the Depth of the Mixed Layer in the North Pacific Ocean," _J. Geophys. Res._, v. 77(36), 1972.

Bernstein, R. L., Breaker and Whritner, "California Current Eddy Formation: Ship Air and Satellite Results," _Science_, v. 195, 1977.

Bourke, R. H. (1983), _The ASRAP III Acoustic Forecast Model_, (unpublished document).

Brown, R. L., _Goestrophic Circulation off the Coast of Central California_, Masters Thesis, Naval Postgraduate School, Monterey, Ca., 1974.

Clancy, R. M. and Martin, P. J., "Synoptic Forecasting of the Oceanic Mixed Layer Using the Navy's Operational Enviromental Data Base: Present Capabilities and Future Applications," _Bull. Am. Met. Soc._, v. 62, 1981.

Crepon, M., Richez, C. and Chartier, "Effects of Coastline Geometry on Upwelling," _J. Phys. Oceanogr._, v. 14, 1984.

Cox, S. A., _Satellite Applications to Acoustic Prediction Systems_, Masters Thesis, Naval Postgraduate School, Monterey, Ca., 1982.

Davis, R., "MODE-1 Temperature Field Statistics," _MODE-1 Hot Line News_, v. 50, 1973.

Davis, R. E., de Szoeke, R. and Miller, P., "Variability of the Upper Ocean During MILE. Part II: Modeling and Mixed Layer Response," _Deep-Sea Res._, v. 28, 1981.

Deschamps, P. Y., Frouin, R. and Wald, L., "Satellite Determination of the Mesoscale Variability of the Sea Surface Temperature," _J. Phys. Oceanogr._, v. 11, 1981.

de Szoeke, R. A and Richman, J. G., "The Role of Wind Generated Mixing in Coastal Upwelling," _J. Phys. Oceanogr._, v. 11, 1981.

Dodimead, A. J., Favorite, F. and Hirano, T., Review of Oceanography of the Subarctic Pacific Region, _INPFC Report_, 1962.

156

Douglas, A. V., "El Nino Signature Patterns in the North Pacific: Analysis of development in the 1982-83 Event," _EOS_ (Abstr. only), v. 64, 1983.

Durban, D. C., _Analysis of Observed and Modeled Mixed Layers: NOCAL Region_, Masters Thesis, Naval Postgraduate School, Monterey, Ca., 1983.

Eber, L. E., _Contoured Depth-Time Charts (0 to 20m, 1950 to 1966) of Temperature, Salinity, Oxygen and Sigma-t at 23 CALCOFI Stations in the California Current_, CALCOFI Report 25., 1977.

Fisher, R. H., _Variability and Sensitivity of Coupled Mixed Layer Acoustic Model Systems_, Masters Thesis, Naval Postgraduate School, Monterey, Ca., 1981

Haidvogel, D. B., Robinson, A. R. and Rooth, C. G. H., _Eddy-Induced Dispersion and Mixing: Eddies in Marine Science_, Springer-Verlag, 1983.

Hamilton, P. and Rattray, M., "A Numerical Model of the Depth-Dependent Wind-Driven Upwelling Circulation on a Continental Shelf," _J. Phys. Oceanogr._, v. 8, 1978.

Heath, G. R., _Oceanographic Studies Through December 1982 at Pacific Study Area W-N_, Low Level Waste Disposal Program, 1983.

Hickey, B. M., "The California Current System-Hypothesis and Facts," _Prog. in Oceanogr._, v. 8(4), 1979.

Holly, R. W., _Temperature and Density Structure of Water Along the California Coast_, Masters Thesis, Naval Postgraduate School, Monterey, Ca., 1968.

Lundell, G. W., _Rapid Oceanographic Data Gathering: Some Problems in Using Remote Sensing to Determine the Horizontal and Vertical Thermal Distributions in the North Pacific Ocean_, Masters Thesis, Naval Postgraduate School, Monterey, Ca., 1981.

Lynn, R., _Seasonal Variation of the Temperature and Salinity at 10 meters in the California Current_, CALCOFI Report: vol XI, 1967.

Lynn, R. J., Bliss, and Eber, L. E., _Vertical and Horizontal Distributions of Seasonal Mean Temperature, Salinity, Sigma-t, Dynamic Height, Oxygen and Oxygen Saturation in the California Current_, CALCOFI Report 30, 1982.

Monsaingeon, L., _Ocean Thermal Analysis and Related Naval Operational Considerations in the Ionian Sea-June 1980_, Masters Thesis, Naval Postgraduate School, Monterey, Ca., 1981.

Mooers, C. K. N., Collins and Smith, "The Dynamic Structure of the Frontal Zone in the Coastal Upwelling Region off Oregon," _J. Phys. Oceanogr._, v. 6(1), 1976.

Nelson, C. S., _Wind Stress and Wind Stress Curl Over the California Current_, Masters Thesis, Naval Postgraduate School, Monterey, Ca., 1976.

Schwaitzlose, H. and Reid, J. L., _Nearshore Circulation in the California Current_, CALCOFI Report 16, 1972.

Schwartzlose, R. A., *Nearshore Currents of the Western United States and Baja California As Measured by Drift Bottles*, CALCOFI Report 9, 1963.

Shepard, F. P., "Submarine Topography off the California Coast," *Geol. Soc. of Am.*, v. 31, 1941.

Wyllis, J. G., *Goestrophic Flow of the California Current at the Surface and at 200 meters*, CALCOFI Report 4, 1966.

INITIAL DISTRIBUTION LIST

		No.	Copies
1.	Defense Technical Information Center Cameron Station Alexandria, VA 22314		2
2.	Library, Code 0142 Naval Postgraduate School Monterey, CA 93943		2
3.	Dr C.K.N. Mooers (Code 68Mr) Chairman Department of Oceanography Naval Postgraduate School Monterey, CA 93943		18
4.	Director of Naval Oceanography and Meteorology Ministry of Defence Old War Office Building Whitehall London SW1A 2EU England		4
5.	Lt Cdr B.J.Brady Royal Navy HMS WARRIOR Northwood Middlesex England		1
6.	Director Naval Oceanography Division Naval Observatory 34th and Massachusetts Avenue NW Washington, DC 20390		1
7.	Commander Naval Oceanography Command NSTL Station Bay St. Louis, MS 39522		1
8.	Commanding Officer Naval Oceanographic Office NSTL Station Bay St. Louis, MS 39522		1
9.	Commanding Officer Fleet Numerical Oceanography Center Monterey, CA 93943		1
10.	Commanding Officer Naval Ocean Research and Development Activity NSTL Station Bay St. Louis, MS 39522		1
11.	Commanding Officer Naval Enviromental Prediction Research Facility Monterey, CA 93943		1

12. Chief of Naval Research 800 N. Quincy Street Arlington, VA 22217	1
13. Office of Naval Research (Ccde 420) 800 N. Quincy Street Arlington, VA 22217	2
14. Scientific Liaison Office Office of Naval Research Scripps Institution of Oceanography La Jolla, CA 92037	1
15. Library School of Oceanography Oregon State University Corvallis, OR 97331	1
16. Commander Oceanographic Systems Pacific Box 1390 Pearl Harbour, HI 96860	1
17. Commander (AIR-370) Naval Air Systems Command Washington, DC 20360	1
18. Chief, Ocean Services Division National Oceanic and Atmospheric Administration 8060 Thirteenth Street Silver Springs, MD 20910	1
19. Commanding Officer Naval Eastern Oceanography Center Naval Air Station Norfolk, VA 23511	1
20. Commanding Officer Naval Western Oceanography Center Box 113 Pearl Harbour, HI 96860	1
21. Commanding Officer Naval Oceanography Command Center, Rota Box 31 FPO San Francisco, CA 09540	1
22. Commanding Officer Naval Oceanography Command Center, Guam Box 12 FPO San Francisco, CA 96630	1
23. Library Acquisitions National Center for Atmospheric Research P.O. Box 3000 Boulder, CO 80307	1

END

FILMED

1-85

DTIC